THE UNIVERSITY OF TULSA

THE GRADUATE SCHOOL

WELL TESTING FOR COMPLEX-GEOMETRY RESERVOIRS

by
Gang Zhao

A dissertation submitted in partial fulfillment of
the requirements for the degree of Doctor of Philosophy
in the Discipline of Petroleum Engineering
The Graduate School
The University of Tulsa
1999

THE UNIVERSITY OF TULSA

THE GRADUATE SCHOOL

WELL TESTING FOR COMPLEX-GEOMETRY RESERVOIRS

by
Gang Zhao

A DISSERTATION
APPROVED FOR THE DISCIPLINE OF
PETROLEUM ENGINEERING

By Dissertation Committee

_____ Chairperson

_____

_____

_____

ABSTRACT

Gang Zhao (Doctor of Philosophy in Petroleum Engineering)
WELL TESTING FOR COMPLEX-GEOMETRY RESERVOIRS
(161 pp.-Chapter 7)
Directed by Dr. Leslie G. Thompson

(232 words)

Complex geometry reservoirs can be encountered in the field for a variety of depositional and tectonic processes. For example, fluvial depositional environments may produce inter-branching channel reservoirs, or reservoirs consisting of relatively high permeability channels in communication with low-permeability splays. This dissertation presents a general methodology for computing pressure responses and flow characteristics in complex geometry reservoirs. The proposed method consists of decomposing the original complex-geometry reservoir into a set of simple-geometry reservoirs, which interact with each other by transfer of fluid and equality of pressure over the regions where they are in hydraulic contact. Analytical solutions are written down for each of the simple reservoir components in terms of the unknown pressures and fluxes at their boundaries, and the coupled systems are solved for the desired wellbore pressure responses. The method of sources and sinks is used to compute the pressure response in the Laplace domain and the results are inverted numerically using the Stehfest Inversion algorithm. We present fast accurate methods of taking numerical Laplace transforms of the source/sink solutions that make the computations reasonably fast and efficient. The proposed methodology can be extended to any system where the Laplace space function can be easily written in

terms of integrals of real-space source/sink functions, including production at constant bottom-hole pressure, wellbore storage effects or naturally fractured systems. We demonstrate the applicability of the method by modeling branching channels and channel/splay systems.

ACKNOWLEDGMENTS

I wish to express my sincere appreciation and gratitude to my advisor, Dr. Leslie G. Thompson, for his creative idea and guidance throughout the process of the this research. My special thanks also go to Dr. Albert C. Reynolds for his sugestion and support during the research. In addition I would like to thank Dr. Dean Oliver and Dr. Redner for taking the time and the effort to be a part of my dissertation committee.

The financial support and the research assistantship provided by TUPREP(Tulsa University Petroleum Reservoir Exploitation Projects) are gratefully acknowledged.

My thanks and appreciation are also extended to faculty members and graduate students for forming the excellent academic environment in Petroleum Engineering Department. I want to thank my parents, Xiongzhi Zhao and Xianjiu Yang, and my parents in law, Jisheng Gao, Guizhen, Nian, for their support and encouragement they have given me dring the time abroad and away.

This dissertation is dedicated to my wife Xiaoxia Gao and to my beloved daughter Michelle Tian Zhao for their understanding, patience and love.

TABLE OF CONTENTS

LIST OF FIGURES

CHAPTER I

INTRODUCTION

1.1 Background

Classical well test analysis has long been used as a valuable tool in characterizing reservoirs from transient pressure versus time behavior. In most classical well test models, the reservoir is idealized as a "homogeneous" single or dual porosity system with a simple reservoir and well geometry. This is done in order to facilitate generation of analytical solutions to the reservoir problem. In fluvial-deltaic reservoir systems, the complex geometry precludes idealizing the reservoir as a simple-shaped homogeneous system and in general, the transient pressure responses do not resemble those of classical simple-geometry systems. Fluvial-deltaic reservoir systems are one example of general complex-geometry reservoirs for which classical well test analysis models may not be applicable.

In this dissertation, we present a general methodology for computing pressure responses in complex geometry reservoirs. Essentially, the method consists of decomposing the original complex-geometry reservoir into a set of simple-geometry reservoirs, which interact with each other by transfer of fluid and equality of pressure over the regions where they are in hydraulic contact. Analytical solutions are written down for each of the simple reservoir components in terms of the unknown pressures and fluxes at their boundaries, and the coupled systems are solved for the desired wellbore pressure responses.

Our efforts in this area are focused on reservoir geometries associated with

fluvial-deltaic systems, such as channel reservoirs with hydraulically connected river splays, branching channels, where the properties of each branch may significantly differ from one another, and intersecting channels such as tees or crosses. Although semi-analytical solutions are obtainable for a wide variety of reservoir geometries, accurate and fast computation of the responses remains a major consideration. This dissertation presents new methods of taking numerical Laplace transforms that provide the required accuracy and speed for our computations.

Final results for the pressure responses of the following four types of complex-geometry reservoirs are shown in this dissertation.

1. Two semi-infinite reservoirs that are isolated from one another by a sealing fault except over a small "hole" in the fault; refer Fig. 1.1. This approximates a system with a "leaky" fault.

2. Tee-shaped channel reservoirs; see Fig. 1.2.

3. Channel and splay reservoirs, refer to Fig. 1.3.

4. Communication between two bounded reservoirs, see Fig. 1.4.

The method of sources and sinks is used to solve the problems in the Laplace domain and the Stehfest Inversion algorithm[1] is used to invert the solution. Unit production rate pressure response is considered without adding wellbore storage and skin factor; addition of wellbore storage and skin effects in Laplace space is trivial. The solutions we generated were verified for limiting cases where well-known analytical results are available.

1.2 Literature Review

Except for work presented by Larsen[2], [3] on a network of interconnected linear reservoirs, there appears to have been very little presented in the literature

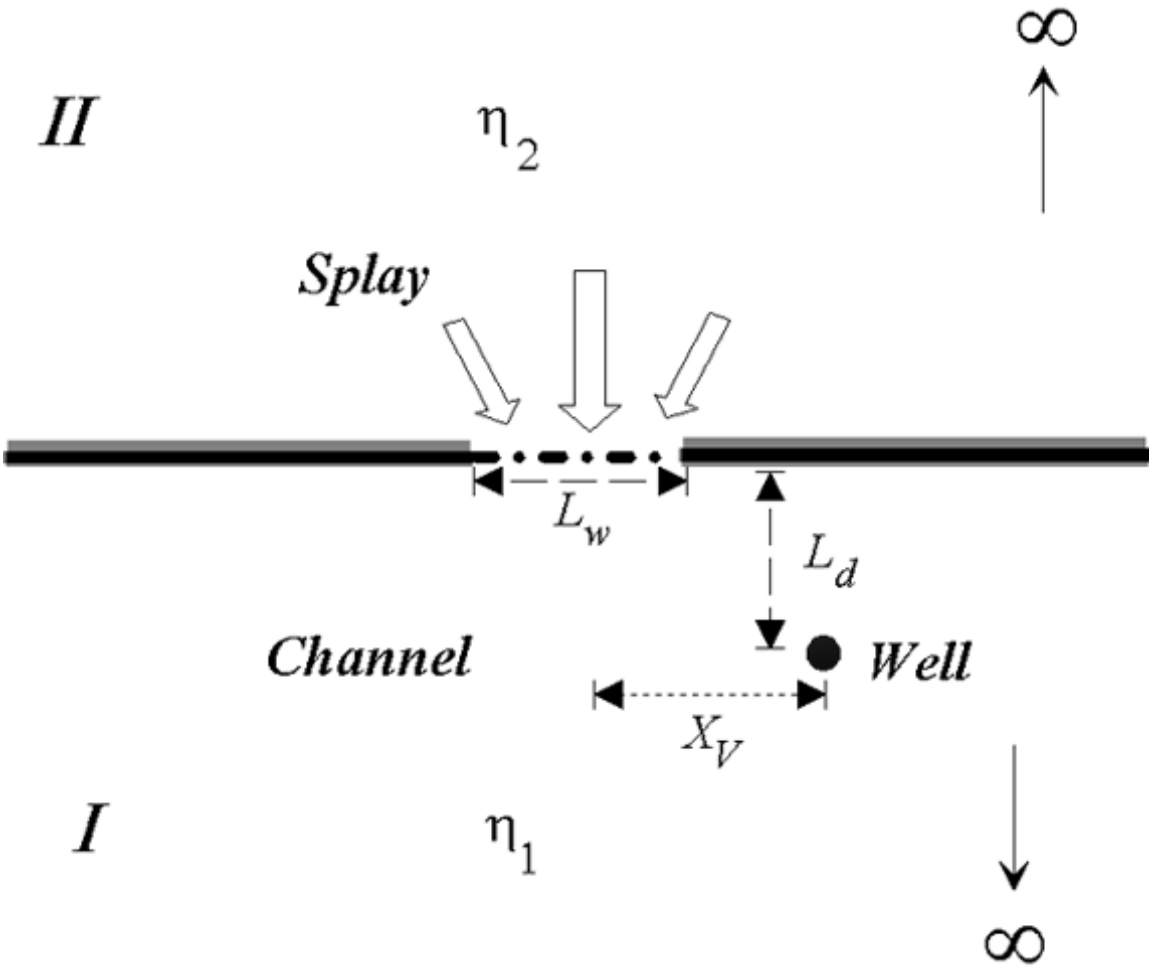

Figure 1.1: Schematic of a well producing from a system with a "leaky" fault

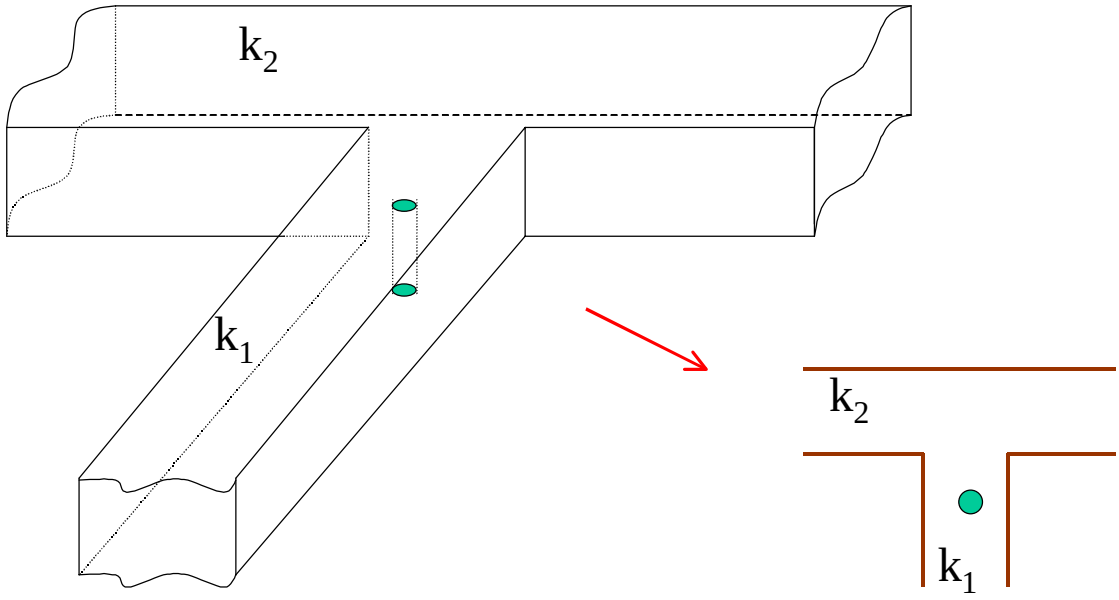

Figure 1.2: Schematic of a well producing from tee-shape reservoir

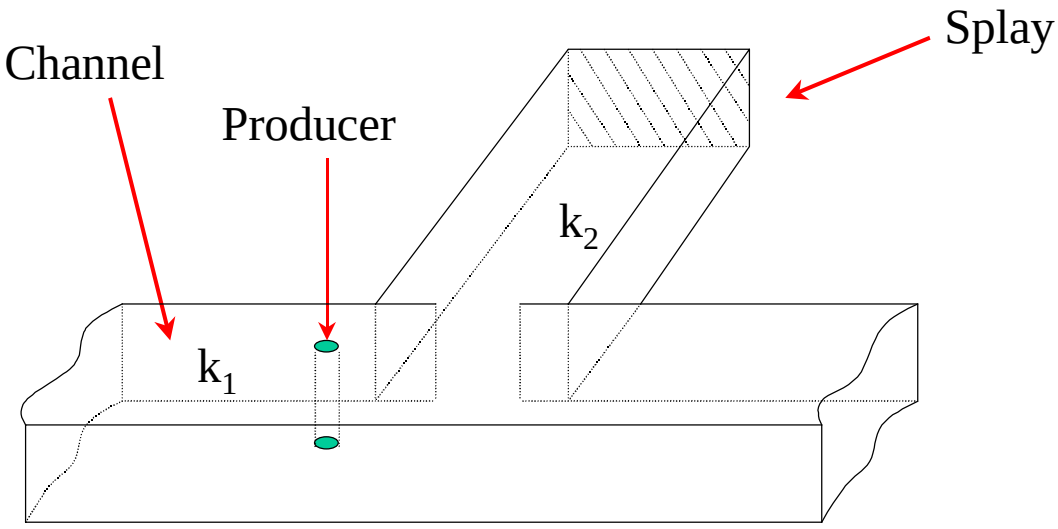

Figure 1.3: Schematic of a well producing from channel and splay reservoir

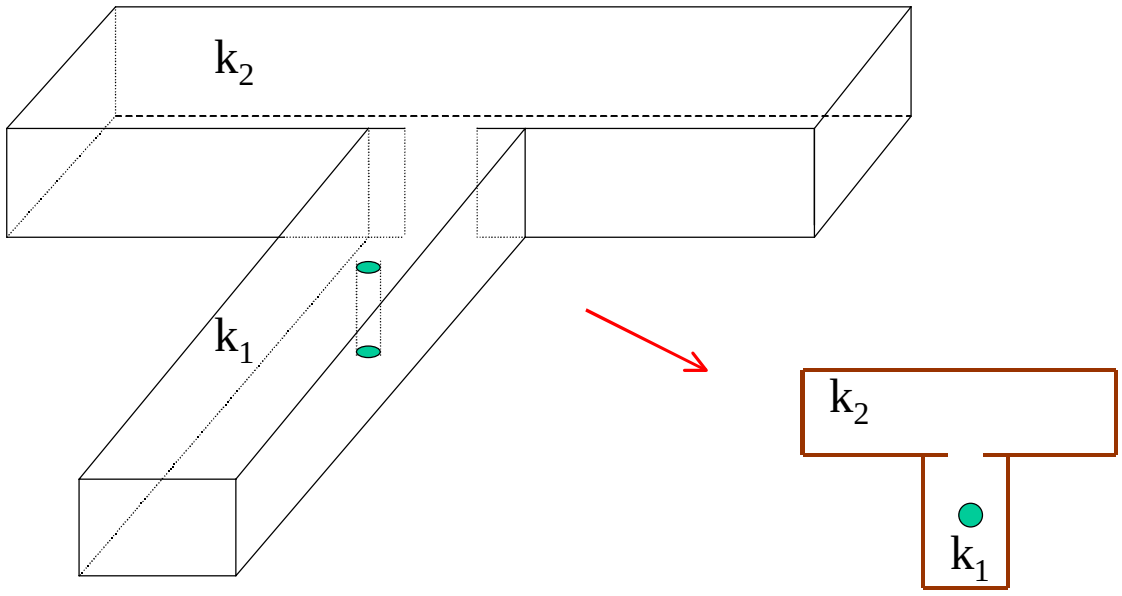

Figure 1.4: Schematic of a well producing from bounded tee-shaped reservoir

in modeling or describing the pressure transient pressure behavior of these types of reservoirs. Larsen's work was primarily concerned with the long time productivity of a network of intersecting linear reservoirs, with no special consideration given to the geometry at the regions of intersection(Larsen tried to account for the intersection geometry by including a "skin factor" at the intersection.). Larsen's work indicated that proper understanding of reservoir type is critical in situations where extrapolation of short-time test data to possible late-time production characteristics is attempted. A schematic of the types of reservoir considered in Larsen's work is depicted in Fig. 1.5.

Sealing and/or non-sealing faults have been a major research topic in pressure transient analysis literature. Instead of focusing on the communication between reservoirs, most of the studies have been focused on the effect of the sealing and/or non-sealing faults. Both numerical and analytical solutions have been presented in the literature to model the pressure behavior in faulted reservoirs and some pertinent papers are discussed below.

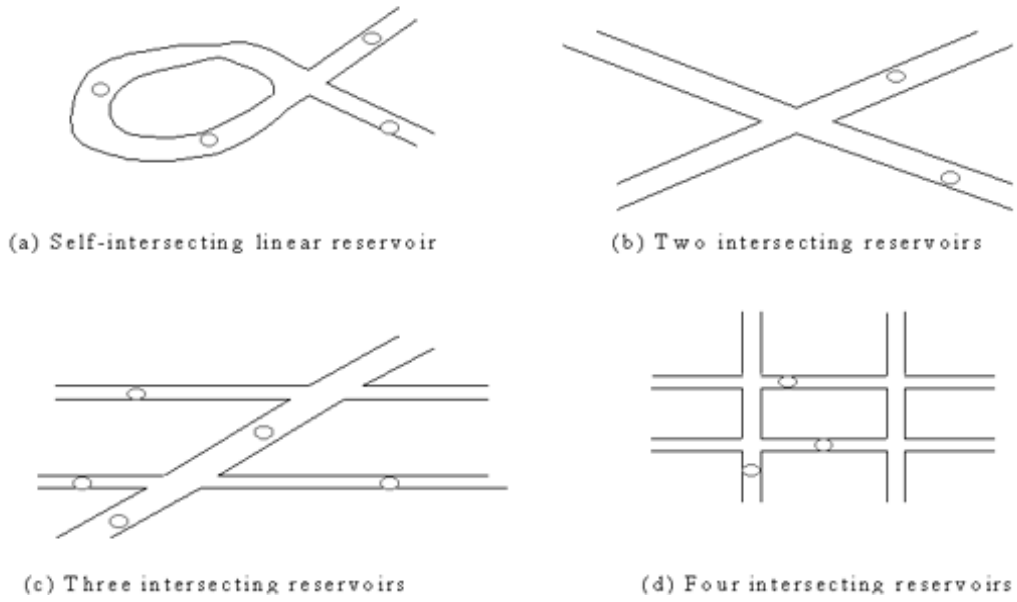

Figure 1.5: Model of intersecting reservoirs and their linear segments (Larsen)

Stewart et al.[4] used numerical simulation to compute the pressure transient response due to a constant rate producing well on an observation well on the far side of a partially communicating fault. The reservoir properties on both sides of the fault were assumed to be identical. They found that at the time when the presence of the fault influences the pressure response, the pressure response becomes steeper at the active well; an almost straight line of slope m_2 is obtained, where $m_1 < m_2 < 2m_1$, and m_1 denotes the slope of the line associated with the homogeneous (infinite-acting) system where the active well is located. The value of m_2 and the duration of this transition period are dependent on the dimensionless fault conductivity, A_{DF}, defined as

$$A_{DF} = \frac{k_f L_{af}}{k h_f}. \tag{1.1}$$

In Eq. 1.1, k_f denotes fault zone permeability, md, k denotes formation permeability, md, L_{af} denotes distance from active well to fault, ft, and h_f is fault zone thickness,

ft. At late time, there is a third straight line period of slope m_3, which is close to m_1 except at small values of A_{DF} (less than 0.04).

Yaxley[5] obtained an analytical solution for the transient pressure behavior of a constant rate well in an infinite reservoir that contained a vertical linear semi-permeable barrier. Interference type curves were generated for the special case of a fault that is perpendicular to a line of intersection joining the active and observation wells. The general analytical solution for the pressure distribution was used to form type curves for other fault orientations. The type curves yield separate estimates of the formation transmissibility and the transmissibility of the fault itself.

Ambastha et al.[6] presented analytical solutions for pressure transient behavior of a line-source, constant-rate well in a composite infinite strip reservoir by modeling the fault as an infinitesimally thin skin boundary, (see Fig. 1.6). Their model was verified by checking it against the line source solution and boundary conditions created either by infinitesimally thin skin or by a linear sealing boundary. The effects of well location, boundary conditions, fault, mobility and diffusivity of the two regions on the drawdown behaviors of an infinite channel reservoir were discussed. A field interference well testing interpretation successfully characterized the properties in Region 1 and Region 2.

They concluded that for large skin factor, the fault serves as a sealing boundary, and the effects of boundaries are felt at a dimensionless time of $t_D = 0.4$, where

$$t_D = \frac{0.000264 k_1 t}{(\phi \mu c_t)_1 a^2}. \tag{1.2}$$

In Eq. 1.2, a denotes the distance between well and fault, and the subscript "1" refers to the properties of the part of the reservoir containing the active well. A doubling or quadrupling of the infinite-reservoir semilog derivative was observed if the well was closer to one sealing boundary or two equidistant perpendicular intersecting sealing boundaries than to the other reservoir boundaries in a homogeneous reservoir. Their study also showed that the analysis of interference tests in composite reservoirs is

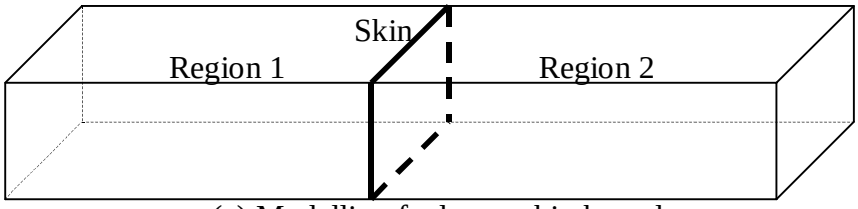

(a) Modelling fault as a skin boundary

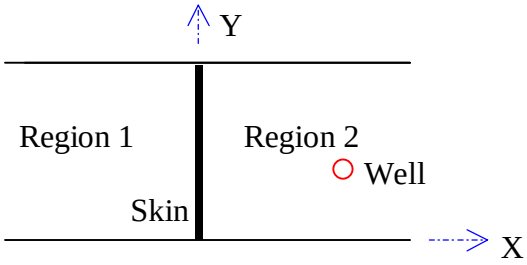

(b) Idealized composite strip reservoir

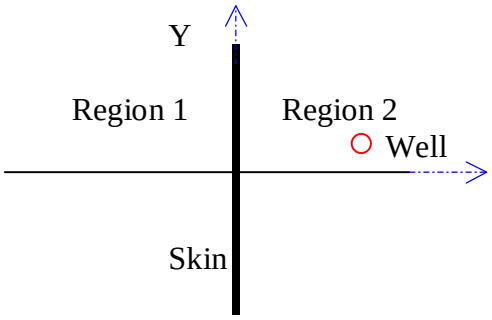

(c) Idealized composite infinite reservoir

Figure 1.6: A. K. Ambastha: Schematic of composite reservoir with a partially communicating fault

not straightforward because the response depends on the property contrasts and the location of the observation well. Therefore, a careful study of the complex geometry reservoir is essential for the reservoir characterization.

Abbaszadeh and Cinco-Ley[7], presented an analytical solution for pressure behavior in a reservoir assuming flow both along and across a non-intersecting finite conductivity fault. Type curves of pressure and pressure derivative were developed for different values of mobility, diffusivity ratio, skin factor and fault conductivities. Their results show that for high fault conductivities and at large times, the pressure derivative exhibits a quarter-slope characteristic of bilinear flow behavior, where the

fault acts like a channel. At very long time the pressure derivative becomes horizontal, exhibiting behavior similar to that of naturally fractured reservoirs. A simple equation for bilinear flow in terms of fault conductivity and reservoir mobility ratio was provided.

Sahni et al.[8] presented an analysis of the transient pressure behavior in a multilayered faulted reservoir with sealing and non-sealing faults. A 3-D numerical model was used to generate the transient pressure response at the producing well. A methodology was developed to estimate the fault and formation transmissibility as well as the distance from the fault to the producing well from newly-derived type curves.

In 1997, Abbaszadeh et al.[9] addressed interference testing in reservoirs with conductive faults. Their results indicated that there are significant differences in interference test responses, depending on the location of the observation well and whether each of the testing well pair is on the same side or opposite sides of the fault. When they are on the same side, the interference response is similar to that of the active well. However, the extent of similarity depends on well arrangement configuration with respect to the fault. When the wells are at the opposite sides of the fault, the interference response is usually similar to that from a hydraulically fractured well. A bilinear flow regime often dominates the observation well response for such cases. In practice, three tests (either all interference or two interference and one buildup) are required to characterize geometrical attributes of a fault with respect to its location and orientation.

CHAPTER II

MODELING PHILOSOPHY AND METHODOLOGY

2.1 Approach

In the following, we illustrate our general modeling approach by applying it to a simple reservoir system. The physical model considered in Fig. 1.1 consists of two semi-infinite reservoirs separated over most of their extent by a hydraulically sealing barrier. One has flow properties of a "channel", while the other has properties of a "splay". The reservoirs are in hydraulic contact only over a small area. A well is producing from one of the reservoirs.

The first step in the modeling procedure is to identify simple-geometry homogeneous reservoir components that make up the complex system. In the preceding example, the complex reservoir is composed of two semi-infinite reservoirs: one with properties of the "channel", which we will refer to as Region 1, and the other with properties of the "splay" or Region 2. Considering Region 1 only, the reservoir behaves as if it contains two wells: a producer at coordinates (x', y') and a planar injection well at the location of the area of communication between the two reservoirs. Similarly, considering Region 2 only, it behaves as if there was a single production plane/fracture well at the location of the area of communication between the two reservoirs. Obviously, since all the fluid leaving Region 2 is entering Region 1, the production and injection rates of the apparent plane/fracture wells in each of the regions must be the same.

The second step in the modeling process involves isolating the various reservoir components from one another at their junction(s) by applying no flow boundaries. For simple reservoir systems that contain wells, this is achieved by creating a mirror

image in the no-flow boundary; that is, the inserted "no-flow boundary" becomes a plane of symmetry for the extended system. For the problem under consideration, Region 1 and Region 2 are each reflected using the fault as a mirror. (See Figs. 2.1 and 2.2.) Planar injection or production wells are added along the plane of symmetry to account for fluid transfer from one system to the other. The separate systems are then coupled at their junctions by equating rates and pressures at the junctions. The coupled systems are solved (in Laplace space) for the unknown flux distributions along the introduced "planar" wells. Finally, the flux profiles from the preceding step are substituted into the pressure equation for the well of interest to obtain the desired pressure response. We illustrate the procedure in more detail for the simple problem under consideration.

2.2 Dimensionless Variables

The coordinate system is defined in Fig. 2.3. In order to generalize our results, we introduce the following dimensionless variables. In general, we define dimensionless distances in the following equations, Eq. 2.1 through Eq. 2.5, based on a characteristic length l in the related reservoir system. For the communication of two semi-infinite reservoirs, (see Fig. 1.1), L_d, the distance from the producer to the boundary, is chosen to be the characteristic length. For other complex-reservoir systems that we will discuss later in this work, appropriate definitions of "l" will be provided.

The dimensionless distances x_D, y_D and L_{wD} are respectively defined as

$$x_D = \frac{x}{l}, \tag{2.1}$$

$$y_D = \frac{y}{l}, \tag{2.2}$$

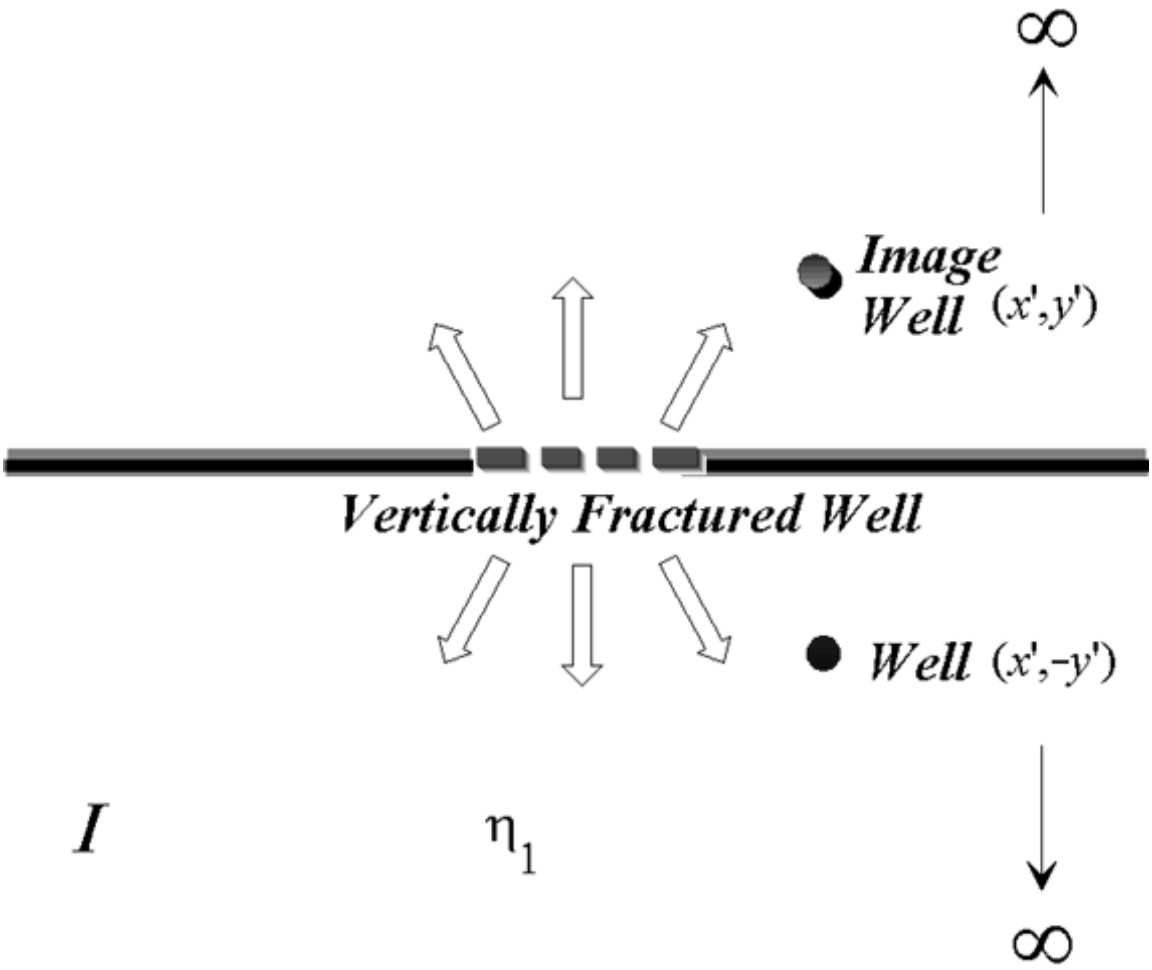

Figure 2.1: The reservoir from the perspective of Region 1

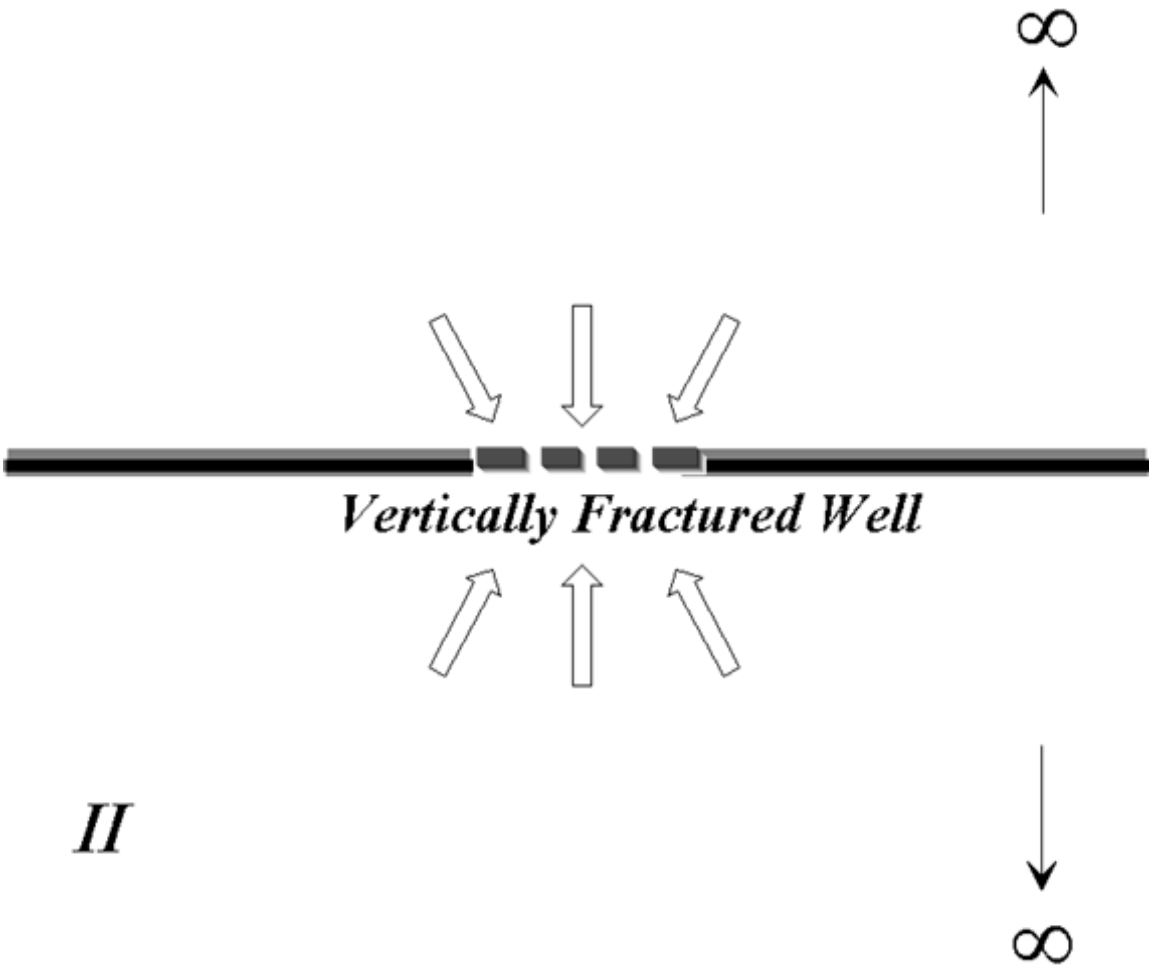

Figure 2.2: The reservoir from the perspective of Region 2

and

$$L_{wD} = \frac{L_w}{l}. \tag{2.3}$$

The dimensionless displacement of the production well from the gap center, X_{DV}, (see Fig. 1.1), is given by

$$X_{DV} = \frac{X_V}{l}. \tag{2.4}$$

Here, x and y refer to coordinates in the $x-y$ plane and L_w denotes the width of the gap.

Dimensionless time, t_D is defined in terms of Region 1 properties, i.e.,

$$t_D = \frac{\eta_1 t}{l^2}, \tag{2.5}$$

where the diffusivity η is defined as

$$\eta = \frac{0.00633k}{\phi c_t \mu} \frac{\text{ft}^2}{\text{day}}. \tag{2.6}$$

Similarly, dimensionless pressure drop, p_D, is defined in terms of Region 1 properties as

$$p_D = \frac{k_1 h_1 \Delta p}{141.2 q B_1 \mu_1}. \tag{2.7}$$

The dimensionless transmissibility, storativity and diffusivity ratios, C_T, C_S, C_R respectively are defined as

$$C_T = \left(\frac{k_2 h_2}{\mu_2}\right)\left(\frac{\mu_1}{k_1 h_1}\right), \tag{2.8}$$

$$C_S = \frac{\phi_2 c_{t2} h_2}{\phi_1 c_{t1} h_1}, \tag{2.9}$$

and

$$C_R = \frac{\eta_2}{\eta_1} = \left(\frac{k_2 h_2}{\mu_2}\right)\left(\frac{\mu_1}{k_1 h_1}\right)\left(\frac{\phi_1 c_{t1} h_1}{\phi_2 c_{t2} h_2}\right) = \frac{C_T}{C_S}, \tag{2.10}$$

respectively.

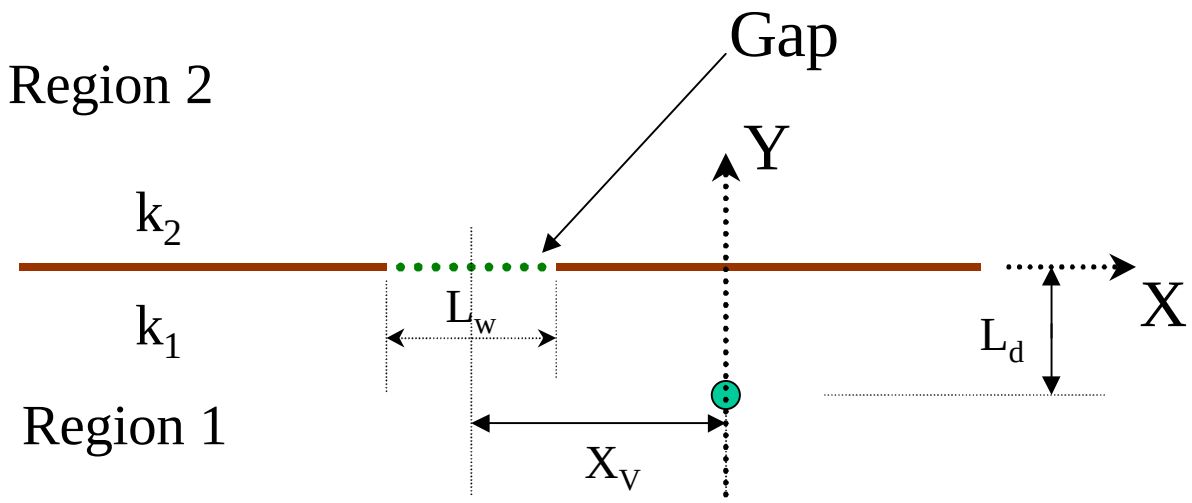

Figure 2.3: The coordinate system definition

2.3 Leaky Fault Problem Formulation and Solution

2.3.1 Discretization of the Fracture Plane

We subdivide the "fracture" injection and production "wells" in Regions 1 and 2 into N_f equal-length "uniform flux" discretized fracture segments. The half width of each discretized fracture segment, L_f , (see Fig. 2.4), is given by

$$L_f = \frac{L_w}{2N_f}. \tag{2.11}$$

The dimensionless half width of any fracture segment is

$$L_{fD} = \frac{L_f}{l} = \frac{1}{2N_f}\frac{L_w}{l}. \tag{2.12}$$

Let $(x_{fD,j}, y_{fD})$ denote the center coordinates of the jth discretized fracture segment. Thus,

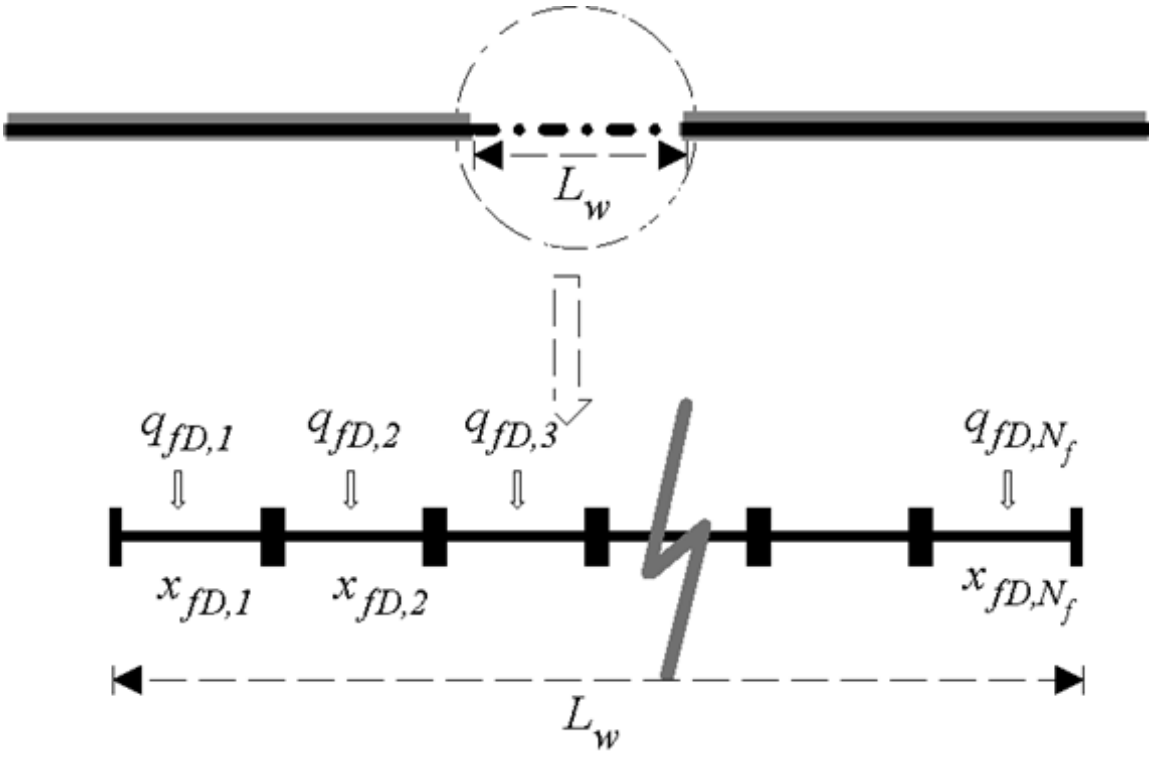

Figure 2.4: Schematic of fracture plane discretization

$$x_{fD,j} = x_{D,j-1} + L_{fD} = x_{D,j} - L_{fD}, \quad \text{for} \quad 1 \leq j \leq N_f \tag{2.13}$$

where, $x_{D,j-1}$ and $x_{D,j}$ represent the left and right hand side dimensionless endpoints of the jth fracture segment.

2.3.2 Region 1 and Region 2 Solution

We assume that the actual well in Region 1 produces at a rate of 1 RB/D. In Laplace space, the pressure drop, $\overline{p}_{D,k_1}$, at any dimensionless location (x_{D,k_1}, y_{D,k_1})

is written in terms of source/sink solutions as

$$\overline{p}_{D,k_1}\left(x_{D,k_1}, y_{D,k_1}, u_D\right) = \frac{K_0\left(\sqrt{\left[\left(x_{D,k_1}-x'_{D,k_1}\right)^2+\left(y_{D,k_1}-y'_{D,k_1}\right)^2\right]u_D}\right)}{u_D} + \frac{K_0\left(\sqrt{\left[\left(x_{D,k_1}-x'_{D,k_1}\right)^2+\left(y_{D,k_1}+y'_{D,k_1}\right)^2\right]u_D}\right)}{u_D} - \sum_{j=1}^{N_f}\overline{q}_{fD,j}\overline{f}_{D,j,k_1}\left(x_{D,k_1}, y_{D,k_1}, u_D\right). \quad (2.14)$$

Here the subscript k_1 denotes that the variable belongs to the region with permeability k_1, i.e., Region 1. The producer is located at (x'_{D,k_1}, y'_{D,k_1}) and the image well is located at $(x'_{D,k_1}, -y'_{D,k_1})$. The three terms on the right side of Eq. 2.14 account for production from the original well, production from an image well , and non-uniform injection from the fracture plane respectively. Our notation in Eq. 2.14 requires clarification. K_0 is the modified Bessel function of the second kind. u_D is the dimensionless Laplace variable for Region 1; that is, if u (with units day^{-1}), is the Laplace variable associated with the transform of time, u_D is defined as

$$u_D = \frac{L_d^2 u}{\eta_1}. \quad (2.15)$$

$(x_{fD,j}, y_{fD})$ denote coordinates along the discretized fracture plane, see Fig. 2.4, while $\overline{q}_{fD,j}$ denotes the Laplace transform of the (unknown) flux at $(x_{fD,j}, y_{fD})$. Finally, $\overline{f}_{D,j,k_1}\left(x_{D,k_1}, y_{D,k_1}, u_D\right)$ denotes the Laplace transform of the dimensionless source/sink function for a "uniform-flux" fracture plane in Region 1. That is, the term $\overline{f}_{D,j,k_1}\left(x_{D,k_1}, y_{D,k_1}, u_D\right)$ denotes the Laplace transform of $f_{D,j,k_1}\left(x_{D,k_1}, y_{D,k_1}, t_D\right)$,

where,

$$f_{D,j,k_1}\left(x_{D,k_1}, y_{D,k_1}, t_D\right) = \frac{\sqrt{\pi}}{2} \frac{\exp\left(-\frac{\left(y_{D,k_1} - y_{fD,k_1}\right)^2}{4t_D}\right)}{\sqrt{t_D}} \times \left[\operatorname{erf}\left(\frac{x_{D,j} - x_{D,k_1}}{2\sqrt{t_D}}\right) - \operatorname{erf}\left(\frac{x_{D,j-1} - x_{D,k_1}}{2\sqrt{t_D}}\right)\right], \quad \text{for } 1 \le j \le N_f. \quad (2.16)$$

We rewrite Eq. 2.16 using the elliptic theta function notation of Appendix A as

$$f_{D,j,k_1}\left(x_{D,k_1}, y_{D,k_1}, t_D\right) = \pi \widehat{\Theta}_L\left(\frac{x_{D,j-1} - x_{D,k_1}}{2}, \frac{x_{D,j} - x_{D,k_1}}{2}, t_D\right) \theta_L\left(\frac{y_{D,k_1} - y_{fD,k_1}}{2}, t_D\right), \quad \text{for } 1 \le j \le N_f \quad (2.17)$$

where, as in Appendix A,

$$\theta_L\left(z,t\right) = \frac{1}{\sqrt{\pi t}} \exp\left(-\frac{z^2}{t}\right) \quad (2.18)$$

and

$$\widehat{\Theta}_L\left(z_1, z_2, t\right) = \frac{1}{2}\left[\operatorname{erf}\left(\frac{z_2}{\sqrt{t}}\right) - \operatorname{erf}\left(\frac{z_1}{\sqrt{t}}\right)\right]. \quad (2.19)$$

To the best of our knowledge, there is no analytical closed form expression for the Laplace Transform of Eq. 2.17, so in our computations, we take the Laplace transform of Eq. 2.17 numerically. Appendix A details a method for taking Laplace Transforms of general source/sink functions that provides the required speed and accuracy.

Let the subscript k_2 denote variables that are measured in Region 2. The corresponding solution to the Region 2 problem is written as

$$\overline{p}_{D,k_2}\left(x_{D,k_2}, y_{D,k_2}, u_D\right) = \sum_{j=1}^{N_f} \overline{q}_{fD,j} \overline{f}_{D,j,k_2}\left(x_{D,k_2}, y_{D,k_2}, u_D\right). \quad (2.20)$$

Here, $\overline{f}_{D,j,k_2}(x_{D,k_2}, y_{D,k_2}, u_D)$ is the Laplace transform of $f_{D,j,k_2}(x_{D,k_2}, y_{D,k_2}, t_D)$ and

$$f_{D,j,k_2}(x_{D,k_2}, y_{D,k_2}, t_D) = \frac{\sqrt{\pi}}{2C_S} \frac{\exp\left(-\frac{(y_{D,k_2} - y_{fD,k_2})^2}{4C_R t_D}\right)}{\sqrt{C_R t_D}} \times \left[\text{erf}\left(\frac{x_{D,j} - x_{D,k_2}}{2\sqrt{C_R t_D}}\right) - \text{erf}\left(\frac{x_{D,j-1} - x_{D,k_2}}{2\sqrt{C_R t_D}}\right)\right], \quad \text{for} \quad 1 \le j \le N_f \quad (2.21)$$

or equivalently,

$$f_{D,j,k_2}(x_{D,k_2}, y_{D,k_2}, t_D) = \frac{\pi}{C_S} \theta_L\left(\frac{y_{D,k_2} - y_{fD,k_2}}{2}, C_R t_D\right) \widehat{\Theta}_L\left(\frac{x_{D,j-1} - x_{D,k_2}}{2}, \frac{x_{D,j} - x_{D,k_2}}{2}, C_R t_D\right), \quad \text{for} \quad 1 \le j \le N_f. \quad (2.22)$$

Eq. 2.20 is the dimensionless pressure drop for a non-uniform flux vertically fractured production well in Region 2.

The coupled problem is solved by equating pressures at the midpoints of each of the fracture segments; i.e., equating the right hand sides of Eq. 2.14 and Eq. 2.20 evaluated at each segment midpoint. The resulting system of N_f equations is solved for the unknown fluxes $\left\{\overline{q}_{fD,j}\right\}_{j=1}^{N_f}$. The fluxes obtained from this step are used in Eq. 2.14 to obtain the desired pressure response at the well.

We did not mention whether $x_{D,j}, x_{D,j-1}$ are in Region 1 or in Region 2 since they have the same value in both regions and $y_{fD,k_1} = y_{fD,k_2} = 0$. Further details on the numerical solution of the problem are provided in the next chapter.

CHAPTER III

COMPUTATIONAL CONSIDERATIONS

3.1 Mathematical Derivation

3.1.1 Method Formulation

By applying Eq. 2.14, the pressure drop at the midpoint, $(x_{fD,i}, y_{fD,k_1})$, of the ith fracture segment in Region 1 is

$$\overline{p}_{D,k_1}(x_{fD,i}, y_{fD,k_1}, u_D) = \frac{K_0\left(\sqrt{\left[\left(x_{fD,i} - x'_{D,k_1}\right)^2 + \left(y_{fD,k_1} - y'_{D,k_1}\right)^2\right] u_D}\right)}{u_D} + \frac{K_0\left(\sqrt{\left[\left(x_{fD,i} - x'_{D,k_1}\right)^2 + \left(y_{fD,k_1} + y'_{D,k_1}\right)^2\right] u_D}\right)}{u_D} - \sum_{j=1}^{N_f} \overline{q}_{fD,j} \overline{f}_{D,j,k_1}(x_{fD,i}, y_{fD,k_1}, u_D), \text{ for } 1 \le i \le N_f, \quad (3.1)$$

where,

$$f_{D,j,k_1}(x_{fD,i}, y_{fD,k_1}, t_D) = \pi \theta_L(0, t_D)\, \widehat{\Theta}_L\left(\frac{x_{D,j-1} - x_{fD,i}}{2}, \frac{x_{D,j} - x_{fD,i}}{2}, t_D\right), \text{ for } 1 \le j \le N_f, \quad 1 \le i \le N_f. \quad (3.2)$$

The pressure drop at each midpoint, $(x_{fD,j}, y_{fD,k_2})$, of the ith fracture segment in Region 2 is

$$\overline{p}_{D,k_2}\left(x_{fD,i},y_{fD,k_2},u_D\right)=\sum_{j=1}^{N_f}\overline{q}_{fD,j}\overline{f}_{D,j,k_2}\left(x_{fD,i},y_{fD,k_2},u_D\right),$$

$$\text{for}\quad 1\le i\le N_f, \tag{3.3}$$

where

$$f_{D,j,k_2}\left(x_{fD,i},y_{fD,k_2},t_D\right)=$$

$$\frac{\pi}{C_S}\theta_L\left(0,C_Rt_D\right)\widehat{\Theta}_L\left(\frac{x_{D,j-1}-x_{fD,i}}{2},\frac{x_{D,j}-x_{fD,i}}{2},C_Rt_D\right),$$

$$\text{for}\quad 1\le j\le N_f,\quad 1\le i\le N_f. \tag{3.4}$$

We introduce the following simplifying notation. Let

$$\Psi\left(x_{fD,i},y_{fD,k_1},u_D\right)=\frac{K_0\left(\sqrt{\left[\left(x_{fD,i}-x'_{D,k_1}\right)^2+\left(y_{fD,k_1}-y'_{D,k_1}\right)^2\right]u_D}\right)}{u_D}+$$

$$\frac{K_0\left(\sqrt{\left[\left(x_{fD,i}-x'_{D,k_1}\right)^2+\left(y_{fD,k_1}+y'_{D,k_1}\right)^2\right]u_D}\right)}{u_D}. \tag{3.5}$$

Equating the right hand sides of Eq.3.1 and Eq.3.3, we have

$$\Psi\left(x_{fD,i},y_{fD,k_1},u_D\right)-\sum_{j=1}^{N_f}\overline{q}_{fD,j}\overline{f}_{D,j,k_1}\left(x_{fD,i},y_{fD,k_1},u_D\right)=$$

$$\sum_{j=1}^{N_f}\overline{q}_{fD,j}\overline{f}_{D,j,k_2}\left(x_{fD,i},y_{fD,k_2},u_D\right), \tag{3.6}$$

which can be rewritten as

$$\sum_{j=1}^{N_f}\overline{q}_{fD,j}\left[\overline{f}_{D,j,k_1}\left(x_{fD,i},y_{fD,k_1},u_D\right)+\overline{f}_{D,j,k_2}\left(x_{fD,i},y_{fD,k_2},u_D\right)\right]=$$

$$\Psi\left(x_{fD,i},y_{fD,k_1},u_D\right),\quad\text{for}\quad 1\le i\le N_f \tag{3.7}$$

where, $\overline{f}_{D,j,k_1}(x_{fD,i}, y_{fD,k_1}, u_D)$ and $\overline{f}_{D,j,k_2}(x_{fD,i}, y_{fD,k_2}, u_D)$ are the Laplace transform of time dependent functions in Eq. 3.2 and Eq. 3.4. Since the planar fracture was discretized by subdividing it into equal-length segments, applying Eq. 2.13 we have

$$x_{D,j} - x_{fD,i} = 2jL_{fD} - (2iL_{fD} - L_{fD}) = [2(j-i)+1]\,L_{fD}, \tag{3.8}$$

and

$$x_{D,j-1} - x_{fD,i} = 2(j-1)L_{fD} - (2iL_{fD} - L_{fD}) = [2(j-i)-1]\,L_{fD}. \tag{3.9}$$

Using the above equations, Eq. 3.2 and Eq. 3.4 can be rewritten as

$$f_{D,j,k_1}(x_{fD,i}, y_{fD,k_1}, t_D) = \pi\theta_L(0, t_D)\,\widehat{\Theta}_L\left(\frac{[2(j-i)-1]\,L_{fD}}{2}, \frac{[2(j-i)+1]\,L_{fD}}{2}, t_D\right), \quad \text{for} \quad 1 \le j \le N_f, \quad 1 \le i \le N_f, \tag{3.10}$$

and

$$f_{D,j,k_2}(x_{fD,i}, y_{fD,k_2}, t_D) = \frac{\pi}{C_S}\theta_L(0, C_R t_D)\,\widehat{\Theta}_L\left(\frac{[2(j-i)-1]\,L_{fD}}{2}, \frac{[2(j-i)+1]\,L_{fD}}{2}, C_R t_D\right), \quad \text{for} \quad 1 \le j \le N_f, \quad 1 \le i \le N_f. \tag{3.11}$$

Eq. 3.10 and Eq. 3.11 are used in Eq. 3.7 to calculate the non-uniform flux distribution.

We express Eq. 3.7 in the following matrix form

$$\begin{bmatrix} \overline{a}_{11} & \overline{a}_{12} & ... & \overline{a}_{1j} & ... & \overline{a}_{1N_f} \\ \overline{a}_{21} & \overline{a}_{22} & ... & \overline{a}_{2j} & ... & \overline{a}_{2N_f} \\ ... & ... & ... & ... & ... & ... \\ \overline{a}_{i1} & \overline{a}_{i2} & ... & \overline{a}_{ij} & ... & \overline{a}_{iN_f} \\ ... & ... & ... & ... & ... & ... \\ \overline{a}_{N_f 1} & \overline{a}_{N_f 2} & ... & \overline{a}_{N_f j} & ... & \overline{a}_{N_f N_f} \end{bmatrix} \begin{bmatrix} \overline{q}_{fD,1}(u_D) \\ \overline{q}_{fD,2}(u_D) \\ ... \\ \overline{q}_{fD,i}(u_D) \\ ... \\ \overline{q}_{fD,N_f}(u_D) \end{bmatrix} = \begin{bmatrix} \Psi(x_{fD,1}, y_{fD,k_1}, u_D) \\ \Psi(x_{fD,2}, y_{fD,k_1}, u_D) \\ ... \\ \Psi(x_{fD,i}, y_{fD,k_1}, u_D) \\ ... \\ \Psi\left(x_{fD,N_f}, y_{fD,k_1}, u_D\right) \end{bmatrix} \tag{3.12}$$

where,

$$\overline{a}_{ij} = \overline{f}_{D,j,k_1}(x_{fD,i}, y_{fD,k_1}, u_D) + \overline{f}_{D,j,k_2}(x_{fD,i}, y_{fD,k_2}, u_D), \quad \text{for} \quad 1 \le j \le N_f, \quad 1 \le i \le N_f, \tag{3.13}$$

or,

$$\overline{a}_{ij} = L\left\{\pi\theta_L(0, t_D)\,\widehat{\Theta}_L\left(\frac{[2(j-i)-1]L_{fD}}{2}, \frac{[2(j-i)+1]L_{fD}}{2}, t_D\right)\right\} + L\left\{\frac{\pi}{C_S}\theta_L(0, C_R t_D)\,\widehat{\Theta}_L\left(\frac{[2(j-i)-1]L_{fD}}{2}, \frac{[2(j-i)+1]L_{fD}}{2}, C_R t_D\right)\right\}. \tag{3.14}$$

Denote the above matrix as A, with elements a_{ij}. It is clear that the matrix A has the following properties:

1. $\overline{a}_{i,j} = \overline{a}_{j,i}$, i.e. A is a symmetric matrix.

2. $\overline{a}_{ij} = \overline{a}_{i+1,j+1}$.

Therefore for a N_f fracture plane discretization, we only need to compute N_f matrix elements.

Note that the derivation for the non-uniform flux "gap" reverts to a uniform-flux gap if the fracture plane is modeled as a single fracture segment; i.e., $N_f = 1$.

3.1.2 Laplace Transformation

For the dimensionless time dependent functions in Eq. 3.2 and Eq. 3.4, the Laplace transformation can be computed by applying the methodology in Appendix C. Using this approach, we generated a tabulated Laplace transform function that provided a very efficient algorithm. However, the numerical methods in Appendix C were not applicable in other kinds of complex geometry reservoirs, such as the tee-shape reservoir, channel splay reservoirs and complex bounded reservoirs. We therefore had to resort to other numerical methods. Our experience with the numerical transform methods of References [10] and [11] is that they do not provide sufficient accuracy for determining flux and pressure derivatives in complex systems. A general fast and sufficiently accurate method of taking numerical Laplace transforms of general source/sink solutions is provided in Appendix A.

3.2 Model Validity and Results

3.2.1 Limiting cases

The limiting model cases we derived were not only vital for us to verify the proposed model but also essential for our better understanding of the behavior of complex geometry reservoirs. We validated the "leaky fault" model by checking it against the following limiting cases.

- The model must approach the behavior of a well in a semi-infinite system if the diffusivity in Region 2 approaches zero .

- At early time, the model must approach the behavior of a well in a semi-infinite system if the width of the gap (L_w in Fig. 1.1) approaches zero.

- The model must approach the behavior of a well in an infinite system if the diffusivities are the same on both sides of the gap, and the width of the gap

becomes very large.

The late-time asymptotic behavior of the pressure derivative solution is derived in Appendix D. At very large times when all of the dimensionless pressure drop terms in Regions 1 and 2 are given by semilog approximations, and when the rate of fluid flow through the gap becomes approximately constant, the stabilized rate of flow through the gap in RB/D per RB/D of production from the actual well is

$$Q_{fD} \rightarrow \frac{2C_T}{1+C_T}. \tag{3.15}$$

For $C_T = 1$, note that $Q_{fD} \rightarrow 1$. This may seem surprising since the fracture injection rate approaches the active well production rate. Recall however that in our model (see Fig. 2.1) half of the "fracture well" injection fluid flows into the physical Region 1, while the other half flows into the image of Region 1; thus at late times, the volume of fluid entering Region 1 through the "gap" approaches half the production rate from the active well. This result is intuitively and physically reasonable.

At late time, the pressure derivative in is approximately given by

$$\frac{dp_{D,1}}{d(\ln t_{D,1})} \rightarrow \frac{1}{1+C_T}. \tag{3.16}$$

Note that for a system with a vanishingly small gap width, the initial pressure derivative behavior will approximate that of a semi-infinite system, while at late time the derivative will approach the value given by Eq. 3.16.

Fig. 3.1 shows a plot of dimensionless pressure and pressure derivative for the limiting cases used to check the modeling results; i.e., for a well in an infinite homogeneous system where the pressure derivative is always flat, and for a well in a semi-infinite system, where there is a doubling in the value of pressure derivative after the effect of the fault is felt. In this case, the distance from the well to the sealing fault is chosen to be the characteristic length.

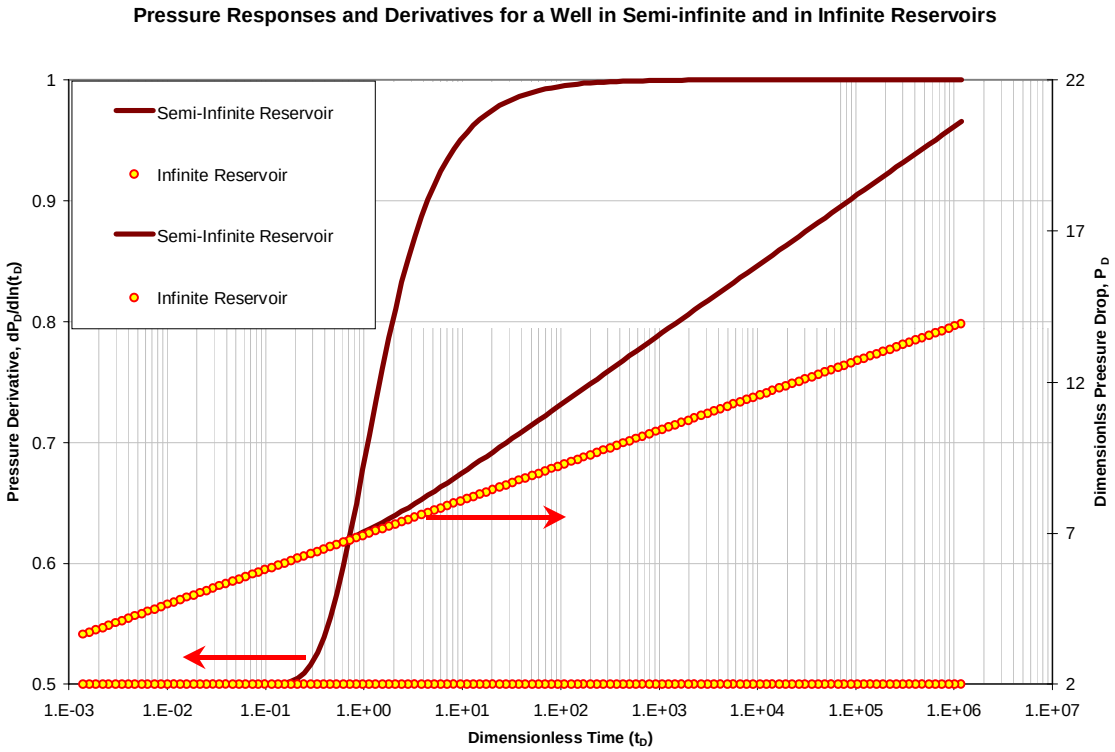

Figure 3.1: Limiting cases used to check modeling results

3.2.2 Effect of the number of "fracture" segments

Fig. 3.2 shows the difference of applying uniform and non-uniform flux assumptions in modeling communication between two semi-infinite reservoirs. The well is located right below the center of the leaky fault and $L_{wD} = 4$; this means the width of the leaky fault is 4 times the distance from the well to the boundary. Since $C_R = 1$ (because $C_T = 1$, $C_S = 1$, i.e., both regions have the same diffusivity), the dimensionless pressure derivative physically can not attain a value less than 0.5 in this case. That is, it is physically impossible for the system to behave as if it has a permeability greater than the permeability of each region. In this case, although the dimensionless pressure drops given by the uniform and non-uniform flux models (100 "fracture" segments) are virtually identical, the pressure derivative from the uniform flux model is physically unreasonable.

In Fig. 3.3 we examine the effect of the number of "fracture" segments, N_f, on the model results. We see that for $N_f > 50$, the computational results are virtually identical. Note that Fig. 3.3 also gives us a clear indication that at very late time, $t_D > 10^{13}$, the dimensionless pressure derivative is approaching 0.5 smoothly and is always slightly larger than 0.5. This is also an indication of accurate and correct modeling.

Generally speaking, the larger the N_f value, the more accurate the results will be, but larger fracture segments will also increase the computational time rapidly. However, it is hard to determine the minimum N_f value since it depends on the boundary conditions, well and leaky fault locations and the property contrast and varies from case to case. In order to compare the results in a consistent and accurate way, a relatively higher N_f value was selected. Unless otherwise stated, we used a value of $N_f = 100$ for our runs.

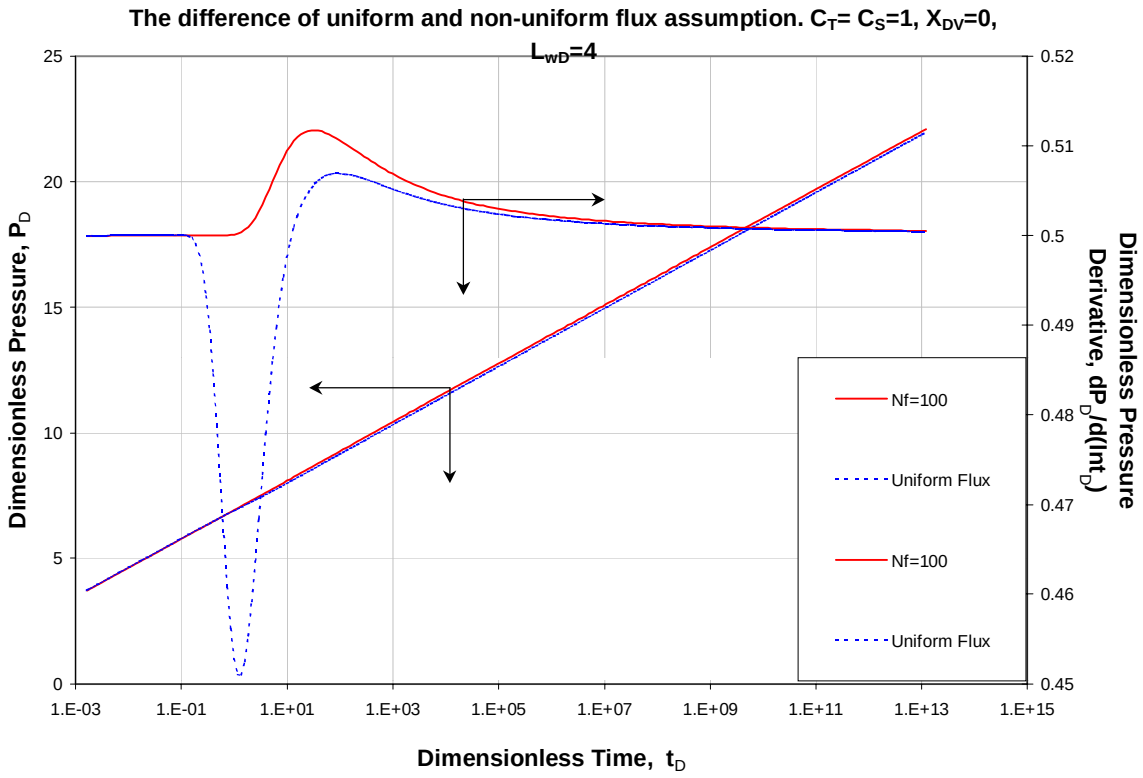

Figure 3.2: Comparison of uniform-flux and non-uniform flux pressure responses

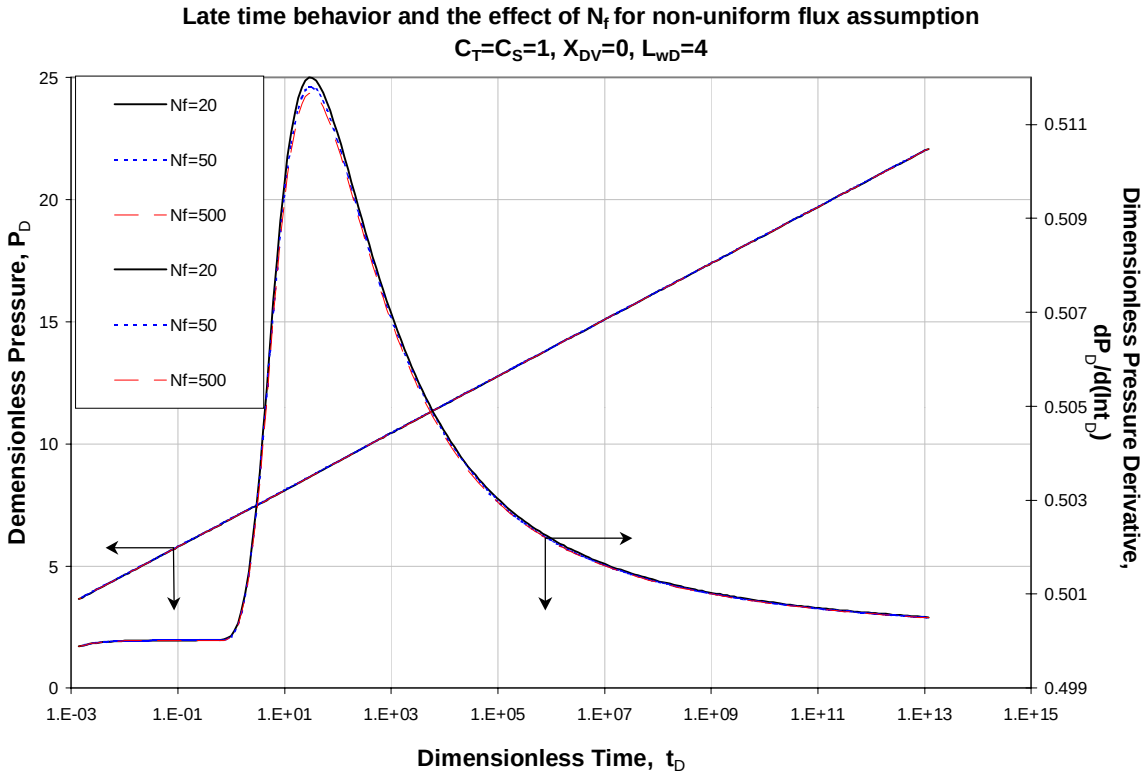

Figure 3.3: The effect of the number of fracture segments on the model results

3.2.3 Effects of variation of dimensionless model parameters

In Fig. 3.4, the producing well is aligned horizontally with the center of the gap, i.e., $X_{DV} = \dfrac{X_V}{L_d} = 0.-$ see Fig. 1.1. Fig. 3.4 shows pressure and pressure derivative responses for a system where the diffusivities on both sides of the leaky fault are the same, i.e. $C_R = 1$ and $C_T = 1$, $C_S = 1$, but the dimensionless width of the gap is varied; the notation LWD in the legend corresponds to values of the dimensionless gap length L_{wD} defined in Eq. 2.3. For large values of the dimensionless gap width ($L_{wD} = 8$ in Fig. 3.4), the model approaches the behavior of a well in an infinite system; that is, the derivative remains approximately flat with a dimensionless value of 0.5. For small values of dimensionless gap width, the pressure derivatives approach the behavior of a semi-infinite system, but as time increases, they deviate from semi-infinite behavior and gradually approach the long-time asymptotic value of 0.5.

Fig. 3.5 shows the effect of varying the ratio of transmissibilities, $\left(\dfrac{kh}{\mu}\right)$, in the two regions; i.e., the value of the dimensionless ratio C_T, see Eq. 2.8. When the value of C_T is very small, (i.e., the transmissibility of Region 2 is small), the system approaches the behavior of a semi-infinite reservoir. (Note that this is also predicted by the asymptotic behavior of Eq. 3.16.) Note that for a value of $C_T = 0.01$, Eq. 3.16 predicts that the dimensionless pressure derivative should approach a value of $\frac{1}{1.01} = 0.99$; the results of Fig. 3.5 agree almost perfectly with this prediction. As the value of C_T is increased to a value greater than 1, the pressure derivative approaches values less than 0.5. Physically, this is because fluid can flow easily from Region 2 to Region 1, and the overall transmissibility of the system appears bigger than the transmissibility of Region 1 itself - i.e., the late-time pressure derivative falls below the homogeneous reservoir value of 0.5. As shown in the figure, the pressure and pressure derivative curves will approach the constant pressure boundary case when the C_T value becomes larger.

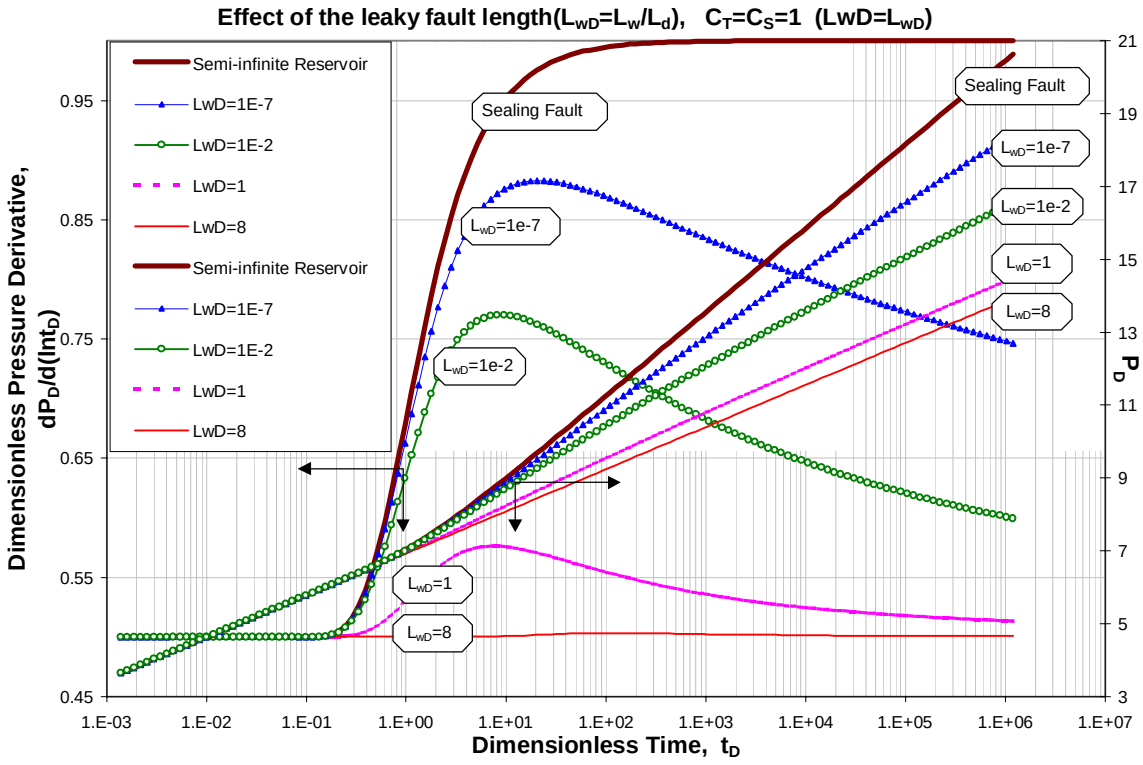

Figure 3.4: Effect of reducing the width of the leaky fault, $C_T = 1$, $C_S = 1$

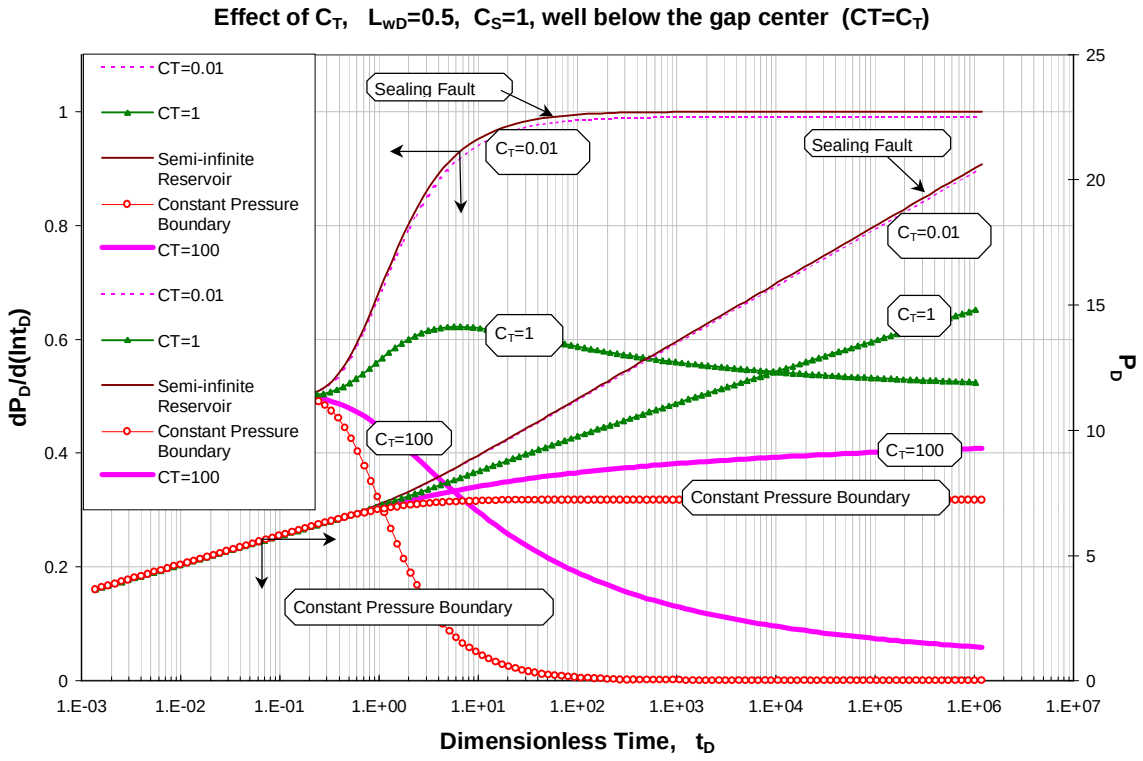

Figure 3.5: The effect of transmissibility ratio, C_T

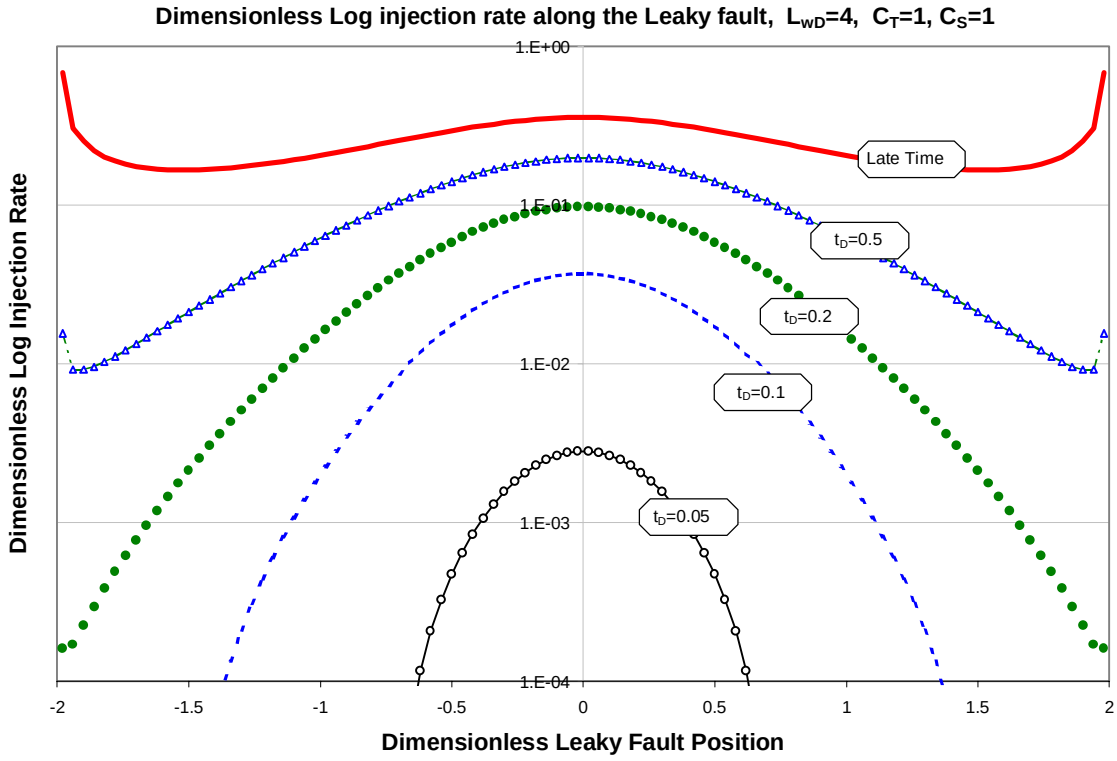

Figure 3.6: Dimensionless log injection rate along the leaky fault (early time behavior)

Since displaying all of the flux distribution plots is impossible, some of the typical flux distributions are selected and shown here. Fig. 3.6 and Fig. 3.7 show the injection rate from Region 2 for a well whose x-location coincides with the center of the gap. Note that the logarithm of the injection rate is plotted on the ordinate in Fig. 3.6. At very early time, fluid flow is at a maximum at the center of the gap where pressure drop is the greatest. As time proceeds, fluid flows across an increasing portion of the gap, and the flux at the tips of the gap increases as more fluid flows from beyond the gap tips in Region 2. Note that since the well was aligned with the center of the gap, ($X_{DV} = 0$), the injection rate (or flux) profiles at all times are symmetric about the gap center.

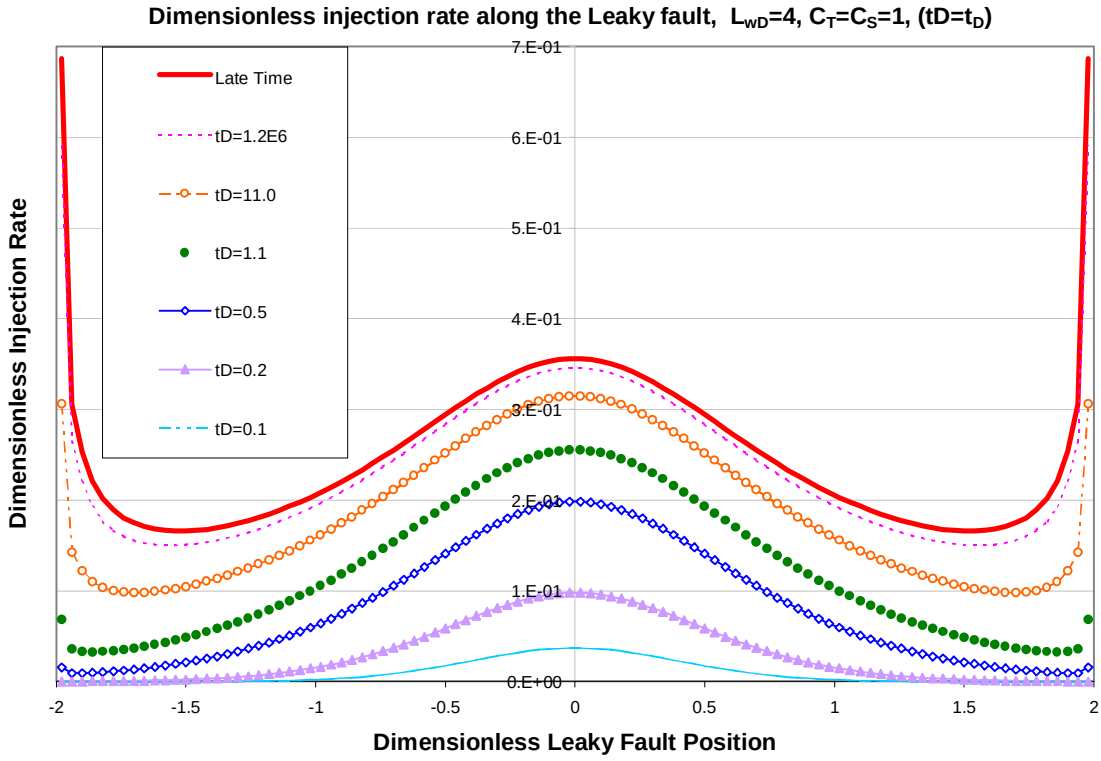

Figure 3.7: Dimensionless injection rate along the leaky fault (late time behavior)

Fig. 3.8 displays the effect of the relative position of the active well and the gap; i.e., X_{DV} refers to Fig. 1.1, where, $X_{DV} = \frac{X_V}{L_d}$. The farther the active well is displaced from the gap center, the more dominant is the effect of the sealing-fault boundary. However, at late time all of the derivative curves approach the derivative value given by Eq. 3.16. In Fig. 3.8, the lowest curve corresponds to the production well being aligned with the gap center. Curves displaying a successively increasing derivative hump correspond to increasing displacement of the producing well from the gap center. Physically, the system initially behaves like a semi-infinite system to wells displaced horizontally from the gap center. When fluid flows from Region 2, the pressure in Region 1 is maintained at a higher level than in the semi-infinite system, and the rate of pressure decline (or equivalently, the pressure derivative) decreases.

Fig. 3.9 shows the flux distribution across the gap when the producing well is horizontally displaced beyond the right end of the gap (i.e., $X_{DV} > 0.5$, see inset in Fig. 3.9). The flux distribution is skewed to the right since the pressure drop due to the well's production is largest at the gap's right end. These curves also shows how the transmissibility, C_T, affects the fluid injection. Generally speaking, higher C_T will make the fluid flow easier and quicker towards the place where the pressure drop is larger. Therefore, the higher the C_T value, the more slanted is the injection rate distribution.

Fig. 3.10 highlights the effect of dimensionless transmissibility C_T. Note that all pressure derivatives approach the value given by Eq. 3.16 at late time. However, at intermediate times, the shapes of the pressure derivative curves vary over a large extent and are affected by the values of L_{wD}, X_{DV} and C_S. The curves plotted in this figure are used to give us a visual indication that the late-time behavior of the various systems approaches the predicted asymptotic values; for this reason, no legend is included.

Figure 3.11 shows the "fracture well" injection rate (or twice the total rate flowing through the gap) as a function of time. At late time, these rates approach

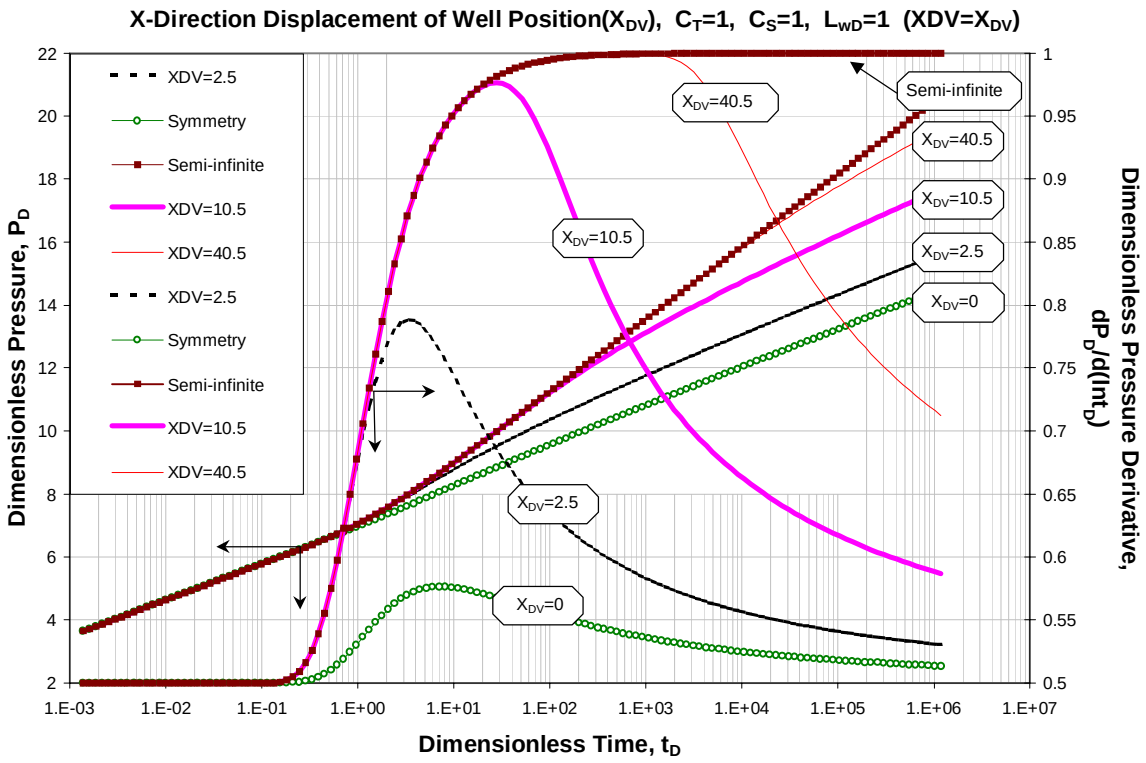

Figure 3.8: The effect of x-direction displacement of well from the center of the leaky fault

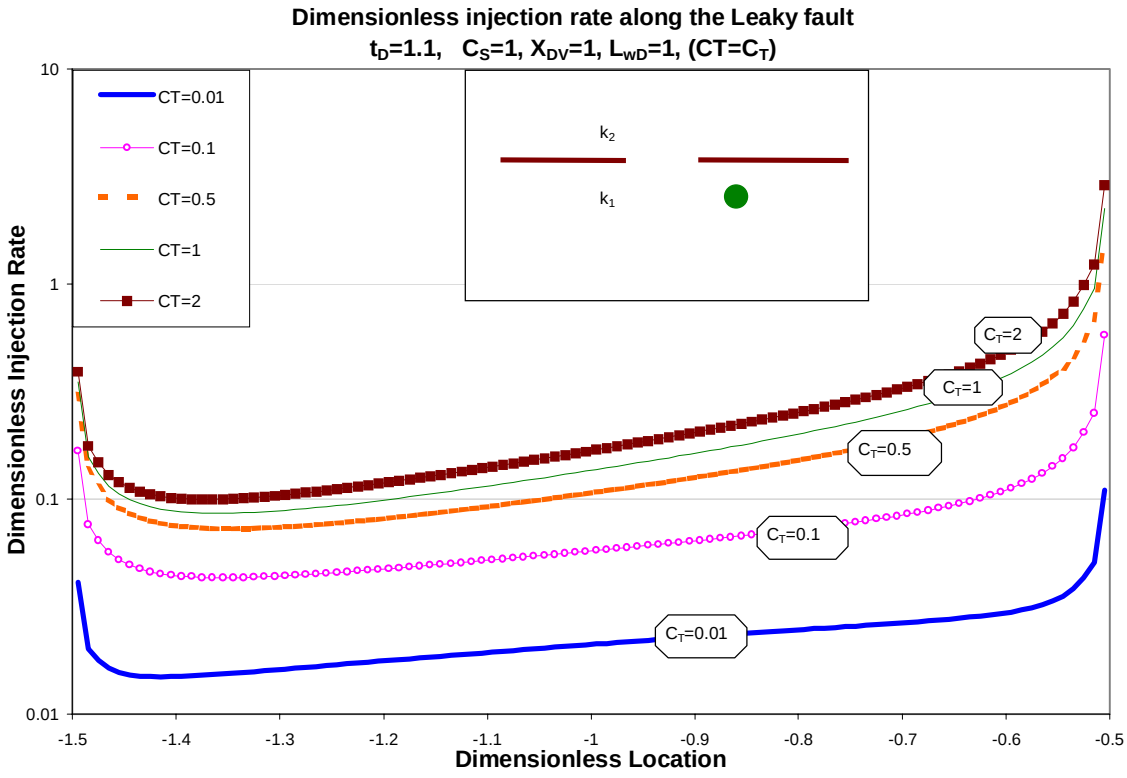

Figure 3.9: Dimensionless injection rate profile for a well displaced from the leaky fault center

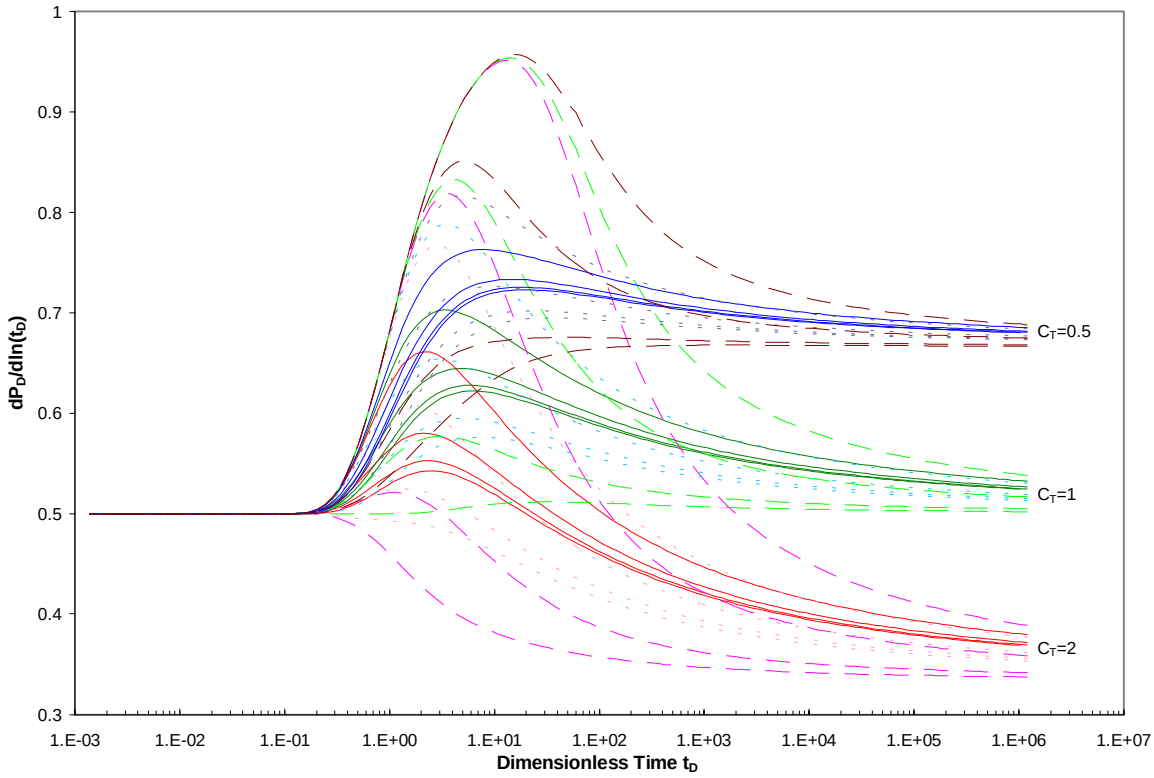

Figure 3.10: Effect of C_T and X_{DV}

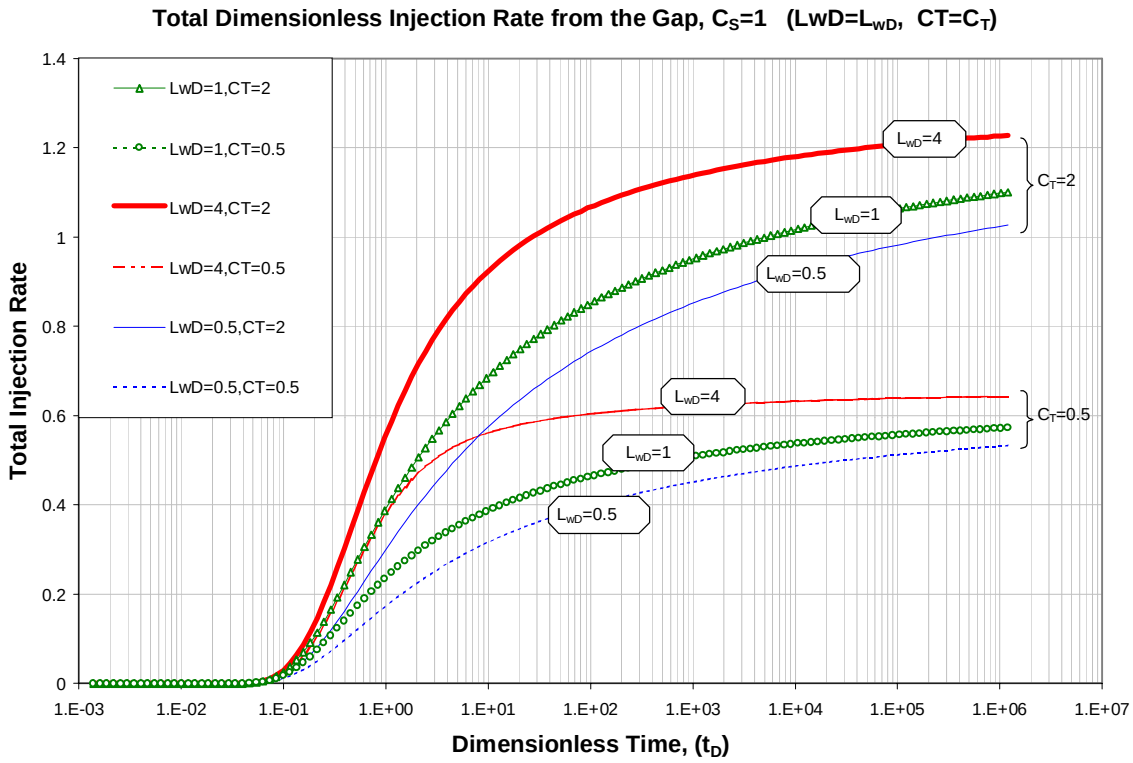

Figure 3.11: Asymptotic rate of fluid flow through the leaky fault

the values given by Eq. 3.16.

The influence of the porosity is shown in Fig. 3.12. Higher C_S and L_{wD} values prevent the pressure derivative curves from increasing. Physically, higher values of C_S and/or L_{wD} expose the producing part of the reservoir to more fluid support from Region 2. This has the effect of maintaining the pressure in Region 1 and causes the pressure derivative to be smaller than in the $C_S = 1$, $L_{wD} = 1$ case. Note that the effects of C_S and/or L_{wD} are very small; refer to the scales in Fig. 3.12. Pressure and pressure derivatives are much more sensitive to contrasts in transmissibility (i.e., C_T) than contrasts in storativity, C_S.

Our results indicate that reasonable prediction of pressure transient behavior

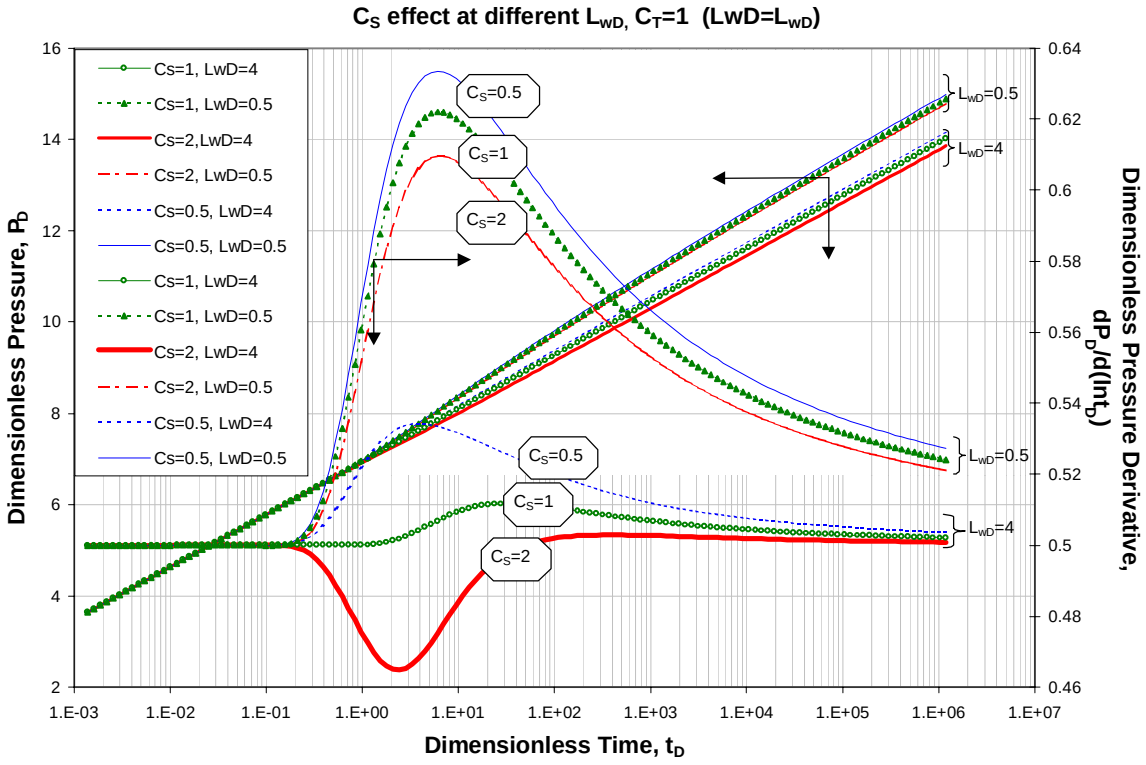

Figure 3.12: The effect of the porosity(or, Cs) at different leaky fault length(or, L_{wD})

in complex-geometry reservoirs may be obtained using our modeling approach. In the following sections, we apply our methodology to more complex geometry reservoirs.

CHAPTER IV

TEE-SHAPED CHANNEL RESERVOIRS

4.1 Mathematical Derivation

4.1.1 Formulas in Region 1 and Region2

As in the previous chapter, the complex model is solved by decomposing it into two simpler homogeneous models that are coupled at their plane of contact; see Fig. 4.1. A tee-shaped channel reservoir can be viewed as two channel components. One with the properties of the vertical channel, referred to as Region 1 and the other with the properties of the horizontal channel is called Region 2. To model the boundary conditions in Region 1, a mirror image is placed $2L_d$ away from the producer along the channel and an injection plane is placed right on the"no-flow boundary" to account for the fluid injection from Region 2. The fluid flow in Region 2 can be taken into account by placing a producing fracture plane along the center of the infinite channel, which has a width of $2L_{y2}$. Note, in both Region 1 and Region 2 the fracture plane is fully-penetrating and has a width of L_x.

Solutions to each of the simpler problems are written in Laplace space and solved for the unknown fluid transfer between the systems. The resulting flux distributions are then used to obtain the desired pressure behavior.

The fracture plane is defined in the same way as in Fig. 2.4. The actual well in Region 1 still produces at a rate of 1 RB/D. We apply Eq. B.10 and Eq. B.13 to compute the dimensionless pressure drop at any location in Region 1; see Fig. 4.1. The pressure drop, $\overline{p}_{D,k_1}$, in the Laplace domain at any dimensionless location (x_{D,k_1}, y_{D,k_1}) can be written in terms of source/sink solutions as

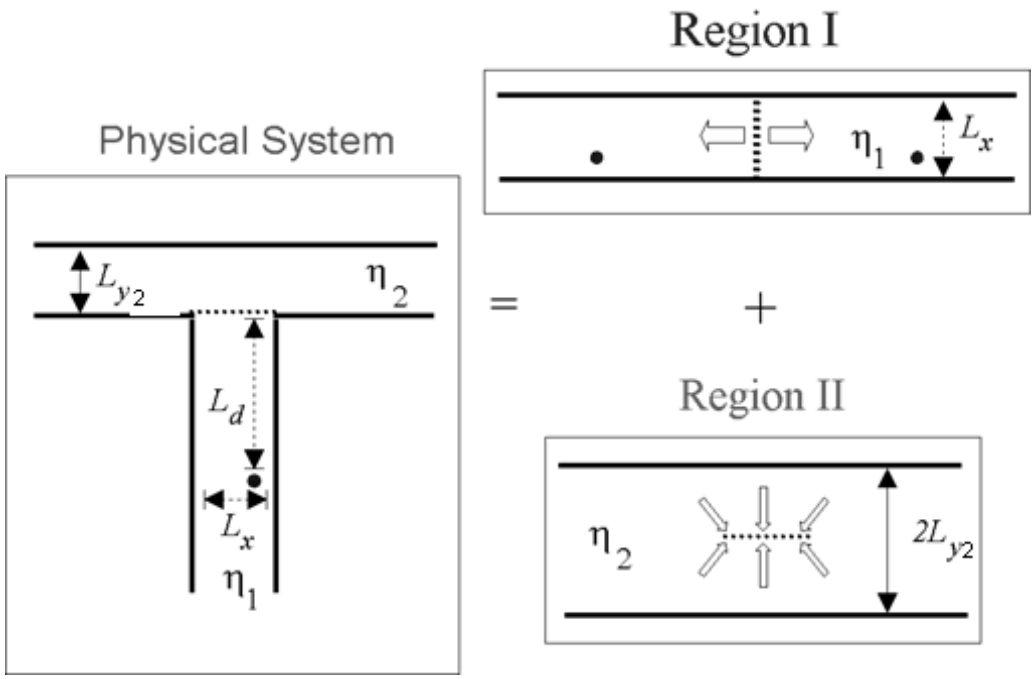

Figure 4.1: Schematic of decoupled tee-shaped reservoir

$$\begin{aligned}\overline{p}_{D,k_1}(x_D,y_D,u_D) &= \overline{p}_{D,wv,k_1}(x_D,y_D,u_D)+\overline{p}_{D,w'v,k_1}(x_D,y_D,u_D)- \\ &\qquad \sum_{j=1}^{N_f}\overline{p}_{D,hv,j,k_1}(x_D,y_D,u_D) \\ &= \overline{q}_{0D}(u_D)\,\overline{f}_{wv,k_1}(x_D,y_D,L_{xD},x'_D,y'_D,u_D)+ \\ &\overline{q}_{0D}(u_D)\,\overline{f}_{w'v,k_1}(x_D,y_D,L_{xD},x'_D,-y'_D,u_D)- \\ &\sum_{j=1}^{N_f}\overline{q}_{fD,j}(u_D)\,\overline{f}_{hv,j,k_1}(x_D,y_D,L_{xD},x_{D,j-1},x_{D,j},y_{fD,k_1},u_D) \quad (4.1)\end{aligned}$$

where the producer is located at (x'_{D,k_1}, y'_{D,k_1}) and the image well is located at $(x'_{D,k_1}, -y'_{D,k_1})$.The three terms on the right side of Eq. 4.1 account for the dimensionless pressure drop caused by a well, its image well, and non-uniform injection from the fracture plane respectively in a vertical channel, respectively; see Fig. 4.1.

u_D is the dimensionless Laplace variable for Region 1; that is, if u is the Laplace variable associated with the transform of time (in units day^{-1}), u_D is defined as

$$u_D = \frac{L_{xD}^2 u}{\eta_1}. \tag{4.2}$$

Note that the above definition is employed only when the producer is located in the vertical channel. $\overline{q}_{fD,j}$ denotes the Laplace transform of the (unknown) flux at the center of fracture segment $(x_{fD,j}, y_{fD,k_1})$. Finally, $\overline{f}_{wv,k_1}$ and $\overline{f}_{w'v,k_1}$ denote the Laplace transforms of the dimensionless source/sink functions for the well and its image well in the vertical channel. $\overline{f}_{hv,j,k_1}$ represents the Laplace transform of the dimensionless source/sink function for a "uniform-flux" line sink. The nomenclature for the source/sink functions employed here corresponds to that employed in Appendix B. That is,

$$f_{wv,k_1}(x_D, y_D, L_{xD}, x_D', y_D', t_D) = \frac{\pi}{2L_{xD}}\left[\theta_3\left(\frac{x_D - x_D'}{2L_{xD}}, \frac{t_D}{L_{xD}^2}\right) + \theta_3\left(\frac{x_D + x_D'}{2L_{xD}}, \frac{t_D}{L_{xD}^2}\right)\right]\theta_L\left(\frac{y_D - y_D'}{2}, t_D\right), \tag{4.3}$$

$$f_{w'v,k_1}(x_D, y_D, L_{xD}, x_D', -y_D', t_D) = \frac{\pi}{2L_{xD}}\left[\theta_3\left(\frac{x_D - x_D'}{2L_{xD}}, \frac{t_D}{L_{xD}^2}\right) + \theta_3\left(\frac{x_D + x_D'}{2L_{xD}}, \frac{t_D}{L_{xD}^2}\right)\right]\theta_L\left(\frac{y_D + y_D'}{2}, t_D\right), \tag{4.4}$$

and

$$f_{hv,j,k_1}(x_D, y_D, L_{xD}, x_{D,j-1}, x_{D,j}, y_{fD,k_1} t_D) = \pi\left[\widehat{\Theta}_3\left(\frac{x_{D,j-1} - x_D}{2L_{xD}}, \frac{x_{D,j} - x_D}{2L_{xD}}, \frac{t_D}{L_{xD}^2}\right) + \widehat{\Theta}_3\left(\frac{x_{D,j-1} + x_D}{2L_{xD}}, \frac{x_{D,j} + x_D}{2L_{xD}}, \frac{t_D}{L_{xD}^2}\right)\right] \times \theta_L\left(\frac{y_D - y_{fD,k_1}}{2}, t_D\right). \tag{4.5}$$

Methods for computing these terms and their Laplace transforms are discussed in detail in Appendix A.

The dimensionless pressure drop solution to the Region 2 problem is written as

$$\overline{p}_{D,k_2}\left(x_{D,k_2}, y_{D,k_2}, u_D\right) = \sum_{j=1}^{N_f} \overline{q}_{fD,j}\left(u_D\right) \overline{f}_{hh,j,k_2}\left(x_D, y_D, 2L_{yD}, x_{D,j-1}, x_{D,j}, y_{fD,k_2}, u_D\right), \tag{4.6}$$

where, $\overline{f}_{hh,j,k_2}$ represents the Laplace transform of the dimensionless source/sink function for a "uniform-flux" line sink in Region 2 . Following the notation in Appendix B, the inverse Laplace transform of $\overline{f}_{hh,j,k_2}$ is given by

$$f_{hh,j,k_2}\left(x_D, y_D, L_{yD}, x_{D,j-1}, x_{D,j}, y_{fD,k_2}, t_D\right) = \frac{\pi}{C_S L_{yD}} \widehat{\Theta}_L\left(\frac{x_{D,j-1}-x_D}{2}, \frac{x_{D,j}-x_D}{2}, C_R t_D\right) \times \left[\theta_3\left(\frac{y_D - y_{fD,k_2}}{2L_{yD}}, \frac{C_R t_D}{L_{yD}^2}\right) + \theta_3\left(\frac{y_D + y_{fD,k_2}}{2L_{yD}}, \frac{C_R t_D}{L_{yD}^2}\right)\right]. \tag{4.7}$$

The coordinate systems in each region are chosen to make $x_{D,j}$ and $x_{D,j-1}$have the same value in both Region 1 and Region 2. Note that $y_{fD,k_1} = 0$ and $y_{fD,k_2} = L_{yD}$.

4.1.2 Method Formulation and computational details

The same methodology as we had derived in the leaky fault problem was applied to generate the formulas for tee-shaped reservoirs. In Region 1, by applying Eq. 4.1, the pressure drop at the midpoint, $\left(x_{fD,i}, y_{fD,k_1}\right)$, of the ith fracture segment can be expressed as

$$\overline{p}_{D,k_1}\left(x_{fD,i},y_{fD,k_1},u_D\right)=\overline{p}_{D,wv,k_1}\left(x_{fD,i},y_{fD,k_1},u_D\right)+$$
$$\overline{p}_{D,w'v,k_1}\left(x_{fD,i},y_{fD,k_1},u_D\right)-$$
$$\sum_{j=1}^{N_f}\overline{p}_{D,hv,j,k_1}\left(x_{fD,i},y_{fD,k_1},u_D\right)$$
$$=\overline{q}_{0D}\left(u_D\right)\overline{f}_{wv,k_1}\left(x_{fD,i},y_{fD,k_1},L_{xD},x'_D,y'_D,u_D\right)+$$
$$\overline{q}_{0D}\left(u_D\right)\overline{f}_{w'v,k_1}\left(x_{fD,i},y_{fD,k_1},L_{xD},x'_D,-y'_D,u_D\right)-$$
$$\sum_{j=1}^{N_f}\overline{q}_{fD,j}\left(u_D\right)\overline{f}_{hv,j,k_1}\left(x_{fD,i},y_{fD,k_1},L_{xD},x_{D,j-1},x_{D,j},y_{fD,k_1},u_D\right),$$
$$\text{for}\quad 1\leq i\leq N_f. \quad (4.8)$$

The dimensionless pressure drop at each midpoint, $\left(x_{fD,j},y_{fD,k_2}\right)$, of the ith fracture segment in Region 2 is

$$\overline{p}_{D,k_2}\left(x_{fD,i},y_{fD,k_2},u_D\right)=$$
$$\sum_{j=1}^{N_f}\overline{q}_{fD,j}\left(u_D\right)\overline{f}_{hh,j,k_2}\left(x_{fD,i},y_{fD,k_2},L_{yD},x_{D,j-1},x_{D,j},y_{fD,k_2},u_D\right),$$
$$\text{for}\quad 1\leq i\leq N_f. \quad (4.9)$$

We introduce the following simplifying notation. Let,

$$\Psi\left(x_{fD,i},y_{fD,k_1},u_D\right)=\frac{\overline{f}_{wv,k_1}\left(x_{fD,i},y_{fD,k_1},L_{xD},x'_D,y'_D,u_D\right)}{u_D}+$$
$$\frac{\overline{f}_{w'v,k_1}\left(x_{fD,i},y_{fD,k_1},L_{xD},x'_D,-y'_D,u_D\right)}{u_D},$$
$$\text{for}\quad 1\leq i\leq N_f. \quad (4.10)$$

Equating the right hand sides of Eq. 4.8 and Eq. 4.9, we have

$$\sum_{j=1}^{N_f} \overline{q}_{fD,j} \left[\overline{f}_{hv,j,k_1} \left(x_{fD,i}, y_{fD,k_1}, L_{xD}, x_{D,j-1}, x_{D,j}, y_{fD,k_1}, u_D \right) + \right.$$

$$\left. \overline{f}_{hh,j,k_2} \left(x_{fD,i}, y_{fD,k_2}, 2L_{yD}, x_{D,j-1}, x_{D,j}, y_{fD,k_2}, u_D \right) \right]$$

$$= \Psi \left(x_{fD,i}, y_{fD,k_1}, u_D \right), \text{ for } \quad 1 \leq i \leq N_f. \quad (4.11)$$

Considering the equal-length discretization of the planar fracture we can derive the following expressions directly.

$$x_{D,j} - x_{fD,i} = 2jL_{fD} - (2iL_{fD} - L_{fD}) = \left[2\left(j - i\right) + 1 \right] L_{fD}, \quad (4.12)$$

$$x_{D,j-1} - x_{fD,i} = 2(j-1)L_{fD} - (2iL_{fD} - L_{fD}) = \left[2\left(j - i\right) - 1 \right] L_{fD}, \quad (4.13)$$

$$x_{D,j} + x_{fD,i} = 2jL_{fD} + (2iL_{fD} - L_{fD}) = \left[2\left(j + i\right) - 1 \right] L_{fD}, \quad (4.14)$$

$$x_{D,j-1} + x_{fD,i} = 2(j-1)L_{fD} + (2iL_{fD} - L_{fD}) = \left[2\left(j + i\right) - 3 \right] L_{fD}. \quad (4.15)$$

Applying Eqs. 4.12 through 4.15 to Eq. 4.3, Eq. 4.4, Eq. 4.5 and Eq. 4.7, and simplifying, we can write Eq. 4.11 as

$$\begin{bmatrix} \overline{a}_{11}+\overline{b}_{11} & \overline{a}_{12}+\overline{b}_{12} & ... & \overline{a}_{1j}+\overline{b}_{1j} & ... & \overline{a}_{1N_f}+\overline{b}_{1N_f} \\ \overline{a}_{21}+\overline{b}_{21} & \overline{a}_{22}+\overline{b}_{22} & ... & \overline{a}_{2j}+\overline{b}_{2j} & ... & \overline{a}_{2N_f}+\overline{b}_{2N_f} \\ ... & ... & ... & ... & ... & ... \\ \overline{a}_{i1}+\overline{b}_{i1} & \overline{a}_{i2}+\overline{b}_{i2} & ... & \overline{a}_{ij}+\overline{b}_{ij} & ... & \overline{a}_{iN_f}+\overline{b}_{iN_f} \\ ... & ... & ... & ... & ... & ... \\ \overline{a}_{N_f1}+\overline{b}_{N_f1} & \overline{a}_{N_f2}+\overline{b}_{N_f2} & ... & \overline{a}_{N_fj}+\overline{b}_{N_fj} & ... & \overline{a}_{N_fN_f}+\overline{b}_{N_fN_f} \end{bmatrix} \begin{bmatrix} \overline{q}_{fD,1}(u_D) \\ \overline{q}_{fD,2}(u_D) \\ ... \\ \overline{q}_{fD,i}(u_D) \\ ... \\ \overline{q}_{fD,N_f}(u_D) \end{bmatrix}$$

$$= \begin{bmatrix} \Psi(x_{fD,1}, y_{fD,k_1}, u_D) \\ \Psi(x_{fD,2}, y_{fD,k_1}, u_D) \\ ... \\ \Psi(x_{fD,i}, y_{fD,k_1}, u_D) \\ ... \\ \Psi(x_{fD,N_f}, y_{fD,k_1}, u_D) \end{bmatrix}. \quad (4.16)$$

Here, $\overline{a}_{ij}$ and $\overline{b}_{ij}$ are the Laplace transforms of the following a_{ij} and b_{ij},

$$a_{ij} = \pi \left[\widehat{\Theta}_3 \left(\frac{[2(j-i)-1] L_{fD}}{2L_{xD}}, \frac{[2(j-i)+1] L_{fD}}{2L_{xD}}, \frac{t_D}{4L_{xD}^2} \right) + \frac{1}{C_S} \widehat{\Theta}_L \left(\frac{[2(j-i)-1] L_{fD}}{2}, \frac{[2(j-i)+1] L_{fD}}{2}, C_R t_D \right) \right] \times \left(\theta_3 \left(0, \frac{C_R t_D}{4L_{yD}^2} \right) + \theta_3 \left(\frac{1}{2}, \frac{C_R t_D}{4L_{yD}^2} \right) \right), \quad (4.17)$$

and

$$b_{ij} = \pi \widehat{\Theta}_3 \left(\frac{[2(j+i)-3] L_{fD}}{2L_{xD}}, \frac{[2(j+i)-1] L_{fD}}{2L_{xD}}, \frac{t_D}{4L_{xD}^2} \right) \theta_L(0, t_D). \quad (4.18)$$

Denote the above matrix as $A+B$, where the matrix A has elements $\overline{a}_{ij}$ and the matrix B has elements $\overline{b}_{ij}$. It is clear that the matrix A and matrix B have the following properties.

1. $\overline{a}_{i,j} = \overline{a}_{j,i}$, i.e., A is a symmetric matrix.
2. $\overline{a}_{ij} = \overline{a}_{i+1,j+1}$.
3. $\overline{b}_{i,j} = \overline{b}_{j,i}$, i.e., B is a symmetric matrix.
4. $\overline{b}_{ij} = \overline{b}_{i-1,j+1}$.

Therefore for a N_f fracture plane discretization, the total number of independent matrix elements we need to compute is $3N_f - 1$.

4.2 Model Verification and Results

The following dimensionless variables are defined for tee-shaped reservoirs; (see Fig. 4.1 for dimensions). The dimensionless distances x_D, y_D and D_D are respectively defined as

$$x_D = \frac{x}{L_x}, \tag{4.19}$$

$$y_D = \frac{y}{L_x}, \tag{4.20}$$

and

$$D_D = \frac{L_d}{L_x}. \tag{4.21}$$

Here, x and y refer to coordinates in the $x-y$ plane. L_x is the width of the vertical channel and L_d is the distance from the producer to the gap, see Fig. 4.1. Note that $L_{xD} = 1$ and the dimensionless width of the upper branch of the tee, L_{y2D}, is defined as

$$L_{y2D} = \frac{L_{y2}}{L_x}. \tag{4.22}$$

Dimensionless time, t_D is defined in terms of Region 1 properties, i.e.,

$$t_D = \frac{\eta_1 t}{L_x^2}, \tag{4.23}$$

where the diffusivity η_1 is defined as before (see Eq. 2.6). As before, dimensionless pressure drop, p_D, is defined in terms of the properties in Region 1, i.e.,

$$p_D = \frac{k_1 h_1 \Delta p}{141.2 q B_1 \mu_1}. \tag{4.24}$$

4.2.1 Limiting cases

In Fig. 4.2 the pressure behavior of a well in an infinite channel, in a semi-infinite channel and in a combined channel and semi-infinite reservoir are shown as the three limiting cases to check the tee-shaped reservoir results. We validated the model's asymptotic behavior by checking it against the following limiting cases.

- The model must approach the behavior of a well in a semi-infinite channel if the diffusivity of the upper channel (η_2 in Fig. 4.1) approaches zero.

- The model must approach the behavior of a well in a semi-infinite channel if the width of the upper channel (L_{y2} in Fig. 4.1) approaches zero .

- The model must approach the behavior of another kind of complex reservoir, which is a combination of a channel and a semi-infinite reservoir, if the width of the upper channel (L_{y2} in Fig. 4.1) becomes very large.

- At early time, if the well is far enough away from the gap, the model must approach the behavior of a well in a channel.

The asymptotic behavior of the pressure derivative solution for tee-shaped reservoirs is presented in Appendix D. At very large times when flow in the vertical channel and horizontal channel become linear and parallel to the channel boundaries, and when the rate of fluid flow through the gap becomes approximately constant, the stabilized rate and the pressure derivative are approximately given by

$$Q_{fD} \rightarrow \frac{2}{1+\dfrac{1}{2L_{y2D}\sqrt{C_T C_S}}}, \tag{4.25}$$

and

$$\frac{dp_{D,1}}{d\left(\ln t_{D,1}\right)} \rightarrow \frac{2\sqrt{\pi t_D}}{1+2L_{y2D}\sqrt{C_T C_S}}, \tag{4.26}$$

respectively. Note that the width of the vertical channel is chosen as the characteristic length; thus we have $L_{xD} = \dfrac{L_x}{L_x} = 1$. As before, Q_{fD} is the stabilized rate of injection from the "vertically-fractured" well or twice the flow through the gap in RB/D per RB/D of production from the actual well.

At very early time a radial flow regime should be observed. Then, if the effect of the upper channel is not "felt", the pressure derivative will display typical channel reservoir behavior (i.e., 0.5 slope on a log-log plot); see Eq. D.10 in Appendix D; i.e.,

$$\frac{dp_{D,1}}{d(\ln t_{D,1})} \rightarrow \sqrt{\pi t_D}. \tag{4.27}$$

When the upper channel, (Region 2), is semi-infinite we get another limiting case for tee-shaped reservoirs, which is a combination of vertical channel and a semi-infinite reservoir. At late time when the fluid flow in the upper channel approaches the late time radial flow, we can show that

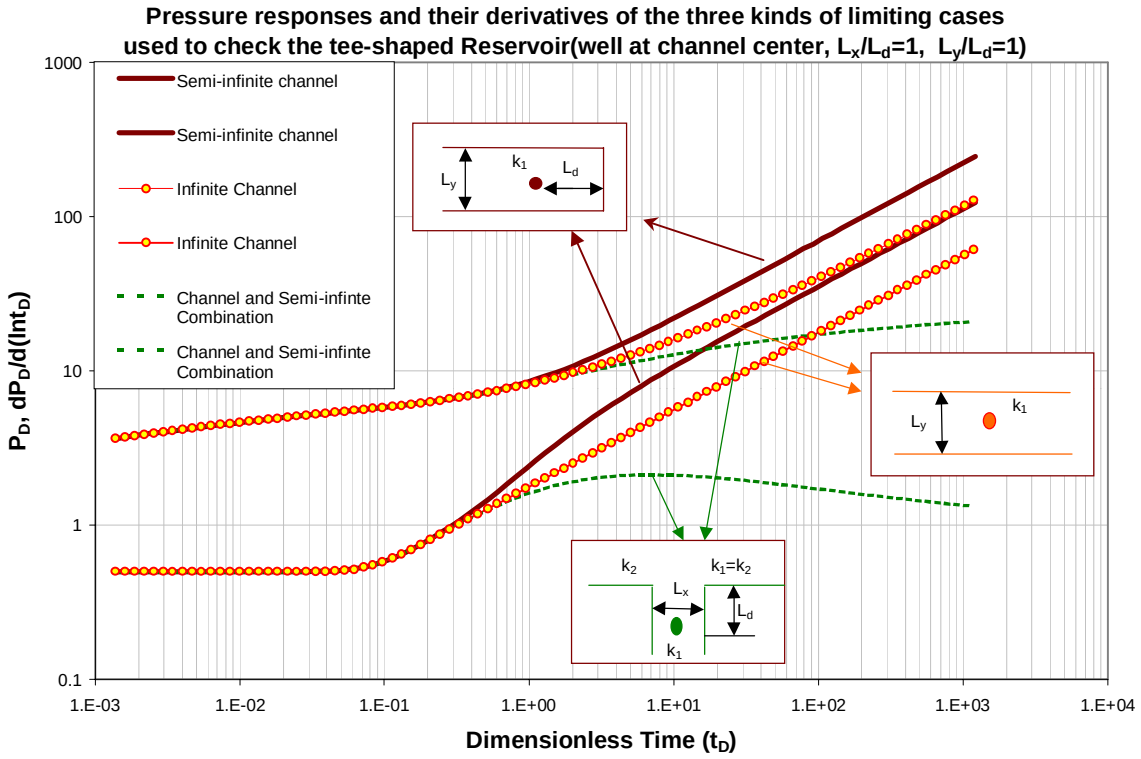

Figure 4.2: Limiting cases used to check tee-shaped reservoir results

$$\frac{dp_{D,1}}{d(\ln t_{D,1})} \rightarrow \frac{1}{C_T + \dfrac{1}{2\sqrt{\pi t_D}}}. \tag{4.28}$$

This equation tells us two facts; one is that, at very large times, the pressure derivative will be inversely proportional to C_T, and another is that the system will approach the semi-infinite channel case as the C_T value becomes very small. This case can be understood further by viewing Fig. 4.3.

The importance of considering non-uniform flux distribution is emphasized in the results of Fig. 4.4. As shown, the uniform flux assumption yields incorrect

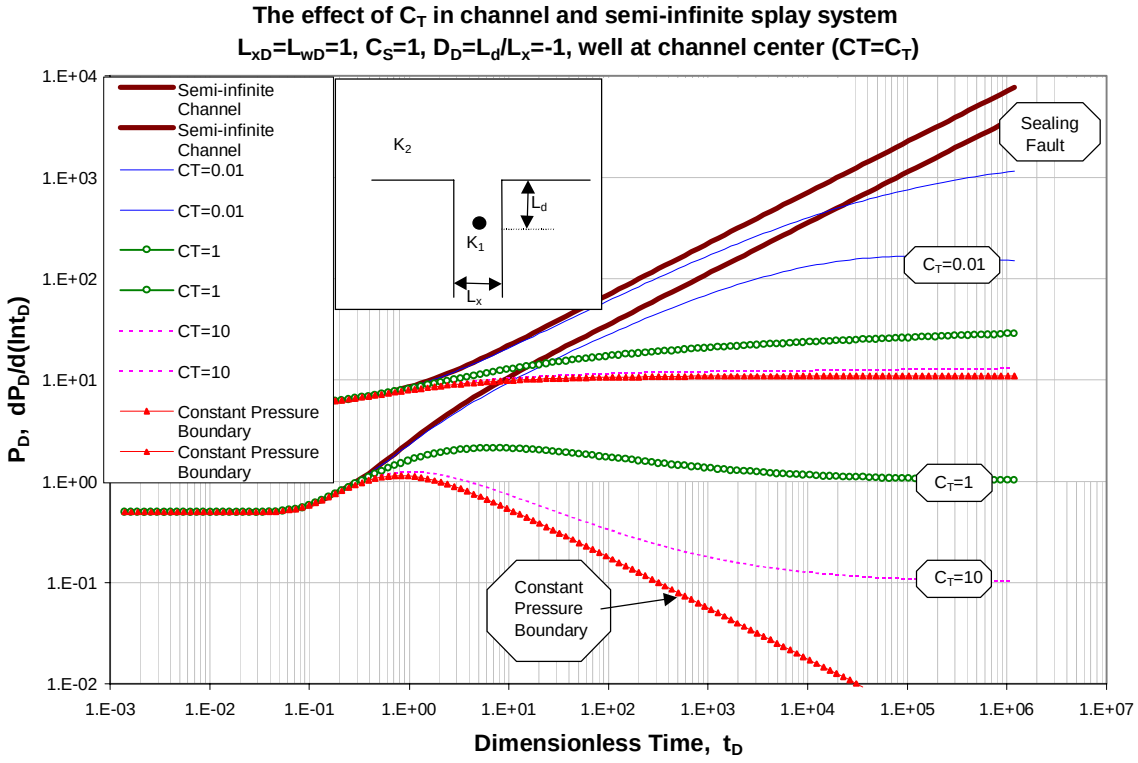

Figure 4.3: The effect of C_T for vertical channel and splay system

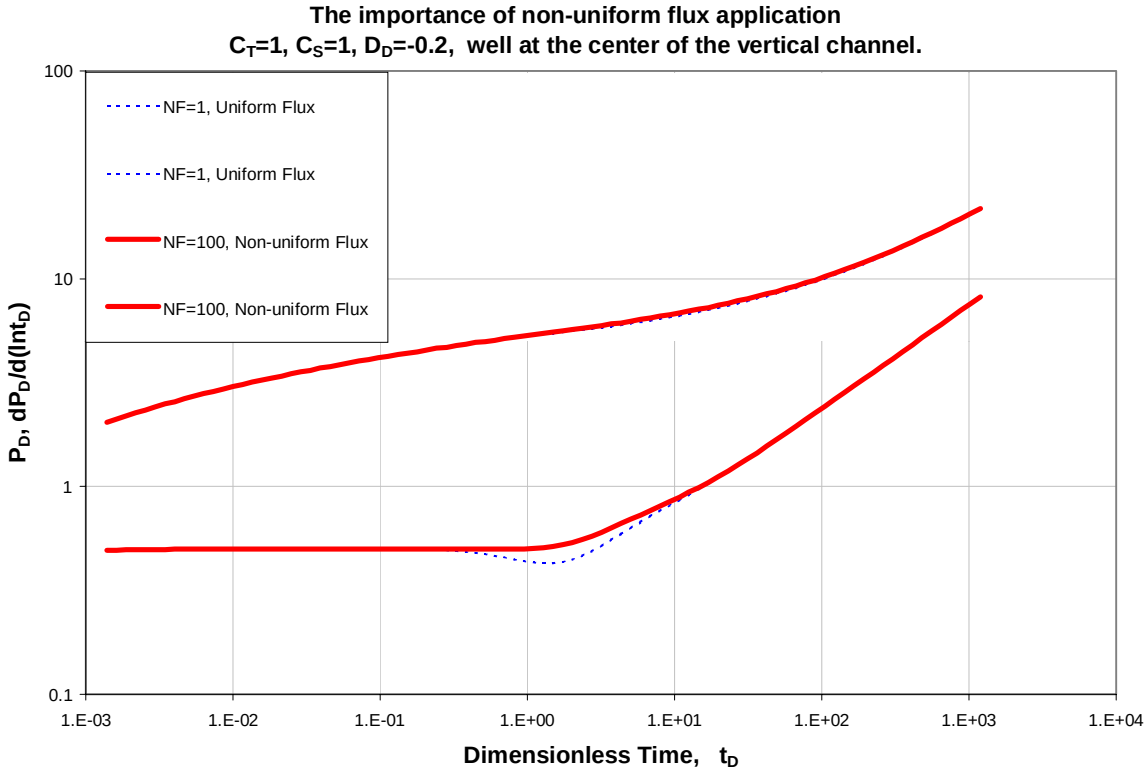

Figure 4.4: The difference between uniform and non-uniform flux distribution assumption

pressure derivative results in the period of transition from radial flow to flow affected by the linear channel geometry; $0.2 < t_D < 2$ in Fig. 4.4.

Fig. 4.5 shows the effect of varying the transmissibility ratio, C_T, in the system. At small values of C_T, the pressure behavior of the system approaches that of a semi-infinite channel. As the ratio increases, the pressure drop at the producer is supported by fluids flowing in from the upper branch, (i.e., the pressure derivative increases at a decreasing rate), until the long-time pressure derivative behavior predicted by Eq. 4.26 is approached. Some of the predictions are shown in Fig. 4.5 by dashed line 1 and 2 for $C_T = 1$ and $C_T = 100$, respectively. Large C_T value means

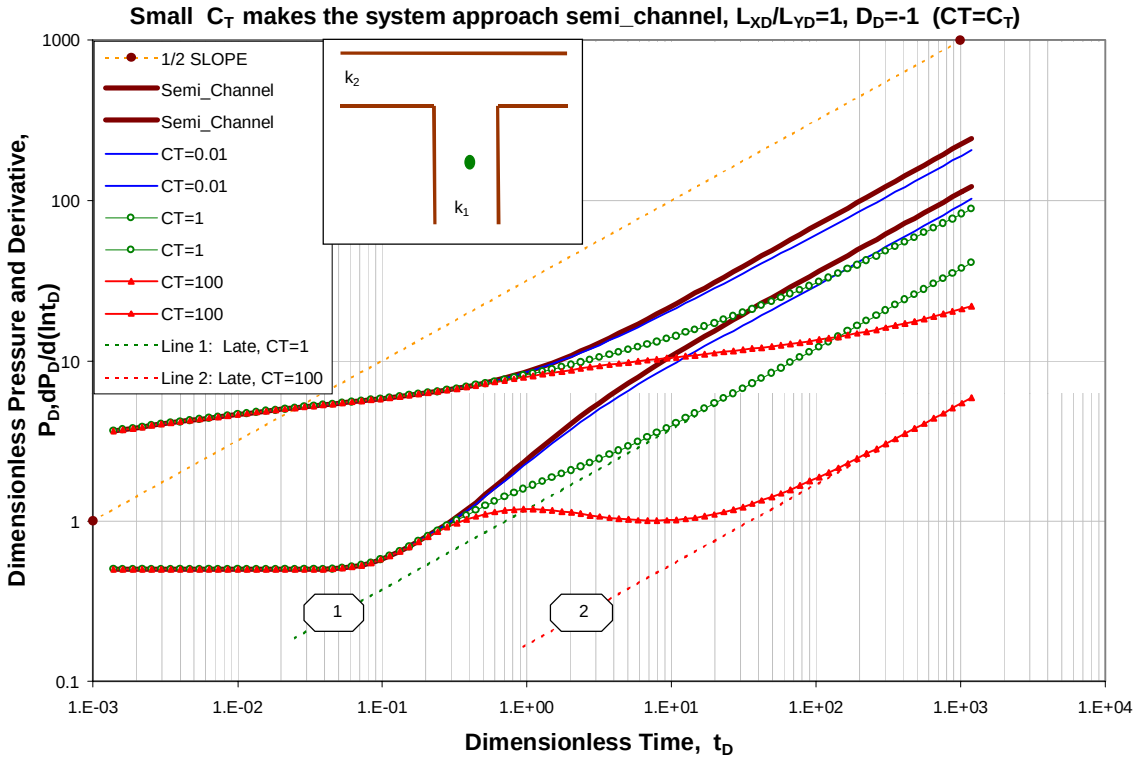

Figure 4.5: The effect of changing C_T, $L_{xD} = L_{y2D} = 1$, $C_S = 1$

a higher permeability and/or better fluid supply from the upper horizontal channel, therefore the larger the C_T value, the more shift of $\frac{dP_D}{d(\ln t_D)}$ curve to the right side will be.

It is very important to mention that for all of the cases studied in Fig. 4.5 and in figures below, the flux distribution (or, injection rate distribution) is peculiar to each case and it is not only a function of dimensionless time, but also a function of the boundary conditions and the property contrasts, such as C_T and C_S. However, it is impossible (and unnecessary) to show all of those profiles. A basic injection rate profile shown in Fig. 4.6, indicates that the injection at each "fracture" tip is higher than at other "fracture" locations when $t_D > 0.1$, in spite of the fact that, at

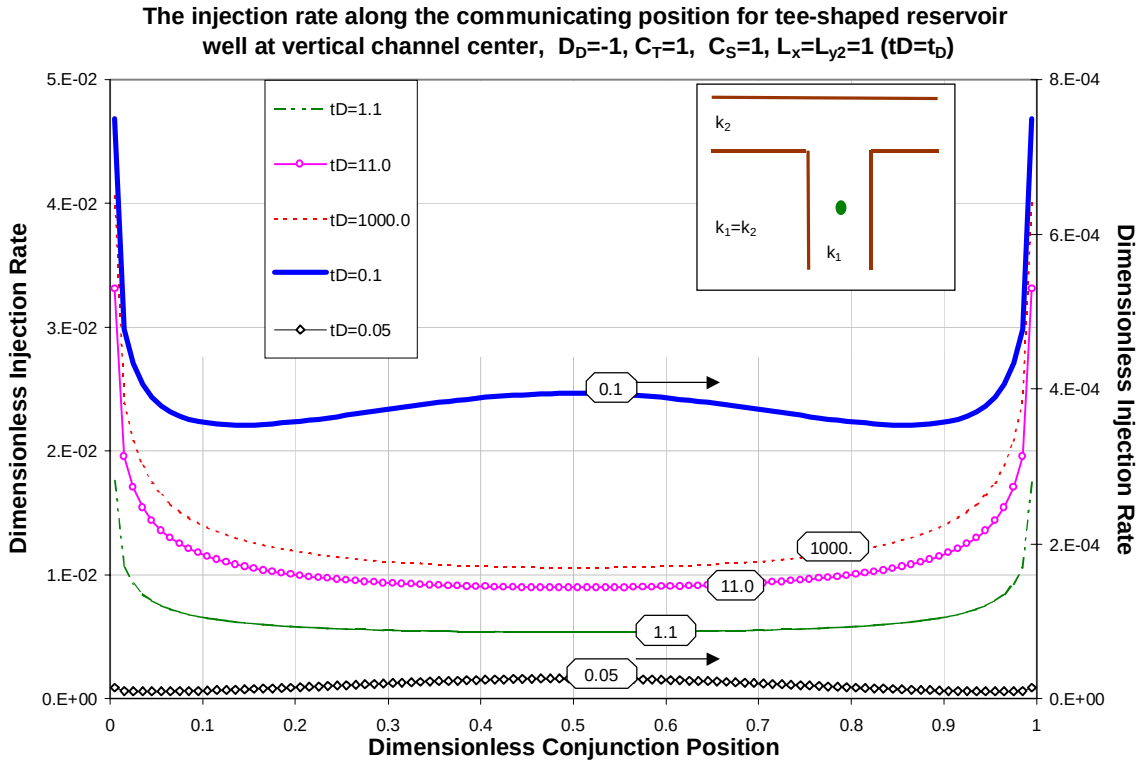

Figure 4.6: The injection rate profile for a basic tee-shaped reservoir

early time, the rate around the center part of the communicating gap may be slightly higher than the other positions away from the center.

Fig. 4.7 shows the effect of changing the upper channel width. A very small value of upper channel width, L_{yD}, will make the system approach a semi-infinite channel, (i.e., without a tee-section). A very large upper channel width will cause the system to approach another kind of complex geometry reservoir - a combination of vertical channel and a semi-infinite reservoir. The late time pressure derivative of this type of reservoir can be predicted by applying Eq. 4.28, which is plotted as line 1. For tee-shaped reservoirs, the late time pressure derivative is approximated by Eq. 4.26. For the cases of $L_{y2D} = 1$ and $L_{y2D} = 10$ their late time behavior is indicated by

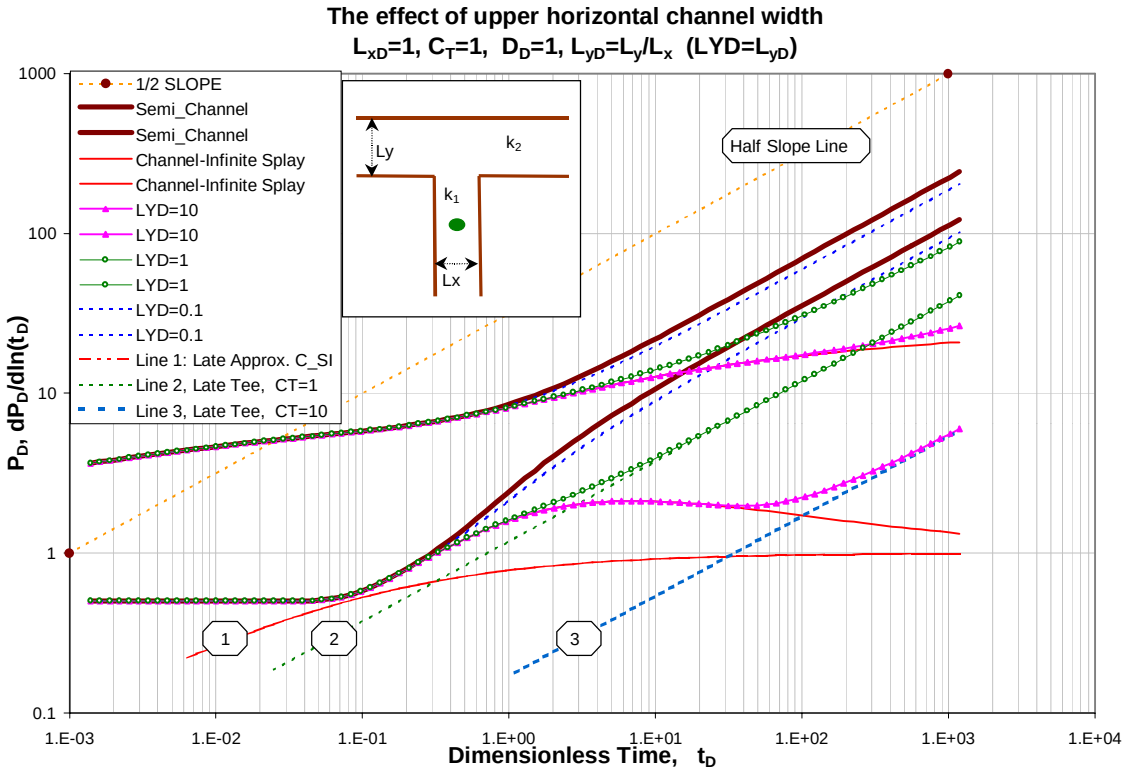

Figure 4.7: The effect of changing the upper channel width

dashed line 2 and 3 in Fig. 4.7. Note that the transition zone follows the behavior of a well in a vertical channel connected to a semi-infinite reservoir. Therefore, the C_T value can be estimated by matching the transition zone with those curves resulting from the vertical channel and semi-infinite splay system, see Fig. 4.3.

In Fig. 4.8, as the distance of the producer from the upper branch, (L_d in Fig. 4.1), is increased, the pressure response will show the distinct behavior of a well in an isolated channel; i.e., the pressure derivative is given by Eq. 4.27. When fluid inflow from the upper branch begins to affect the produced pressure response, the pressure derivative deviates from the early time response and exhibits a slope less than $\frac{1}{2}$. At late time, when flow in the upper branch is linear, the pressure derivative

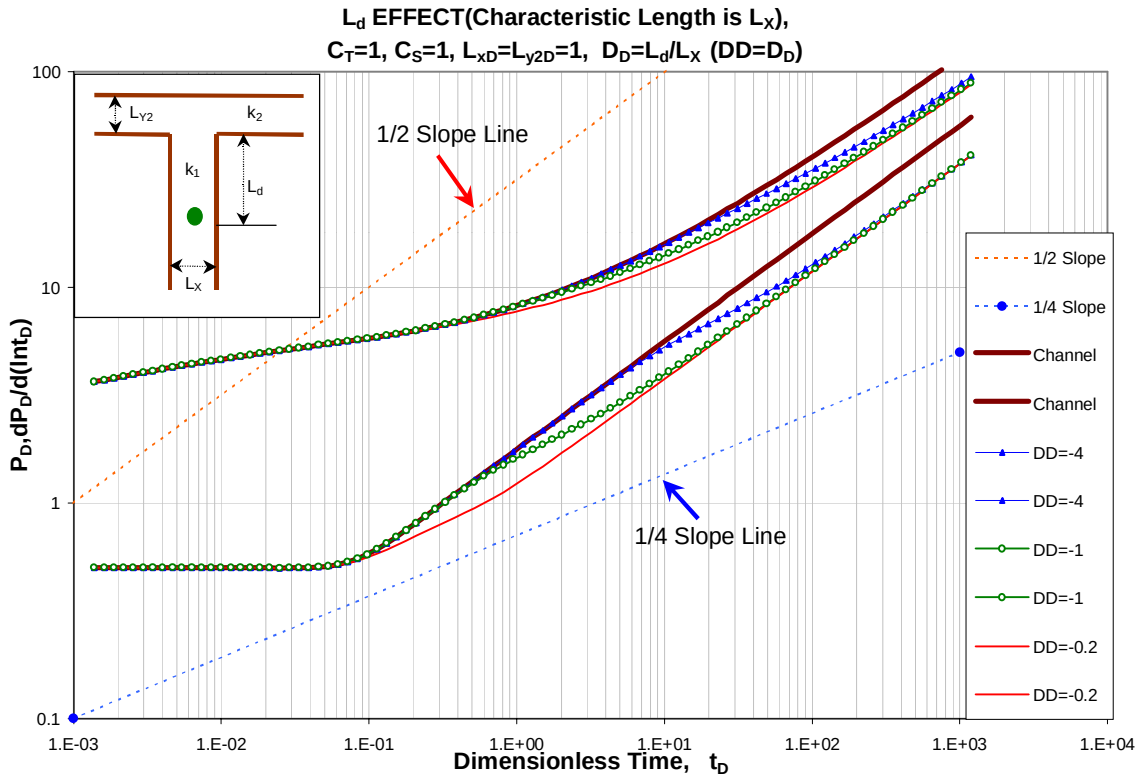

Figure 4.8: The effect of changing the well position

approaches the behavior predicted by Eq. 4.26. The D_D value has no influence on the late time behavior, therefore, the derivative curves are identical at late time for all cases.

Fig. 4.9 shows the a composite of the flow regimes obtainable from a tee-shaped reservoir. At very early time, a radial flow region for the producer in Region 1 may be observed. As time progresses, the sides of the vertical channel affect the pressure response, and an early-time linear flow regime (i.e., $\frac{1}{2}$ slope) is obtained. A transition period where inflow from the upper channel affects the pressure drop follows. Depending on the width and diffusivity of the upper channel, the pressure derivative approaches a second linear flow regime (Eq. 4.26) or the behavior defined

by Eq. 4.28 where the upper branch is infinite in width.

The difference between dashed line 1 and 2 reflects the comparison between the vertical and horizontal parts of tee-shaped reservoir. Applying Eq. 4.27 and Eq. 4.26 at equal $\frac{dp_D}{d(\ln t_D)}$ we can describe the pressure derivative behavior as follows. Note that the points read from line 1 and 2 are point A, with coordinate (31.0,10.0), and point B, with coordinate (970.0,10.0), respectively. From Eq. 4.27 and Eq. 4.26 we have

$$2\sqrt{\pi t_{D,PointB}}\frac{1}{1+2L_{y2D}\sqrt{C_TC_S}} = \sqrt{\pi t_{D,PointA}}, \tag{4.29}$$

or

$$\begin{aligned} L_{y2D}\sqrt{C_TC_S} &= \sqrt{\frac{t_{D,PointB}}{t_{D,PointA}}} - \frac{1}{2} && (4.30)\\ &= \sqrt{\frac{970.0}{31.0}} - \frac{1}{2} && (4.31)\\ &= 5.09. && (4.32) \end{aligned}$$

In this case, if we have identical properties in both Region 1 (vertical part) and Region 2 (horizontal part), then $C_T = C_S = 1$. Therefore, the approximate channel width ratio, L_{y2D}, is 5.09. It is very close to the real ratio value, 5.0. The right hand side of Eq. 4.30 is an composite of C_T, C_S and L_{y2D}, which represents all of the parameters in which we are interested. It is clear that with additional information either from geological, geophysical sources or from another well testing data Eq. 4.30 could facilitate better characterization of this type of reservoir.

Theoretically, a good C_T estimation can be obtained if the well testing data before $t_{D,dev.c\_s}$ are reproduced by choosing the right C_T value, while the comparative C_T value can be computed as (see Eq. 4.26 and Eq. 4.28)

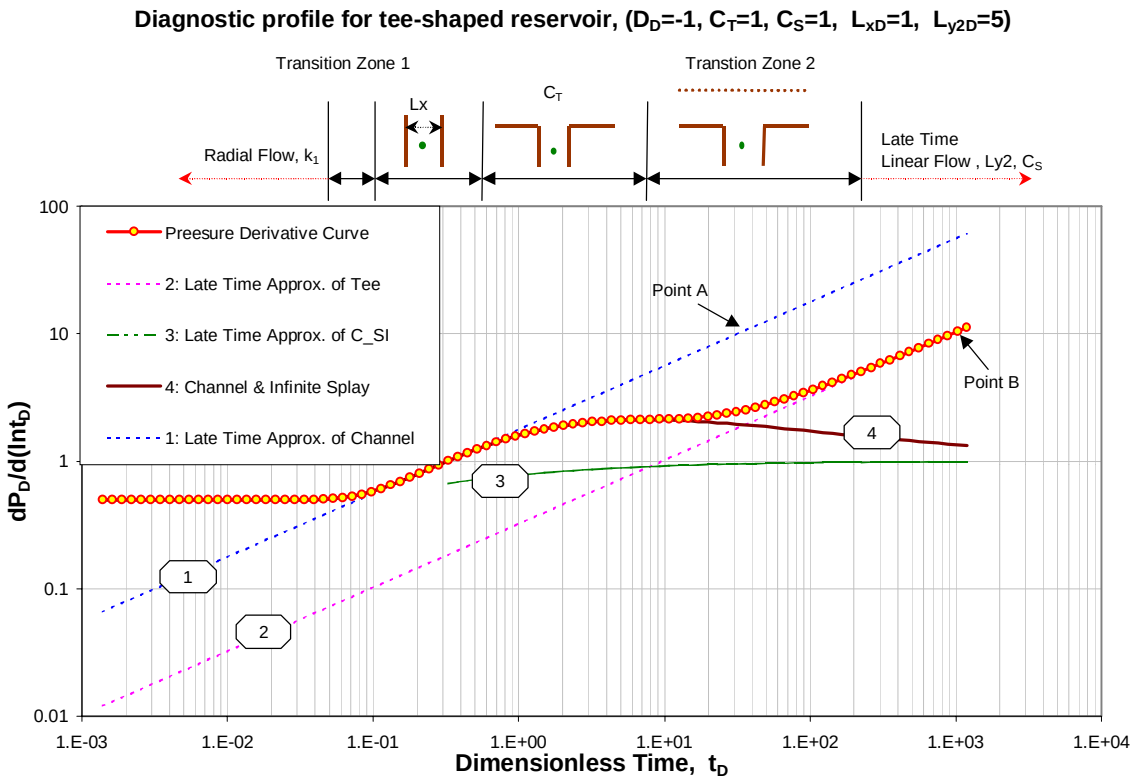

Figure 4.9: Observable flow regimes in a tee-shaped reservoir

$$t_{D,dev.c\_s} = \frac{L_{y2D}^2}{\pi C_R}. \tag{4.33}$$

From Fig. 4.9, we know that $t_{D,dev.c\_s}$ is the crossing point of dashed line 2 and curve 3 and is not the actual time at which the behavior of the tee-shaped reservoir deviates from that of channel and semi-infinite reservoir. However, $t_{D,dev.c\_s}$ can be treated as a good approximation for the actual deviation time.

A special case of a tee-shaped reservoir occurs when the producer is located in the horizontal part of the tee. We refer to this type of reservoir as a "reverse tee-shaped reservoir" in this dissertation. Following our previous dimensionless variable definitions, which assume that the reservoir region where the producing well is located

is Region 1, the late time behaviors of Q_{fD} and $\frac{dp_D}{d(\ln t_D)}$ are derived in Eq. D.49 and Eq. D.50 of Appendix D. In this case, the width of the horizontal channel, L_y, is defined as the characteristic length.

Fig. 4.10 compares the pressure and derivative behaviors for tee-shaped reservoirs and reverse tee-shaped reservoirs. In order to be able to compare the results, the dimensionless widths of all channels are chosen as 1 and identical properties in both regions are assumed. A fact we need to mention here is that the injection rate profile of a reverse tee-shaped reservoir, see Fig. 4.11, is completely different from what we had in Fig. 4.6 for the tee-shaped reservoir; the difference in the boundary conditions cause the dissimilar results.

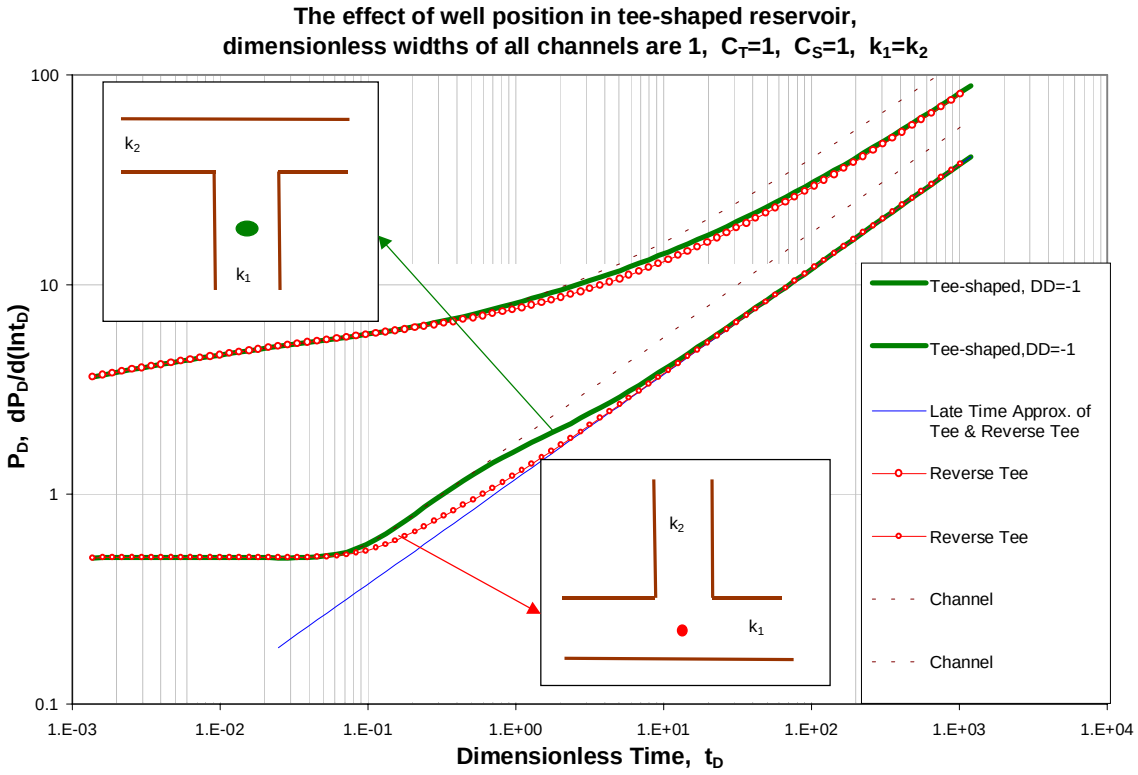

Figure 4.10: The behaviors of tee-shaped and reverse tee-shaped reservoirs(or, the effect of well position)

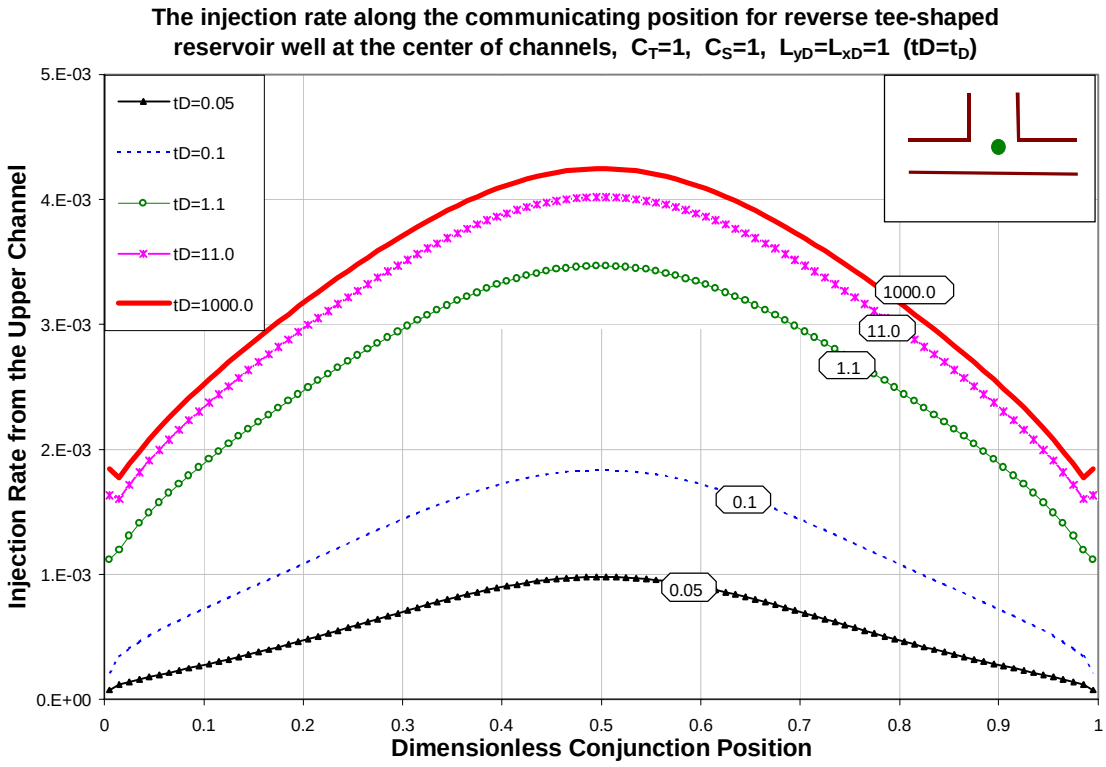

Figure 4.11: The injection rate profile of "reverse tee-shaped" reservoir

CHAPTER V

CHANNEL AND SPLAY RESERVOIRS

5.1 Mathematical Derivation

As in the previous section, the complex model is solved by decomposing it into two simpler homogeneous models that are coupled at their plane of contact; see Fig. 5.1. Solutions to each of the simpler problems are written in Laplace space and solved for the unknown fluid transfer between the systems. The resulting flux distributions are then used to obtain the desired pressure behavior.

The fracture plane is defined in the same way as in Fig. 2.4. The actual well in Region 1 still produces at a rate of 1 RB/D. Applying Eq. B.10 and Eq. B.16 to compute the dimensionless pressure drop caused by a completely-penetrating producer and by a fully-penetrating horizontal fracture plane in the horizontal channel, respectively, the pressure drop, $\overline{p}_{D,k_1}$, in Laplace domain at any dimensionless location (x_{D,k_1}, y_{D,k_1}) can be written in terms of source/sink solutions as

$$\begin{aligned}\overline{p}_{D,k_1}(x_D, y_D, u_D) = {} & \overline{q}_{0D}(u_D)\,\overline{f}_{wh,k_1}(x_D, y_D, 2L_{yD}, x'_D, y'_D, u_D) + \\ & \overline{q}_{0D}(u_D)\,\overline{f}_{w'h,k_1}(x_D, y_D, 2L_{yD}, x'_D, -y'_D, u_D) - \\ & \sum_{j=1}^{N_f} \overline{q}_{fD,j}(u_D)\,\overline{f}_{hh,j,k_1}(x_D, y_D, 2L_{yD}, x_{D,j-1}, x_{D,j}, y_{fD,k_1}, u_D)\,. \quad (5.1)\end{aligned}$$

Here,

$$L_{yD} = \frac{L_y}{L_y} = 1, \quad (5.2)$$

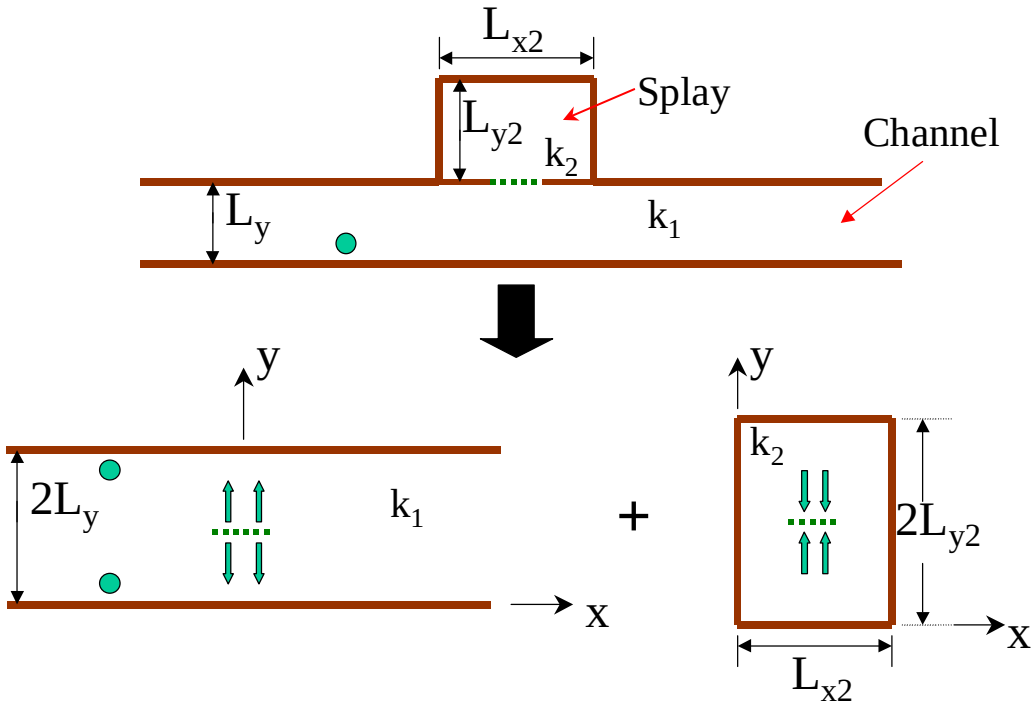

Figure 5.1: Decomposition of channel splay reservoir and their coordinate system

$$L_{x2D} = \frac{L_{x2}}{L_y}, \tag{5.3}$$

and

$$L_{y2D} = \frac{L_{y2}}{L_y}. \tag{5.4}$$

The three terms on the right side of Eq. 5.1 account for the dimensionless pressure drop caused by a well, its image well located at an equal distance behind the channel boundary on which the splay is located, and non-uniform injection from the fracture plane allowing fluid transfer from Region 2 to Region 1. Note that Eq. 5.1 is evaluated in Region 1. Here, when the producer is located in the horizontal channel, u_D is defined as

$$u_D = \frac{L_{yD}^2 u}{\eta_1}. \tag{5.5}$$

$\overline{q}_{fD,j}$ denotes the Laplace transform of the unknown flux at the center of fracture segment $(x_{fD,j}, y_{fD,k_1})$.

As before, $\overline{f}_{wh,k_1}(x_D, y_D, 2L_{yD}, x'_D, y'_D, u_D)$ and $\overline{f}_{w'h,k_1}(x_D, y_D, 2L_{yD}, -x'_D, y'_D, u_D)$ denote the Laplace transforms of the dimensionless source/sink function for the well and its image well in horizontal channel. Formulas for the inverse Laplace transforms of these functions can be found in Appendix B; the method we use to compute the Laplace transform can be found in Appendix A. Similarly, the term $\overline{f}_{hh,j,k_1}(x_D, y_D, 2L_{yD}, x_{D,j-1}, x_{D,j}, y_{fD,k_1}, u_D)$ represents the Laplace transform of the dimensionless source/sink function for a "uniform-flux" line sink as described in Appendix B. That is

$$f_{wh,k_1}(x_D, y_D, 2L_{yD}, x'_D, y'_D, t_D) =$$
$$\frac{\pi}{4L_{yD}}\left[\theta_3\left(\frac{y_D - y'_D}{4L_{yD}}, \frac{t_D}{4L_{yD}^2}\right) + \theta_3\left(\frac{y_D + y'_D}{4L_{yD}}, \frac{t_D}{4L_{yD}^2}\right)\right]\theta_L\left(\frac{x_D - x'_D}{2}, t_D\right), \tag{5.6}$$

$$f_{w'h,k_1}\left(x_D, y_D, 2L_{yD}, -x_D^{'}, y_D^{'}, t_D\right) =$$
$$\frac{\pi}{4L_{yD}}\left[\theta_3\left(\frac{y_D - y_D^{'}}{4L_{yD}}, \frac{t_D}{4L_{yD}^2}\right) + \theta_3\left(\frac{y_D + y_D^{'}}{4L_{yD}}, \frac{t_D}{4L_{yD}^2}\right)\right]\theta_L\left(\frac{x_D + x_D^{'}}{2}, t_D\right), \quad (5.7)$$

and

$$f_{hh,j,k_1}\left(x_D, y_D, 2L_{yD}, x_{D,j-1}, x_{D,j}, y_{fD,k_1}, t_D\right) =$$
$$\frac{\pi}{2L_{yD}}\widehat{\Theta}_L\left(\frac{x_{D,j-1} - x_D}{2}, \frac{x_{D,j} - x_D}{2}, t_D\right) \times$$
$$\left[\theta_3\left(\frac{y_D - y_{fD,k_1}}{4L_{yD}}, \frac{t_D}{4L_{yD}^2}\right) + \theta_3\left(\frac{y_D + y_{fD,k_1}}{4L_{yD}}, \frac{t_D}{4L_{yD}^2}\right)\right]. \quad (5.8)$$

The dimensionless pressure drop solution to the Region 2 problem is written as

$$\overline{p}_{D,k_2}\left(x_{D,k_2}, y_{D,k_2}, u_D\right) = \sum_{j=1}^{N_f}\overline{q}_{fD,j}\left(u_D\right)\overline{f}_{hb,k_2}\left(x_D, y_D, L_{x2D}, 2L_{y2D}, x_{D,j-1}, x_{D,j}, y_{fD,k_2}, u_D\right), \quad (5.9)$$

where, $\overline{f}_{hb,k_2}\left(x_D, y_D, L_{x2D}, 2L_{y2D}, x_{D,j-1}, x_{D,j}, y_{fD,k_2}, u_D\right)$ represents the Laplace transform of the dimensionless source/sink function for a "uniform-flux" line sink in Region 2. Following the notation in Appendix B, the inverse Laplace transform of $\overline{f}_{hb}$ is given by

$$f_{hb,k_2}\left(x_D, y_D, L_{x2D}, 2L_{y2D}, x_{D,j-1}, x_{D,j}, y_{fD,k_2}, t_D\right) =$$
$$\frac{\pi}{2C_S L_{yD}}\left[\widehat{\Theta}_3\left(\frac{x_{D,j-1} - x_D}{2L_{x2D}}, \frac{x_{D,j} - x_D}{2L_{x2D}}, \frac{C_R t_D}{L_{x2D}^2}\right) + \widehat{\Theta}_3\left(\frac{x_{D,j-1} + x_D}{2L_{x2D}}, \frac{x_{D,j} + x_D}{2L_{x2D}}, \frac{C_R t_D}{L_{x2D}^2}\right)\right]$$
$$\times\left[\theta_3\left(\frac{y_D - y_{fD,k_2}}{4L_{y2D}}, \frac{C_R t_D}{4L_{y2D}^2}\right) + \theta_3\left(\frac{y_D + y_{fD,k_2}}{4L_{y2D}}, \frac{C_R t_D}{4L_{y2D}^2}\right)\right]. \quad (5.10)$$

For the coordinate systems displayed in Fig. 5.1, note that $y_{fD,k_1} = L_{yD}$ and $y_{fD,k_2} = L_{y2D}$. The procedure used to solve the problem is the same as what is described in the previous chapters, and is not repeated here.

5.2 Model Verification and Results

5.2.1 Limiting cases

In Fig. 5.2 the pressure behaviors of wells in an infinite channel, in a reverse tee-shaped channel reservoir and in a parallel two channel reservoir (with a leaky fault between these two channels) are shown as the three limiting cases to check the channel splay reservoir results. We validated the model by checking it against the following limiting cases.

- The model must approach the behavior of a well in an infinite channel if the diffusivity and/or the size of the splay part approaches zero.

- The model must approach the behavior of a well in a tee-shaped channel reservoir if the vertical direction length of the splay part (L_{y2} in Fig. 5.1) becomes infinite.

- The model must approach the behavior of another kind of complex reservoir, which is a combination of two parallel channels with a leaky fault separating them, if the width of the splay part (L_{x2} in Fig. 5.1) becomes infinite.

- The model must approach the behavior of another kind of complex reservoir, which is a combination of an infinite channel and a semi-infinite splay with a leaky fault separating them, if the splay size (both L_{x2} and L_{y2} in Fig. 5.1 become infinite) becomes infinite.

- At early time, if the well is far enough away from the gap, the model must approach the behavior of a well in a channel.

The asymptotic behavior of the pressure derivative solution of channel and splay reservoir is derived in Appendix D. At very large times when flow in the horizontal channel becomes linear and parallel to the channel boundaries, and when the rate of fluid flow through the communicating position becomes approximately constant, the pressure derivative in this channel and splay system is approximately given by

$$\frac{dp_{D,1}}{d(\ln t_{D,1})} \rightarrow \frac{\sqrt{\pi t_D}}{1 + C_S \dfrac{L_{x2D} L_{y2D}}{2\sqrt{\pi t_D}}}, \tag{5.11}$$

see Appendix D. Note that the width of the horizontal channel is selected as the characteristic length.

The stabilized rate of flow from the "vertically-fractured" well at the communicating position (in RB/D per RB/D of production from the actual well), can be expressed as

$$Q_{fD} \rightarrow \frac{1}{\frac{1}{2} + \dfrac{1}{C_S} \dfrac{\sqrt{\pi t_D}}{L_{x2D} L_{y2D}}}. \tag{5.12}$$

The system behaves like an infinite linear channel reservoir when the diffusivity or dimensions of the splay part approach zero. The pressure response at late time can be approximated by

$$\frac{dp_{D,1}}{d(\ln t_{D,1})} \rightarrow \sqrt{\pi t_D}. \tag{5.13}$$

If the vertical length of the splay (Region 2), L_{y2}, goes to infinity we get a "reverse tee-shaped" limiting case as we had discussed in Fig. 4.10 of Chapter

4 for channel splay reservoirs. At late time when the pressure derivative can be approximated by Eq. D.14. We can show that, (see Eq. D.50)

$$\frac{dp_{D,1}}{d(\ln t_{D,1})} \rightarrow \frac{\sqrt{\pi t_D}}{1+\frac{1}{2}L_{x2D}\sqrt{C_T C_S}}. \tag{5.14}$$

If the width of the splay (Region 2), L_{x2}, is infinite we get another limiting case for channel splay reservoirs, which is a combination of two parallel channel reservoirs with a leaky fault between them. At late time when the pressure derivative can be approximated by Eq. D.18, we can show that, (see Eq. D.57)

$$\frac{dp_{D,1}}{d\,(\ln t_{D,1})} \rightarrow \frac{\sqrt{\pi t_D}}{1+L_{y2D}\sqrt{C_T C_S}}. \tag{5.15}$$

If the splay size, $L_{x2} \times L_{y2}$, becomes infinite(both L_{x2} and L_{y2} in Fig. 5.1 become infinite), another kind of limiting case for channel splay reservoirs can be reached , which is a combination of an infinite channel reservoirs and a semi-infinite splay with a leaky fault separating them. At late time when the dimensionless pressure term in Eq. 5.9 is given by the semilog approximation, and when the fluid injection from the splay part becomes nearly stable, we can show that

$$\frac{dp_{D,1}}{d\,(\ln t_{D,1})} \rightarrow \frac{1}{C_T+\frac{1}{\sqrt{\pi t_D}}}. \tag{5.16}$$

The asymptotic behavior of the pressure derivative solution by using Eq. 5.13, Eq. 5.14, Eq. 5.15 and Eq. 5.16 are also shown in Fig. 5.2 as dashed line 1, 2, 3 and dashed curve 4, respectively.

The pressure responses in the system will be affected by the properties and the boundary conditions of both the channel and splay. The effect of each relevant factor can be identified by applying our model. Fig. 5.3 shows the effect of the size

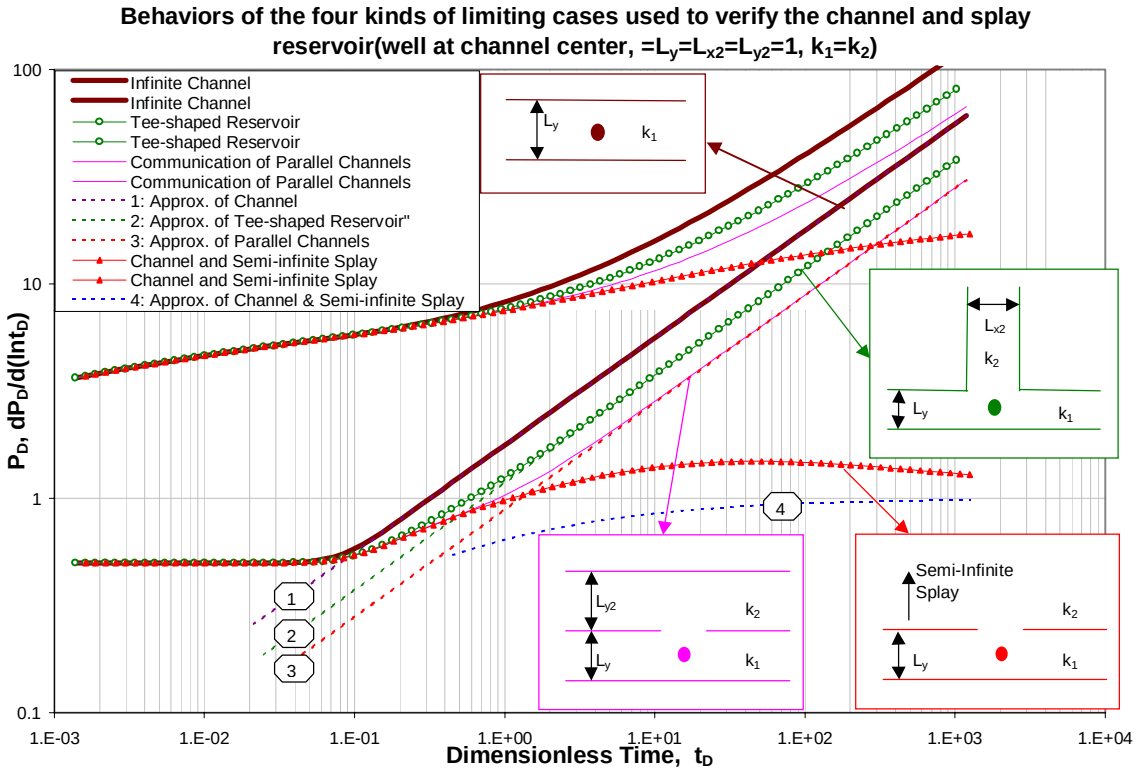

Figure 5.2: The four limiting cases designed to verify the computational results

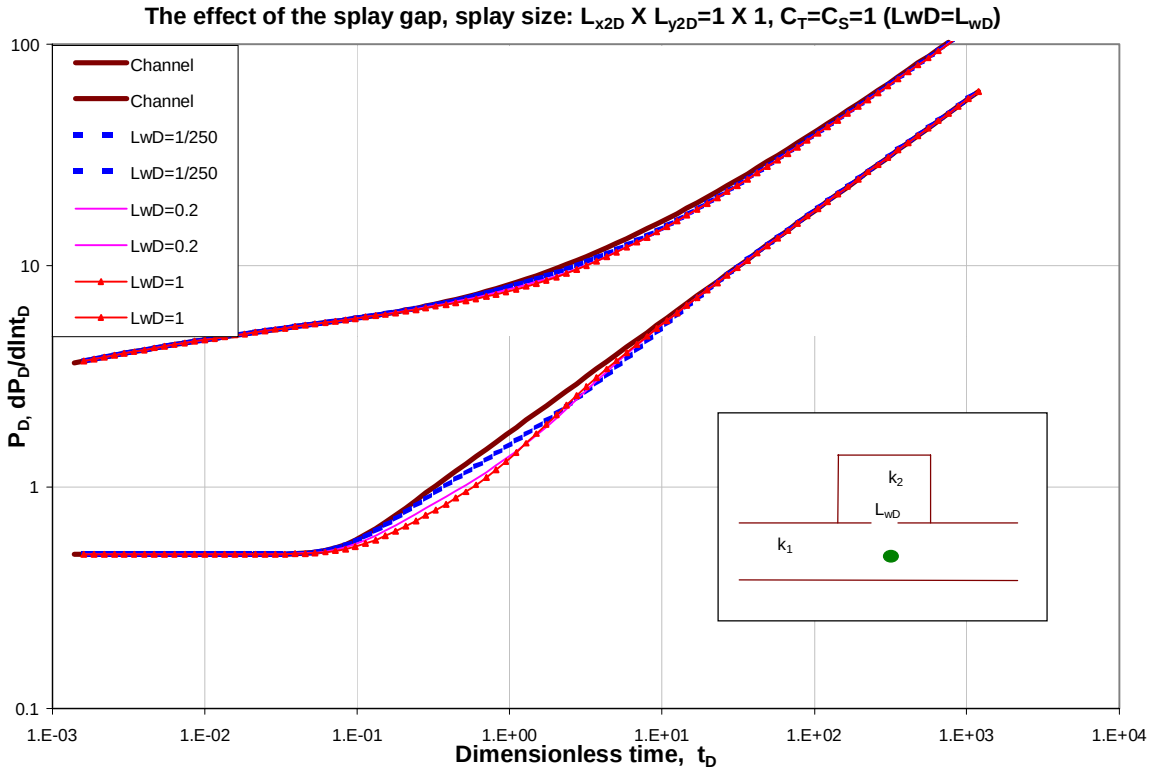

Figure 5.3: The effect of the size of the area of communication between channel and splay

of the opening (L_{wD}) where the splay and the channel communicate, see Fig. 5.1. Fig. 5.3 shows that even a relatively small opening, (e.g., $L_{wD} = \frac{1}{250}$), will give a change in the derivative curves. Although the changes in the derivative curves appear significant in Fig. 5.3, these differences would be difficult to discern in actual field data, and would have a negligible impact on analysis of field data. Further, as we shall show later, the impact of the splay on the pressure derivative is maximized when the horizontal location of the well is in the middle of the gap. This means that the overall impact of the gap opening on well test data is expected to be minimal. At very late time the system approaches the typical behavior of linear flow in a channel.

Although the flux distribution for each case was also computed to examine the fluid flow in detail, a simple symmetric case was chosen to exemplify the flux behavior. Fig. 5.4 and Fig. 5.5 show the early and late time flux distribution for channel and splay reservoir, respectively. At any instant, the flux near the center of the zone of communication is larger than positions away from the center since the pressure drop caused by the well is larger at the center of the gap. As time proceeds, fluid flows across an increasingly larger part of the gap. However, the fluxes at the tips are prevented from increasing too much because of the splay boundary condition; that is, because of its finite volume, the splay does not contain sufficient fluid to support large fluid transfer close to the tips of the gap - this behavior contrasts with the flux behavior of semi-infinite splays. At late time, $t_D > 1.1$ in this case, fluid in the channel begins to enter the splay part (indicated by the negative flux in Fig. 5.5) as the pressure in the splay becomes relatively depleted. The amount of fluid entering into the splay continuously increases as time progresses.

Physically, we expect that the size of the splay must play a dominant role in system's pressure transient behavior. Fig. 5.6 examines the effect of the splay size; for this case, we assume the splay is a square, i.e., $L_{x2D} = L_{y2D}$. We also assume that the x-coordinate of the well corresponds to the center of the gap in order to maximize the effect of the splay region on the pressure response. Note that the system pressure behavior falls between that of a well in an isolated linear channel and a well in a channel connected to a semi-infinite splay; see Fig. 5.2. In general, the larger the volume of the connected splay, the more deviation there is from the curves of a channel (both p_D and $\frac{dp_D}{d(\ln t_D)}$) and the longer the period will be, where the system resembles the channel/semi-infinite splay system.

We checked the approximation of Eq. 5.11 to the late-time behavior of the channel-splay system. Line 1 and Line 2 are the late time $\frac{dp_D}{d(\ln t_D)}$ approximation of Eq. 5.11 for the cases with splay sizes ($L_{x2D} \times L_{y2D}$) 4×4 and 40×40, respectively. Apparently, line 2 didn't match very well at late time and a careful examination

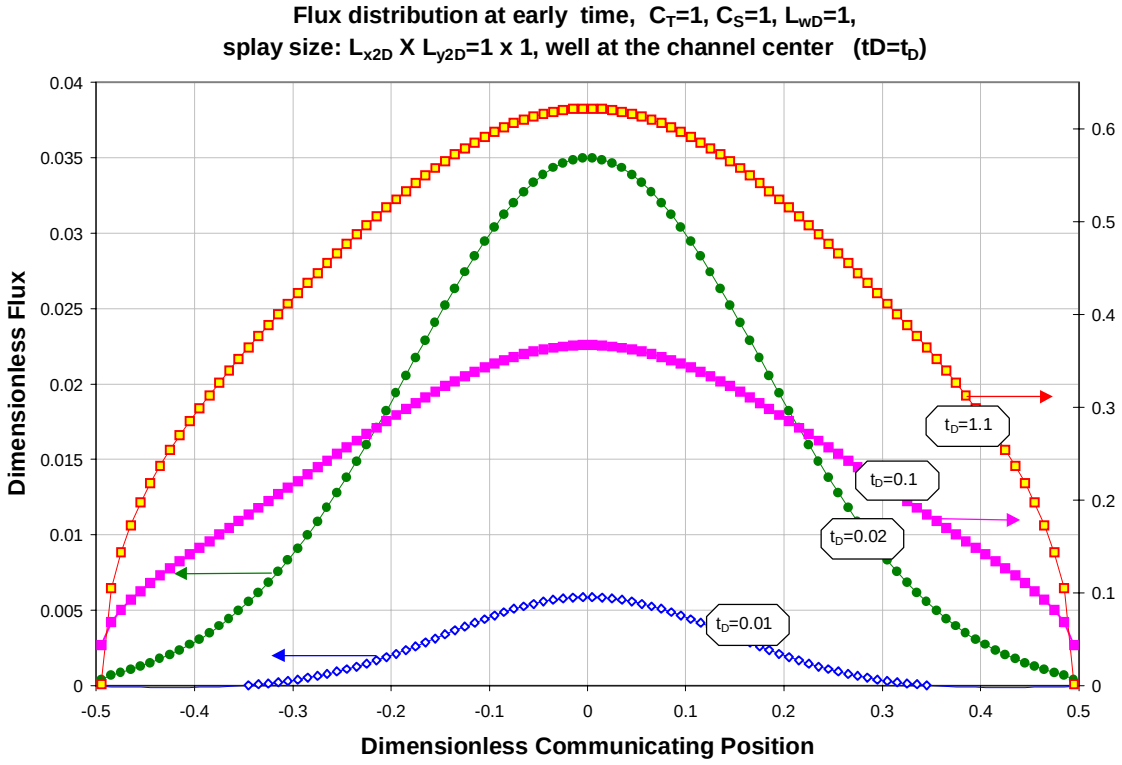

Figure 5.4: Flux distribution at early time channel splay reservoir, splay size: 1×1

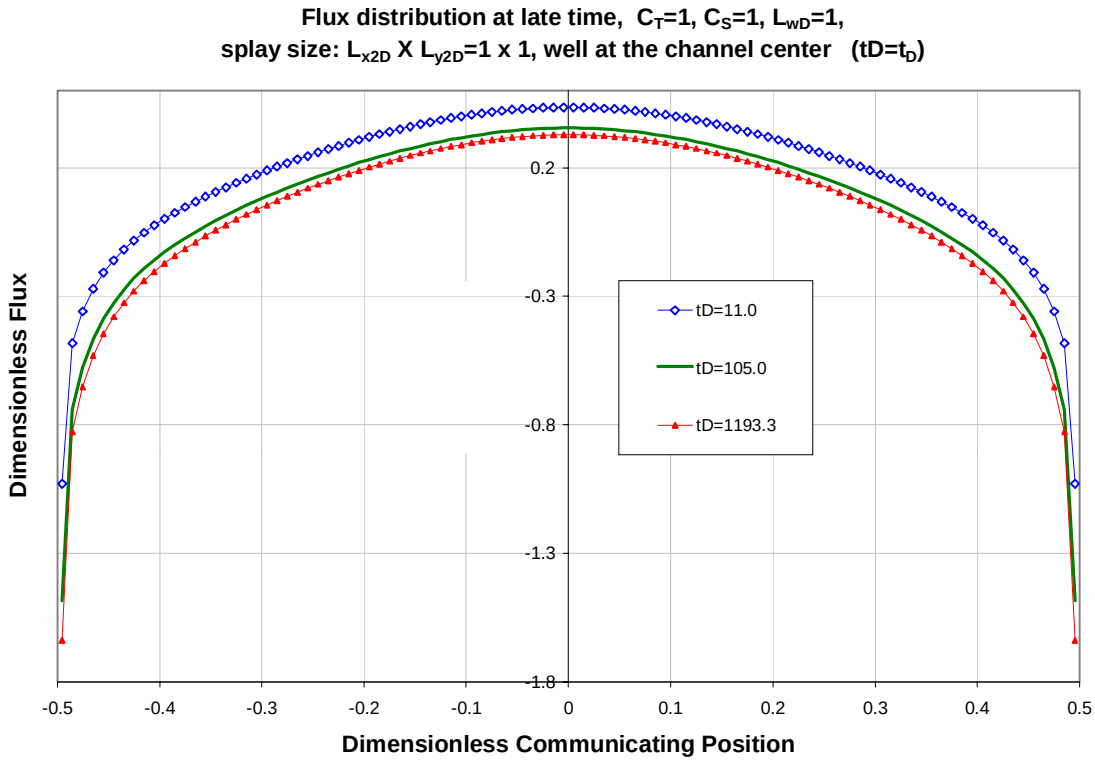

Figure 5.5: Flux distribution at late time for channel splay reservoir, splay size: 1×1

of Line 1 also indicated a discrepancy at late time. This apparent failure can be explained by examining the related total injection rate from the splay, see Fig. 5.7. For the smaller splay of size 4×4, the lack of agreement is because of the difficulty to reach stabilized behavior in the splay part since the fluid from the infinite channel is constantly injected into splay. For the splay of size 40×40, the late time Q_{fD} approximation is not accurate enough even at $t_D > 10^6$, indicating that the larger the size of the splay, the harder it would be to attain a pseudosteady state flow condition in splay part. Therefore, the prediction from Eq. 5.11 is not very good since a pseudosteady state flow in splay part is assumed. These results reveal two facts. One is the importance of the knowledge of the flux distribution along the communicating position and another is a difficulty in applying the late time approximation equations in complex geometry reservoirs.

The approximate dimensionless time, t_{Dc_s}, when the curves deviate from the behavior of channel and semi-infinite splay system can be computed roughly by equating Eq. 5.16 and Eq. 5.11. Then, we have

$$t_{Dc\_s} = \frac{C_S L_{x2D} L_{y2D}}{2\pi C_T} \tag{5.17}$$

$$= \frac{L_{x2D} L_{y2D}}{2\pi C_R}. \tag{5.18}$$

As we have mentioned before the t_{Dc_s} value is only an approximate value. Our numerical experience indicates that the real deviation time should be before t_{Dc_s}. In Fig. 5.6 t_{Dc_s} are $0.1591, 2.546, 254.6$ and 25464.8 for cases of sizes 1×1, $4 \times 4, 40 \times 40$ and 400×400, respectively.

Obviously, for the same splay size/volume the dimension of the splay may vary widely. Fig. 5.8 examines the effect of splay dimensions on pressure transient response. The results in Fig. 5.8 shows that the splay orientation has an effect on the pressure responses, particularly in the transition period between infinite-acting flow and the boundary-dominated flow in the splay. If the width of the splay is

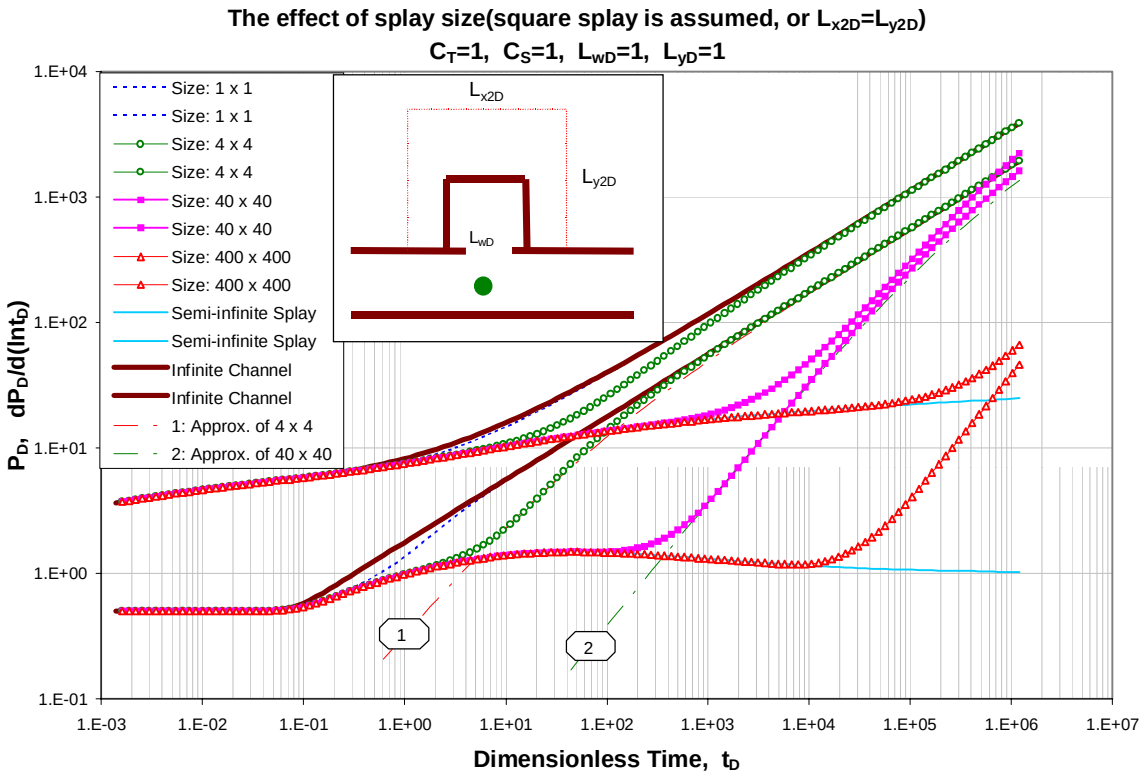

Figure 5.6: The effect of the splay size

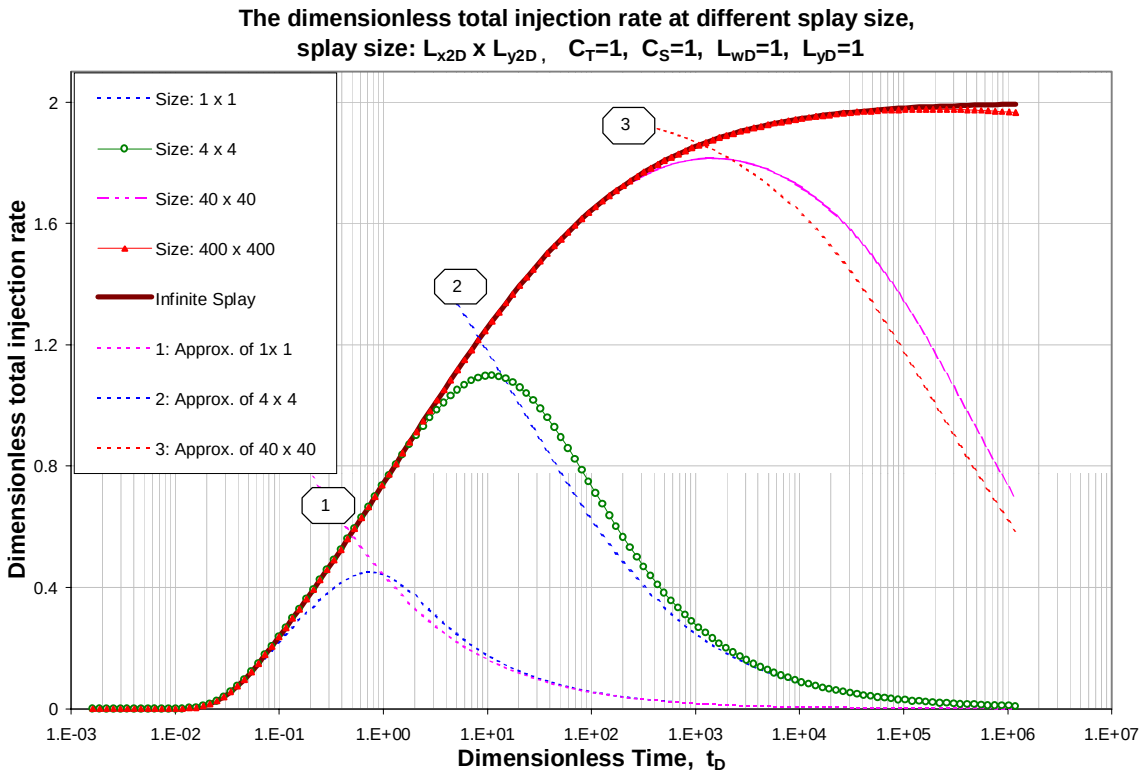

Figure 5.7: The effect of splay size on dimensionless total injection rate

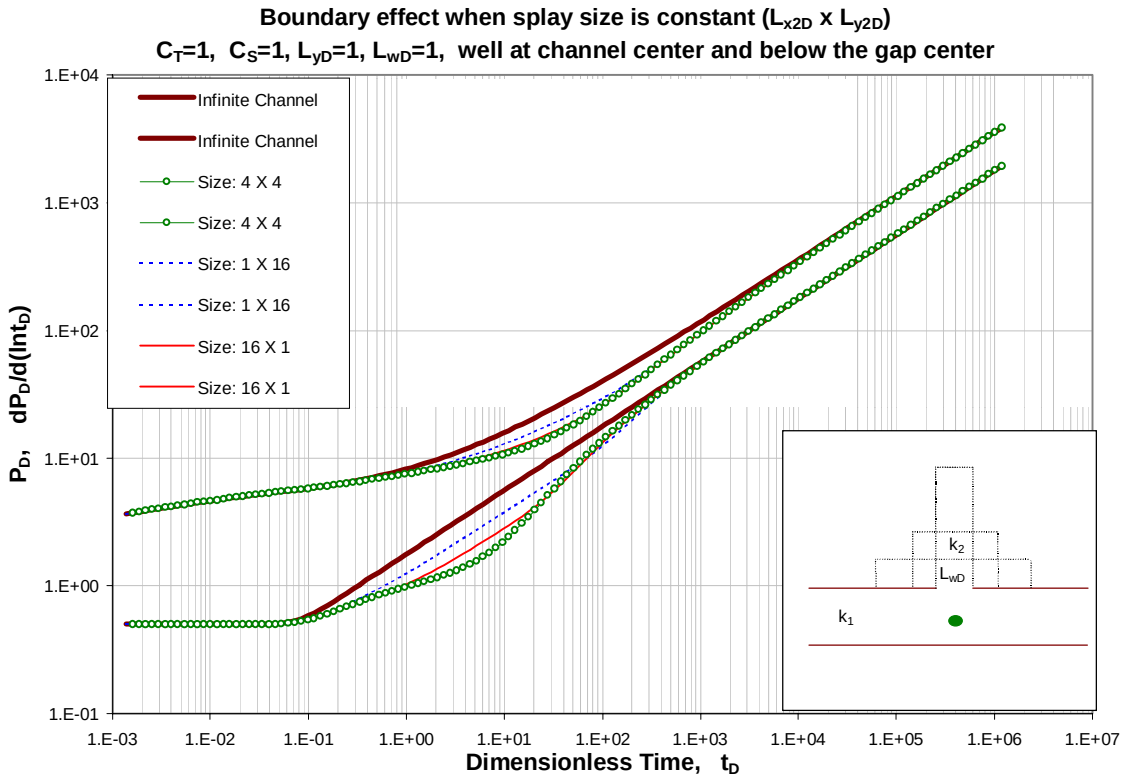

Figure 5.8: The effect of splay dimensions on pressure transient response

approximately the same as the width of the gap, the vertical splay boundaries are felt immediately, and the time to pseudosteady-state flow is solely determined by the distance to the horizontal splay boundary. Conversely, for splays with widths appreciably larger than the gap width, the transition to pseudosteady state flow is affected by distances to both the vertical and horizontal splay boundaries. Note that the late-time pressure derivative behavior is closely described by the asymptotic formula, Eq. 5.11.

Fig. 5.9 and Fig. 5.11 serve as two verifications for our modeling. As the splay length (L_{y2D}) in vertical direction increases, the model results will approach the reverse tee-shaped reservoir that we modeled in Chapter 4. The limiting case

of two hydraulically contacted parallel horizontal channels can be approximated by increasing the splay width (L_{x2D}) in horizontal direction. Both Fig. 5.9 and Fig. 5.11 give us the results expected. The total dimensionless injection rate curves for these two figures are shown in Fig. 5.10 and Fig. 5.12 respectively. Under the assumed conditions, Fig. 5.10 indicates that the total dimensionless injection rate from the vertical splay part approaches $2 \times \frac{1}{3}$ as L_{y2D} increases and Fig. 5.12 tells us that if L_{x2D} is large enough that the total dimensionless injection rate will be close to $2 \times \frac{1}{2}$ at late time. All of these values are in agreement with the asymptotic formulas, Eq. D.49 and Eq. D.56. The late time injection approximation for some of those curves are also plotted in Fig. 5.10 and Fig. 5.12 by applying Eq. 5.12.

Fig. 5.13 shows the effect of the well displacement for splay of size 4×4 and $C_T = C_S = C_R = 1$. If the well is located right below the splay gap center, the derivative curve has a maximum difference from the single channel behavior. As the well is displaced away from the gap center in the x-direction, the discrepancy with single infinite-channel behavior is delayed and minimized. This means that if our testing well is too far away from the possible existing splay we will not be able to identify it.

Fig. 5.14 shows the effect of the dimensionless transmissibility ratio (C_T). If the splay properties are not favorable, i.e., the C_T value is small, the fluid contribution from the splay part will also be small. Then the p_D and $\dfrac{dp_D}{d(\ln t_D)}$ curves will resemble the responses of an infinite channel. Curves in Fig. 5.14 for $C_T = 0.001$ are a good example. On the other hand, if C_T is large enough the size of the splay will be the dominant factor in determining the pressure responses.

Fig. 5.15 shows the effect of C_S for splay of size 4×4. The higher the porosity in the splay part, the longer the fluid support from the splay will last and the more curve deviation from channel's curves will be. This figure also shows the late time behavior predicted in Eq. 5.11 for $C_T = 1$, $C_S = 2$ case. (In Eq. 5.11, note that $L_{x2D} L_{y2D}$ represents the area of the splay for our 2-D problem.)

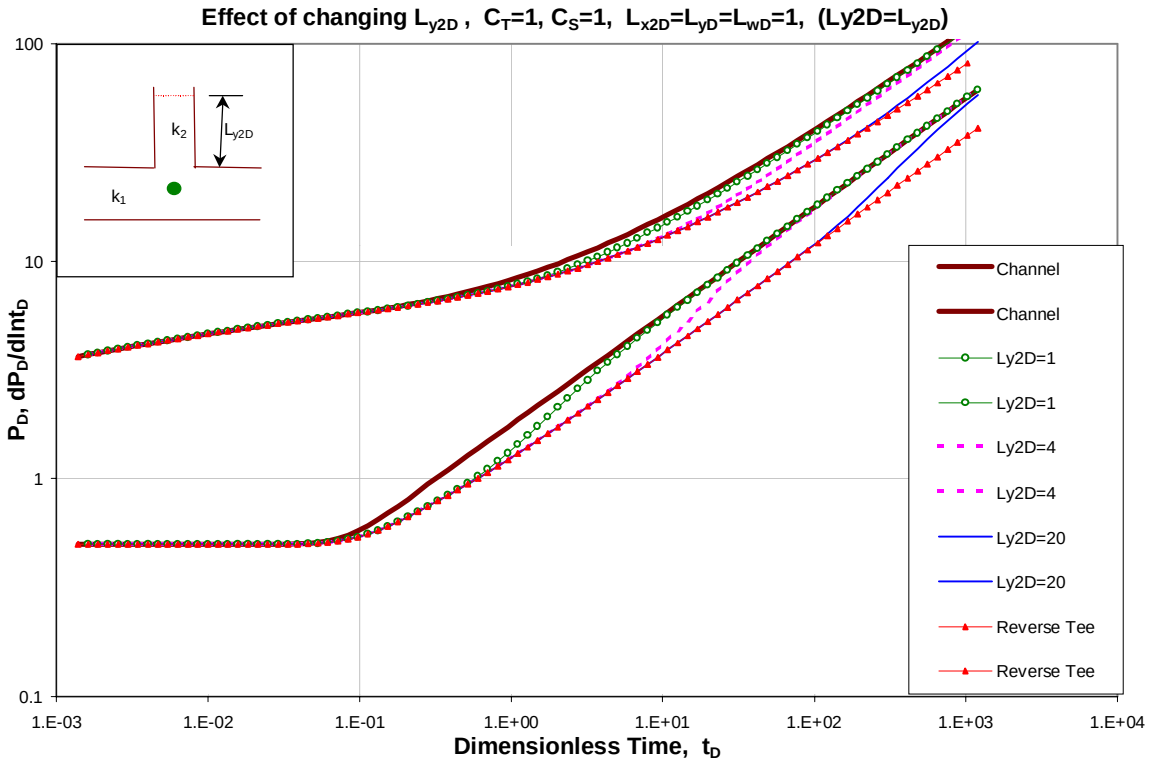

Figure 5.9: The effect of changing the splay size in vertical direction and the limiting case(reverse tee)

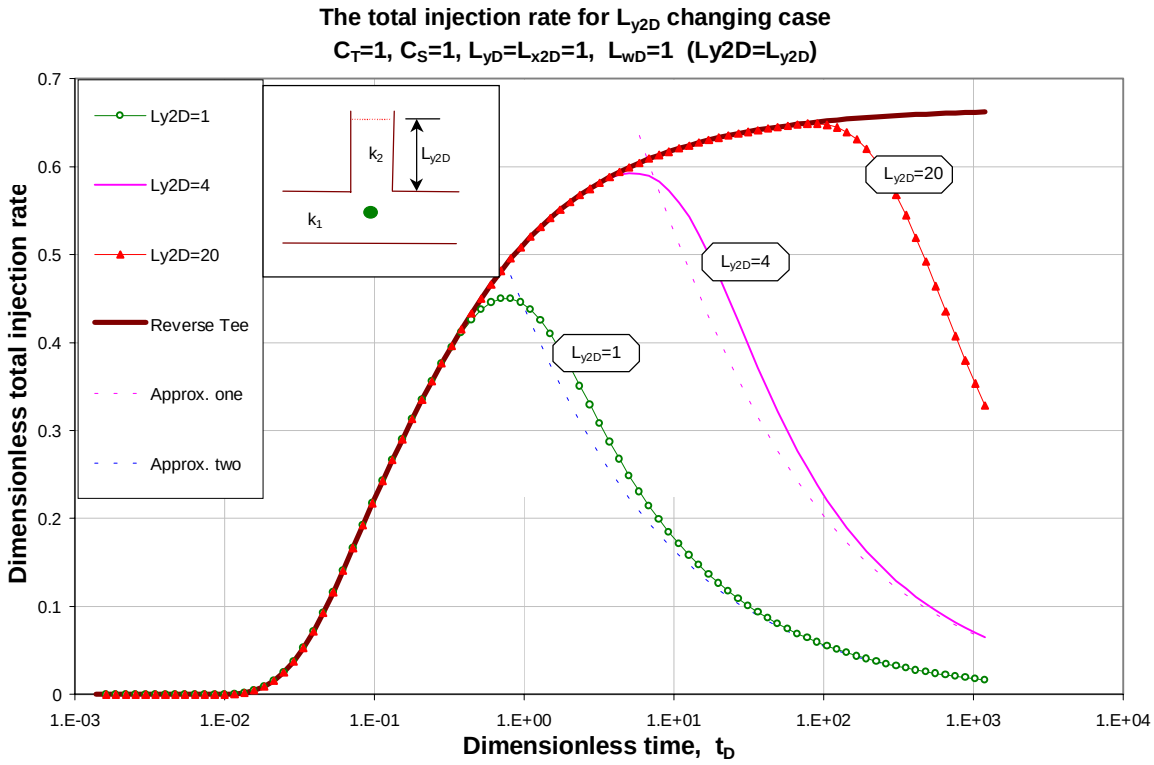

Figure 5.10: The total dimensionless injection rate for the above L_{y2D} changing case

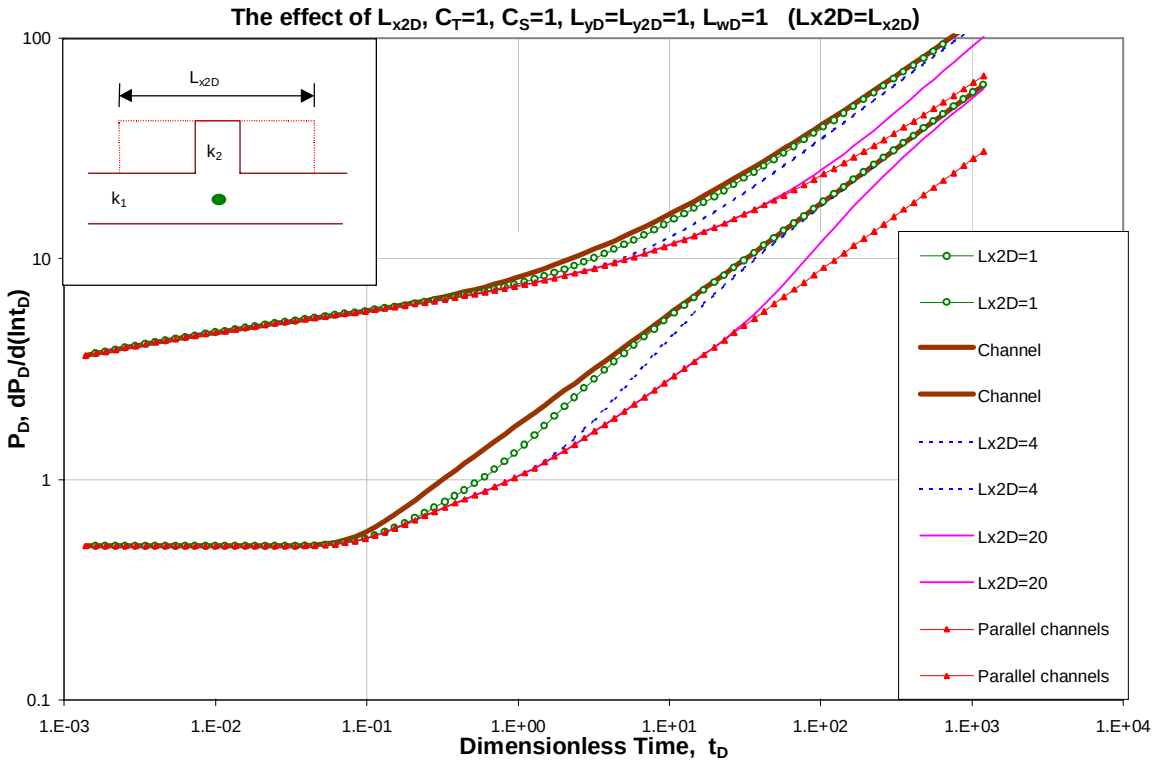

Figure 5.11: The effect of the L_{x2D}, when L_{yD}=L_{y2D}=1

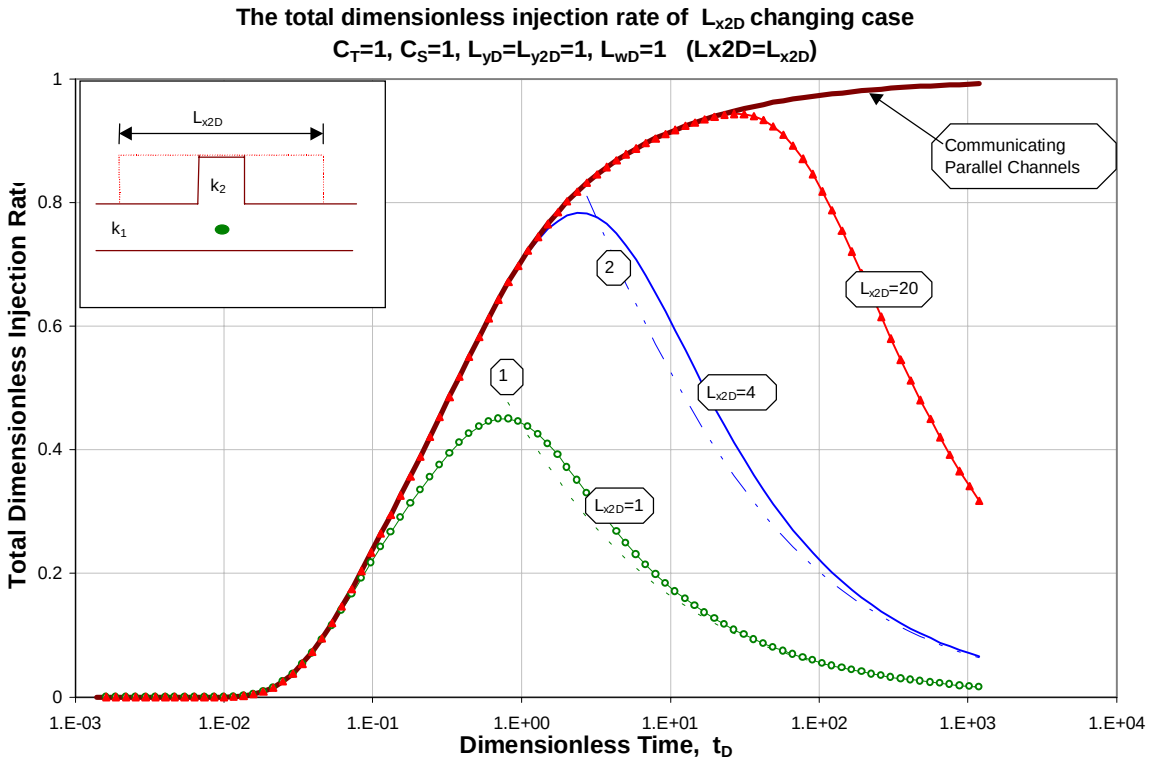

Figure 5.12: The total dimensionless injection rate for the above L_{x2D} changing case

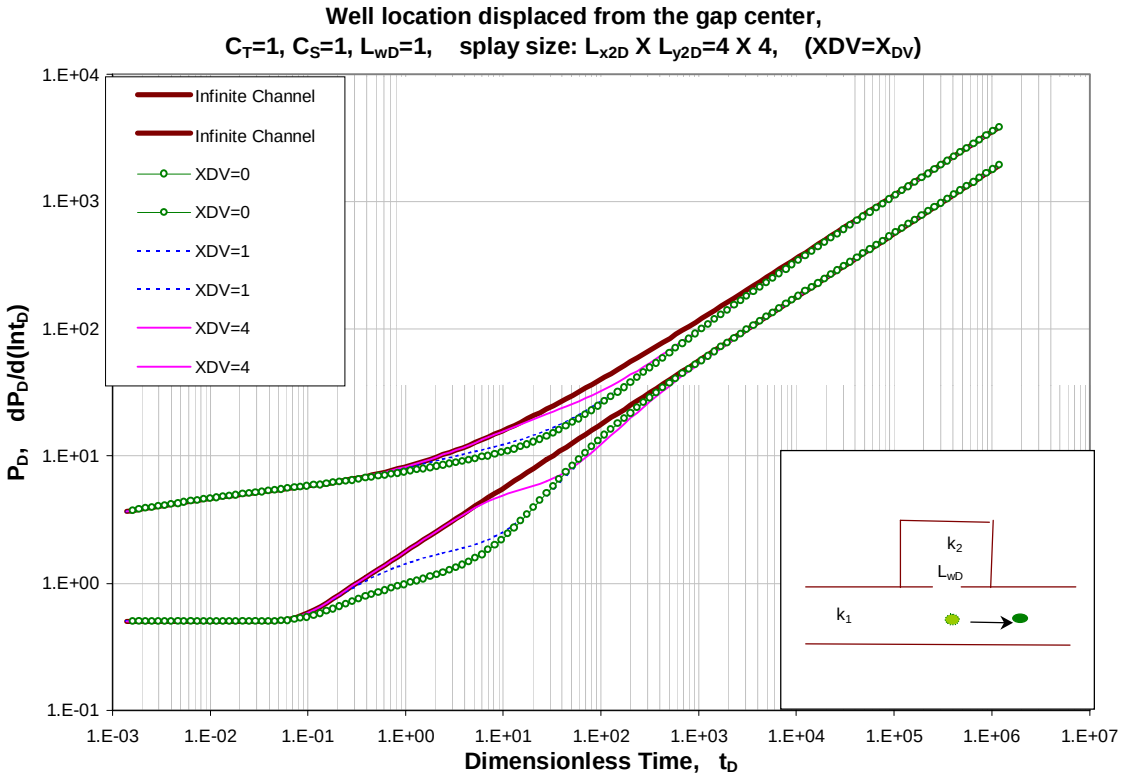

Figure 5.13: The effect of well displacement X_{DV}

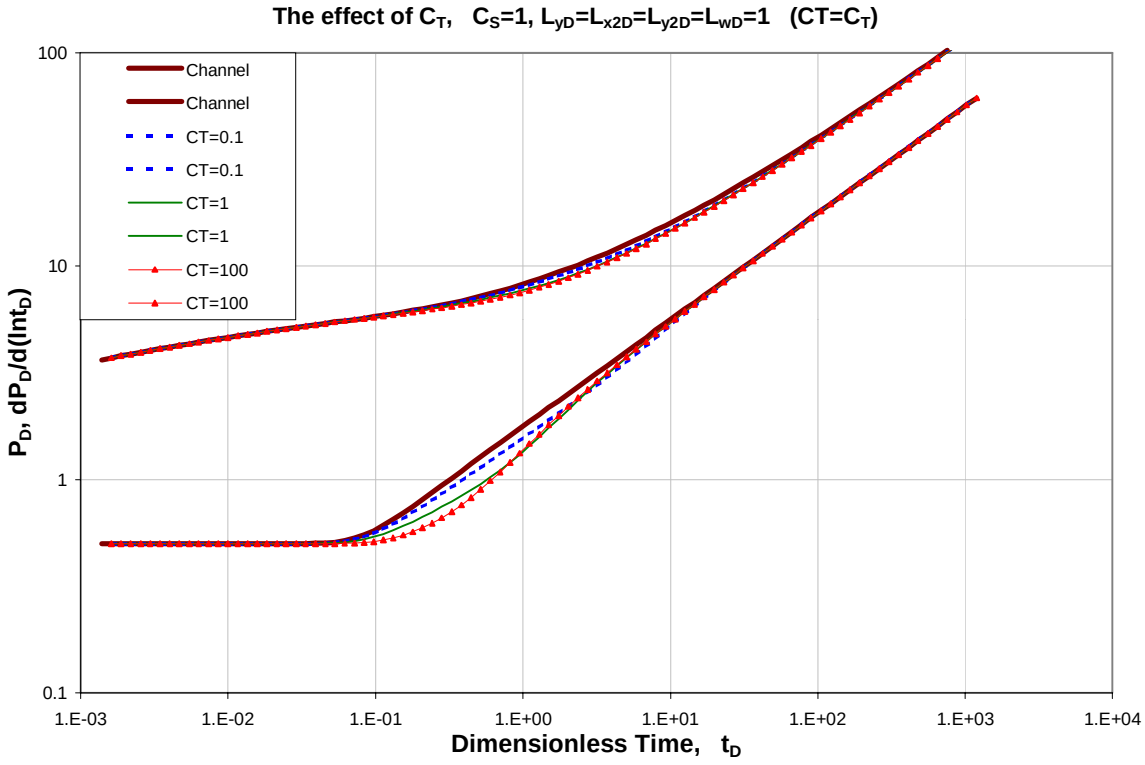

Figure 5.14: The effect of the transmissibility ratio(C_T)

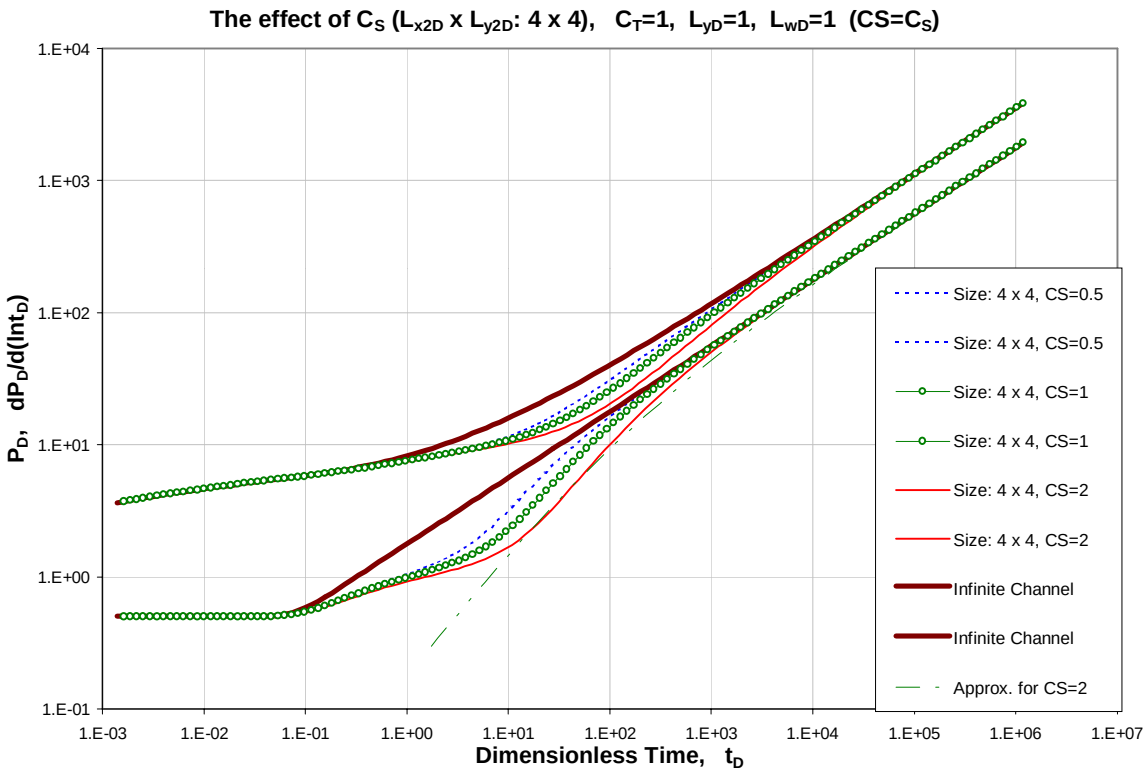

Figure 5.15: The effect of C_S, splay sizes $L_{x2D} \times L_{y2D} = 4 \times 4$

CHAPTER VI

COMMUNICATION OF BOUNDED RESERVOIRS

6.1 Mathematical Derivation

The complex model of communication between two bounded reservoirs is solved by decomposing it into two simpler homogeneous bounded models that are coupled at their plane of contact; see Fig. 6.1. Solutions to each of the simpler problems are written in Laplace space and solved for the unknown fluid transfer between the systems. The resulting flux distributions are then used to obtain the desired pressure behavior as before.

The fracture plane is defined in the same way as in Fig. 2.4. The actual well in Region 1 still produces at a rate of 1 RB/D. Applying Eq. B.19 and Eq. B.22 we can compute the dimensionless pressure drop caused by a completely-penetrating producer and by a fully-penetrating horizontal fracture plane in the bounded reservoirs, respectively. The pressure drop, $\overline{p}_{D,k_1}$, in the Laplace domain at any dimensionless location (x_{D,k_1}, y_{D,k_1}) can be written in terms of source/sink solutions as

$$\begin{aligned}\overline{p}_{D,k_1}(x_D, y_D, u_D) = {} & \overline{q}_{0D}(u_D)\,\overline{f}_{wb,k_1}(x_D, y_D, L_{xD}, 2L_{yD}, x'_D, y'_D, u_D) + \\ & \overline{q}_{0D}(u_D)\,\overline{f}_{w'b,k_1}(x_D, y_D, L_{xD}, 2L_{yD}, x'_D, y''_D, u_D) - \\ & \sum_{j=1}^{N_f} \overline{q}_{fD,j}(u_D)\,\overline{f}_{hb,j,k_1}(x_D, y_D, L_{xD}, 2L_{yD}, x_{D,j-1}, x_{D,j}, y_{fD,k_1}, u_D) \quad (6.1)\end{aligned}$$

where the producer is located at (x'_D, y'_D) and the image well is located at (x'_D, y''_D).The three terms on the right side of Eq. 6.1 account for the dimensionless pressure drop caused by a well, its image well located at an equal distance from the plane that

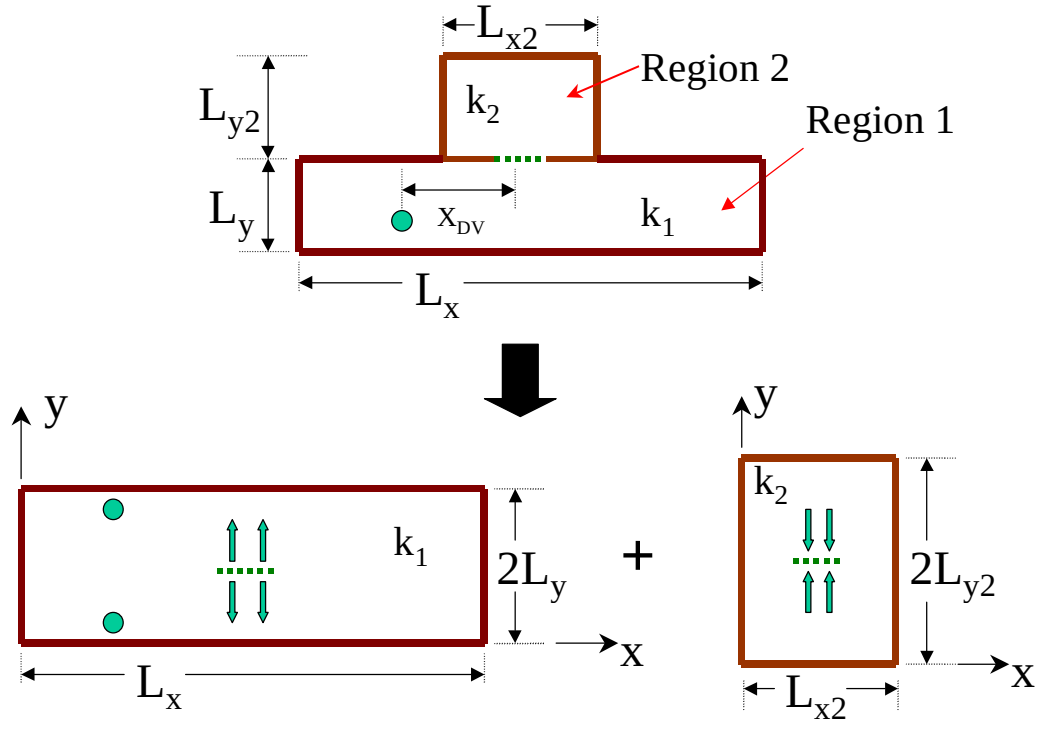

Figure 6.1: Decomposition of bounded reservoir and their coordinate system

defines the boundary between the two communicating reservoirs, and non-uniform injection from the fracture plane respectively. Note that Eq. 6.1 is evaluated in Region 1. Here, u_D is the dimensionless Laplace variable for Region 1 and is defined as

$$u_D = \frac{l^2 u}{\eta_1} \tag{6.2}$$

where u is the Laplace variable associated with the transform of time (in units day^{-1}), l represents the characteristic length which may be different in each case. $\overline{q}_{fD,j}$ still denotes the Laplace transform of the (unknown) flux at the center of fracture segment $(x_{fD,j}, y_{fD,k_1})$. As before, $\overline{f}_{wb,k_1}(x_D, y_D, L_{xD}, 2L_{yD}, x'_D, y'_D, u_D)$ and $\overline{f}_{w'b,k_1}(x_D, y_D, L_{xD}, 2L_{yD}, x'_D, y''_D, u_D)$ denote the Laplace transforms of the dimensionless source/sink functions for the well and its image well in Region 1. The function $\overline{f}_{hb,j,k_1}(x_D, y_D, L_{xD}, 2L_{yD}, x_{D,j-1}, x_{D,j}, y_{fD,k_1}, u_D)$ represents the Laplace transform of the dimensionless source/sink function for the jth "uniform-flux" line sink. The nomenclature for the source/sink functions employed here corresponds to that employed in Appendix B. That is,

$$\begin{aligned} f_{wb,k_1}(x_D, y_D, L_{xD}, L_{yD}, x'_D, y'_D, t_D) = \\ \frac{\pi}{2}\left\{\frac{1}{L_{xD}}\left[\theta_3\left(\frac{x_D - x'_D}{2L_{xD}}, \frac{t_D}{L_{xD}^2}\right) + \theta_3\left(\frac{x_D + x'_D}{2L_{xD}}, \frac{t_D}{L_{xD}^2}\right)\right]\right\} \times \\ \left\{\frac{1}{2L_{yD}}\left[\theta_3\left(\frac{y_D - y'_D}{4L_{yD}}, \frac{t_D}{4L_{yD}^2}\right) + \theta_3\left(\frac{y_D + y'_D}{4L_{yD}}, \frac{t_D}{4L_{yD}^2}\right)\right]\right\}, \end{aligned} \tag{6.3}$$

$$\begin{aligned} f_{w'b,k_1}(x_D, y_D, L_{xD}, L_{yD}, x'_D, y''_D, t_D) = \\ \frac{\pi}{2}\left\{\frac{1}{L_{xD}}\left[\theta_3\left(\frac{x_D - x'_D}{2L_{xD}}, \frac{t_D}{L_{xD}^2}\right) + \theta_3\left(\frac{x_D + x'_D}{2L_{xD}}, \frac{t_D}{L_{xD}^2}\right)\right]\right\} \times \\ \left\{\frac{1}{2L_{yD}}\left[\theta_3\left(\frac{y_D - y''_D}{4L_{yD}}, \frac{t_D}{4L_{yD}^2}\right) + \theta_3\left(\frac{y_D + y''_D}{4L_{yD}}, \frac{t_D}{4L_{yD}^2}\right)\right]\right\}, \end{aligned} \tag{6.4}$$

and

$$f_{hb,j,k_1}\left(x_D, y_D, L_{xD}, 2L_{yD}, x_{D,j-1}, x_{D,j}, y_{fD,k_1}, t_D\right) =$$
$$\frac{\pi}{2L_{yD}}\left[\widehat{\Theta}_3\left(\frac{x_{D,j-1}-x_D}{2L_{xD}}, \frac{x_{D,j}-x_D}{2L_{xD}}, \frac{t_D}{L_{xD}^2}\right) + \widehat{\Theta}_3\left(\frac{x_{D,j-1}+x_D}{2L_{xD}}, \frac{x_{D,j}+x_D}{2L_{xD}}, \frac{t_D}{L_{xD}^2}\right)\right] \times$$
$$\left[\theta_3\left(\frac{y_D - y_{fD,k_1}}{4L_{yD}}, \frac{t_D}{4L_{yD}^2}\right) + \theta_3\left(\frac{y_D + y_{fD,k_1}}{4L_{yD}}, \frac{t_D}{4L_{yD}^2}\right)\right]. \quad (6.5)$$

Methods for computing these terms and their Laplace transforms are also discussed in detail in Appendix A.

The dimensionless pressure drop solution to the Region 2 problem is written as

$$\overline{p}_{D,k_2}\left(x_{D,k_2}, y_{D,k_2}, u_D\right) = \sum_{j=1}^{N_f} \overline{q}_{fD,j}\left(u_D\right) \overline{f}_{hb,j,k_2}\left(x_D, y_D, L_{x2D}, 2L_{y2D}, x_{D,j-1}, x_{D,j}, y_{fD,k_2}, u_D\right) \quad (6.6)$$

where, $\overline{f}_{hb,j,k_2}\left(x_D, y_D, L_{x2D}, 2L_{y2D}, x_{D,j-1}, x_{D,j}, y_{fD,k_2}, u_D\right)$ represents the Laplace transform of the dimensionless source/sink function for a "uniform-flux" line sink in Region 2. Following the notation in Appendix B, the inverse Laplace transform of $\overline{f}_{hb,j,k_2}$ is given by

$$f_{hb,j,k_2}\left(x_D, y_D, L_{x2D}, 2L_{y2D}, x_{D,j-1}, x_{D,j}, y_{fD,k_2}, t_D\right) =$$
$$\frac{\pi}{2C_S L_{y2D}}\left[\widehat{\Theta}_3\left(\frac{x_{D,j-1}-x_D}{2L_{x2D}}, \frac{x_{D,j}-x_D}{2L_{x2D}}, \frac{C_R t_D}{L_{x2D}^2}\right) + \widehat{\Theta}_3\left(\frac{x_{D,j-1}+x_D}{2L_{x2D}}, \frac{x_{D,j}+x_D}{2L_{x2D}}, \frac{C_R t_D}{L_{x2D}^2}\right)\right]$$
$$\times \left[\theta_3\left(\frac{y_D - y_{fD,k_2}}{4L_{y2D}}, \frac{C_R t_D}{4L_{y2D}^2}\right) + \theta_3\left(\frac{y_D + y_{fD,k_2}}{4L_{y2D}}, \frac{C_R t_D}{4L_{y2D}^2}\right)\right]. \quad (6.7)$$

Using the above coordinate system defined in Fig. 6.1, it is clear that $y_{fD,k_1} = L_{yD}$ and $y_{fD,k_2} = L_{y2D}$.

6.2 Model Verification and Results

6.2.1 Limiting cases

The interesting thing for this problem is that all of the limiting cases we mentioned before can be applied as limiting cases for the bounded reservoir communication problem. In other words, our bounded reservoir model has the potential to simulate the behaviors of the former models, i.e., the behaviors of leaky fault infinite reservoirs, tee-shaped reservoirs, channel-splay reservoirs, infinite channel reservoirs, semi-infinite channel reservoirs, infinite reservoirs, semi-infinite reservoirs and some special shaped reservoirs. A detailed study of these limiting cases will allow us to understand a variety of different kinds of complex geometry reservoirs.

The physical realization of these limiting cases are specified as below.

- The model must approach the behavior of a well in a bounded reservoir if the diffusivity of the upper part approaches zero or the size of Region 1 and Region 2 are finite.

- The model must approach the behavior of a well in an infinite or semi-infinite channel reservoir if Region 2 has the same width as Region 1 and its length goes to infinity.

- The model must approach the behavior of the complex reservoir described in Chapter 3, a leaky fault separating two semi-infinite regions, if the vertical extent of each bounded region becomes very large.

- The model must approach the behavior of the complex reservoir we described in Chapter 4, which is a tee-shaped reservoir, if the L_{yD} of Region 1 and L_{x2D} of Region 2 become infinite.

- The model must approach the behavior of the complex reservoir described in Chapter 5, which is a channel-splay reservoir, if the L_{xD} of Region 1 becomes infinite. Furthermore, if both L_{xD} of Region 1 and L_{x2D} of Region 2 become infinite, a the system will approach the behavior of two infinite channel reservoirs communicating over a small area.

The asymptotic behavior of the pressure derivative solution for bounded reservoirs is derived in Appendix D. At very large time when the flow in Region 1 and Region 2 become pseudosteady state flow, and when the rate of fluid flow through the leaky fault becomes approximately constant, the pressure derivative at the producing well is approximately given by

$$\frac{dp_{D,1}}{d(\ln t_{D,1})} \rightarrow \frac{2\pi t_D}{L_{xD}L_{yD} + C_S L_{x2D} L_{y2D}}. \tag{6.8}$$

Note that the characteristic length used differs from case to case. As before, Q_{fD} is the late time stabilized rate of flow from the injection "vertically-fractured" well at the junction of the two regions in RB/D per RB/D of production from the actual well. At late times,

$$Q_{fD} \rightarrow \frac{2}{1 + \frac{1}{C_S}\frac{L_{xD}L_{yD}}{L_{x2D}L_{y2D}}}. \tag{6.9}$$

When the upper channel, (Region 2), is semi-infinite we get another limiting case for tee-shaped reservoirs. We can derive the following limits. At early time where the effect of the upper channel is not "felt",

$$\frac{dp_{D,1}}{d(\ln t_{D,1})} \rightarrow \sqrt{\pi t_D}. \tag{6.10}$$

At late time when the pressure drop in the upper channel is given by the semilog equation, we can show that

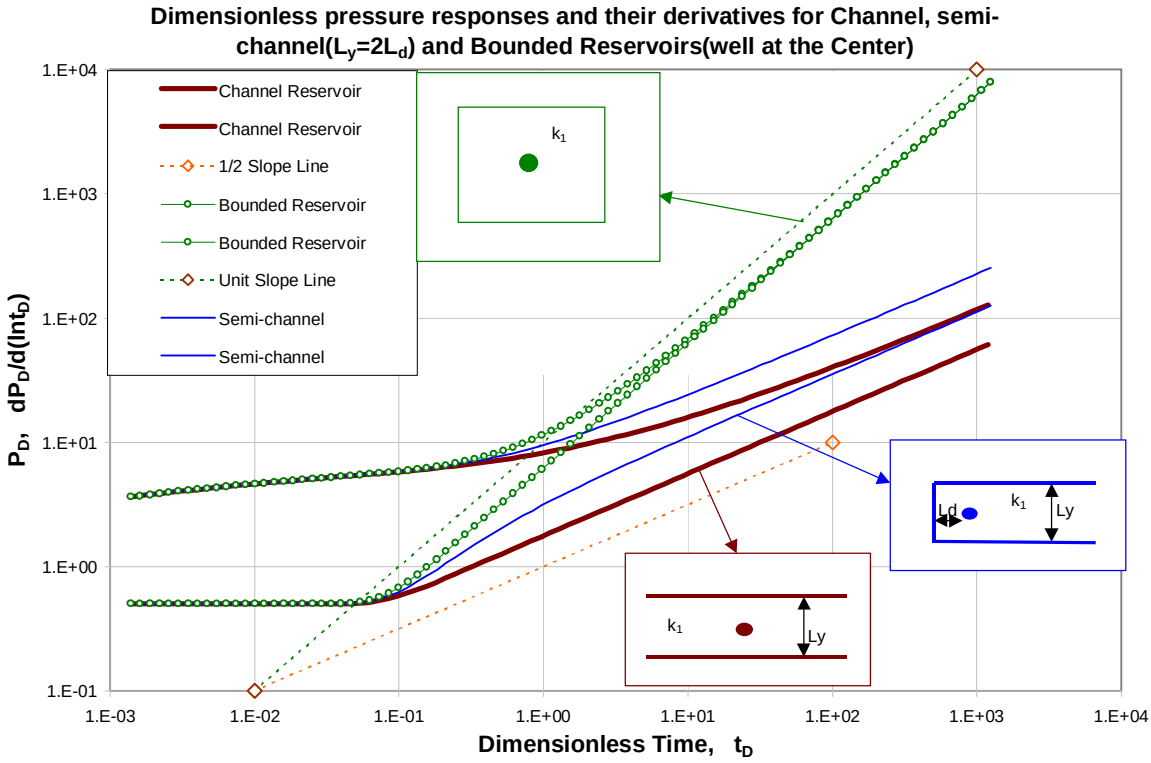

Figure 6.2: The limiting cases for communicating bounded reservoirs

$$\frac{dp_{D,1}}{d(\ln t_{D,1})} \rightarrow \frac{2\sqrt{\pi t_D}}{1+2C_T\sqrt{\pi t_D}}. \tag{6.11}$$

6.2.2 Approximation of infinite channel and semi-infinite channel reservoirs

Basically, there are several ways to form an infinite channel and/or semi-infinite channel by varying the dimensions of Region 1 and Region 2. For example, if we assume $L_{xD} = L_{x2D} = L_{wD}$, we can approach either an infinite channel or a semi-infinite channel reservoir by varying the L_{yD}, L_{y2D} values and/or the well location. Fig. 6.3 shows the effect of increasing the L_{y2D} value only with the well location fixed

at $(\frac{L_{xD}}{2}, \frac{L_{xD}}{2})$. In order to compare with the previously-presented channel reservoir results, the width of Region 1, L_{xD}, is chosen as the characteristic length.

Let $L_{xD} = L_{x2D} = L_{wD} = 1$, so that the well is located at the center of Region 1. A semi-infinite channel reservoir is approached as L_{y2D} goes to infinity. As expected, the derivative response successively reflects radial flow, linear channel flow, and finally bounded reservoir flow. For example, in Fig. 6.3 with $L_{y2D} = 20$, when $t_D < 0.1$, $\frac{dp_D}{d(\ln t_D)} = 0.5$. For $0.1 < t_D < 100$, the pressure derivative is the same as the semi-infinite channel behavior; i.e., linear flow. When $t_D > 100$, the derivative curve has a unit slope which indicates the pseudosteady state flow in a bounded reservoir.

The dimensionless time, $t_{D,dev1}$, when $\frac{dp_D}{d(\ln t_D)}$ deviates from linear flow can be obtained by equating Eq. D.10 and Eq. 6.8 as

$$t_{D,dev1} = \frac{L_{yD}^2}{\pi}\left(1 + C_S\frac{L_{x2D}L_{y2D}}{L_{xD}L_{yD}}\right)^2. \tag{6.12}$$

By using this equation, the computed dimensionless times at which linear flow ends for the cases in Fig. 6.3 are 2.865 and 140.4 for cases of $L_{y2D} = 2$ and $L_{y2D} = 20$ respectively. Checking against those curves in Fig. 6.3, we find that the times to the end of linear flow dimensionless time are reasonably estimated.

The case of varying both L_{yD} and L_{y2D} to approach the infinite channel has been verified and shown as Fig. 6.4. The well location is $(\frac{L_{xD}}{2}, L_{yD} - 1)$. Linear channel flow can be observed when L_{yD} and L_{y2D} are large enough. The dimensionless time, $t_{D,dev2}$, when $\frac{dp_D}{d(\ln t_D)}$ deviates from linear flow can be estimated by the following equation,

$$t_{D,dev2} = \frac{L_{yD}^2}{4\pi}\left(1 + C_S\frac{L_{x2D}L_{y2D}}{L_{xD}L_{yD}}\right)^2. \tag{6.13}$$

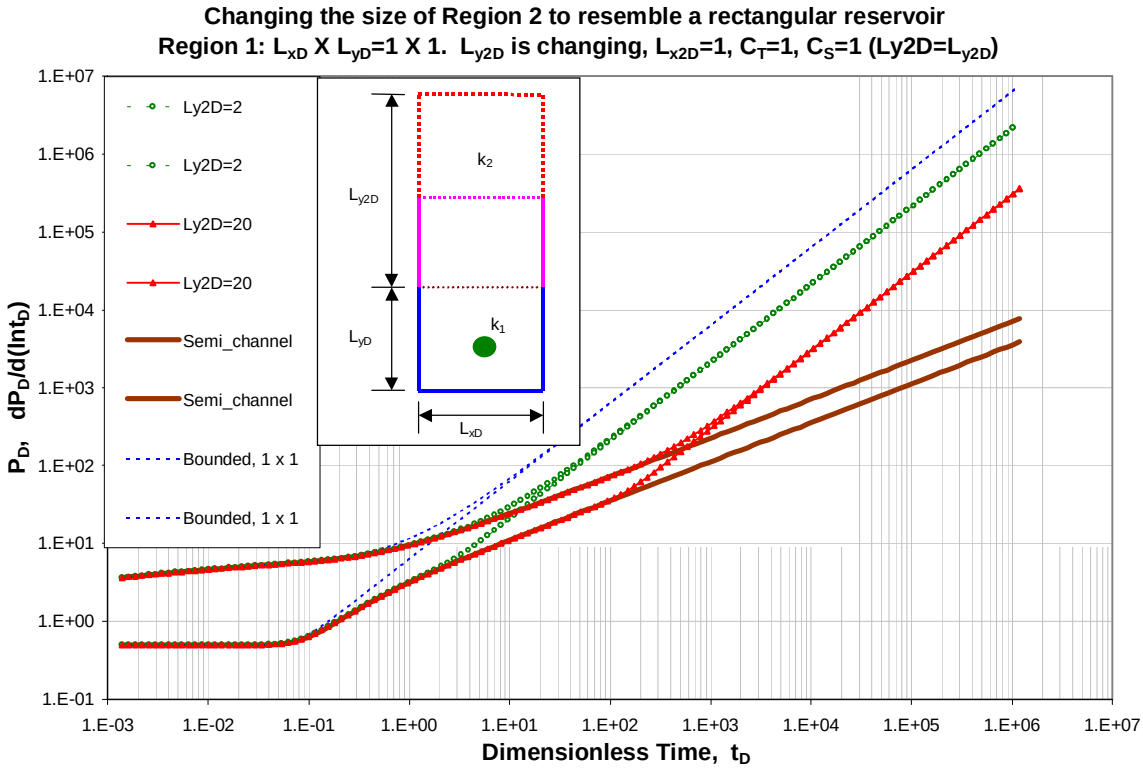

Figure 6.3: Manipulating the size of Region 2 to resemble the responses of a well located in a rectangular reservoir

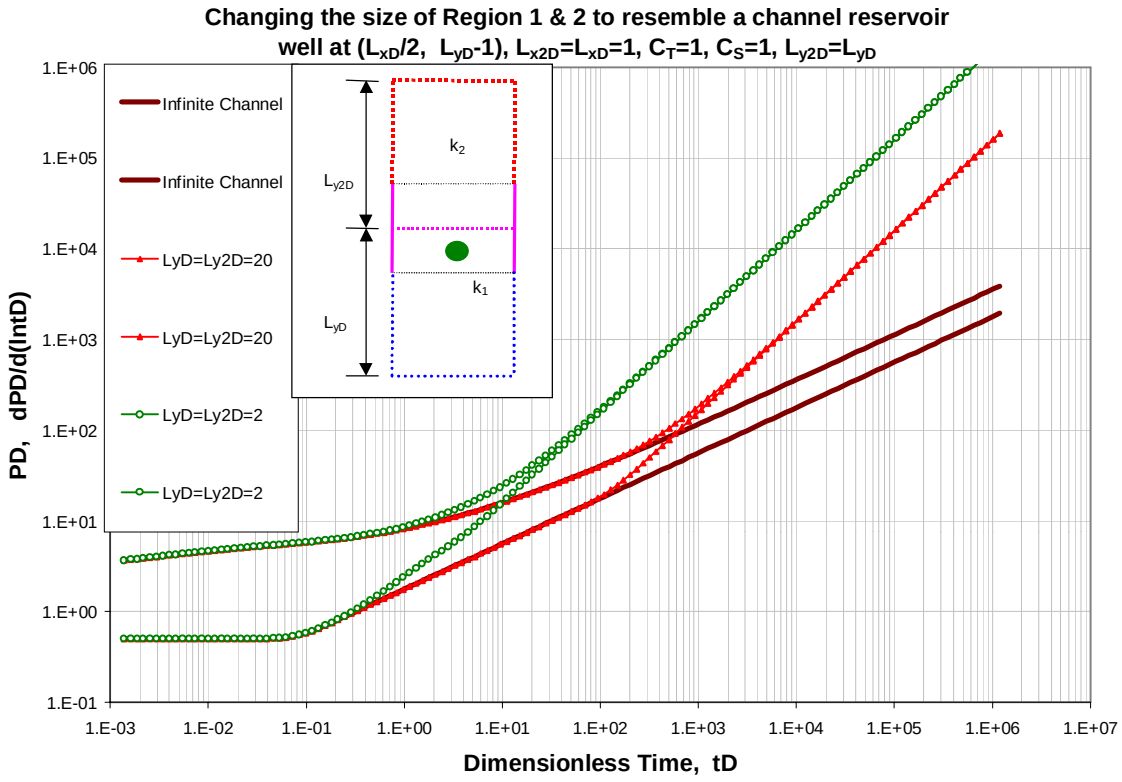

Figure 6.4: Simulating the channel behaviors by setting the well at $(\frac{L_{xD}}{2}, L_{yD} - 1)$

6.2.3 Approximation of leaky fault infinite reservoirs

In this case, the 2-D sizes of Region 1 and Region 2 are increased in both the x-direction and y-direction proportionally to simulate the behavior of a well located in a leaky fault reservoir. The legend of Fig. 6.5 is expressed in terms of $L_{xD} \times L_{yD}$ (or, $L_{x2D} \times L_{y2D}$, since they are the same in this case). The distance from well to the fault, L_d, is selected as the characteristic length as was done in the leaky fault reservoir problem. Fig. 6.5 shows the late derivative can be predicated by Eq. 6.8 and it is still a unit slope line. The corresponding total fluid injection rate from Region 2 is shown in Fig. 6.6. As Eq. 6.9 indicates, the late time injection rate is dominated by the sizes of those two regions. In this case all curves go to a unit value at late time since $\dfrac{L_{xD} \times L_{yD}}{L_{x2D} \times L_{y2D}} = 1$, and $C_S = 1$.

An examination of Fig. 6.5 in detail is given in Fig. 6.7 and also shows us how the leaky fault infinite reservoir behaviors are being approached. All derivative curves are superposed on the leaky fault reservoir curve of $L_{wD} = 1$ in this case. Referring to the curve of $L_{wD} = 1$ in Fig. 3.4, the integration of leaky fault reservoir and communicating bounded reservoir in our simulation model becomes apparent. The dashed lines in this figure are plotted to compare the behaviors of a well located in a bounded reservoir (without a fault) of the same size. Their derivative will remain as 0.5 before feeling the influence from the boundaries. The diagnostic profile is shown in Fig. 6.8.

The dimensionless time, $t_{D,dev3}$, when $\dfrac{dp_D}{d\ln t_D}$ deviates from the derivative curve of the leaky fault reservoir can be derived by equating Eq. 3.16 and Eq. 6.8; this yields

$$t_{D,dev3} = \frac{L_{xD}L_{yD} + C_S L_{x2D} L_{y2D}}{2\pi\,(1 + C_T)} \tag{6.14}$$

$$= \frac{L_{xD}L_{yD}}{2\pi\,(1 + C_T)} \left(1 + C_S \frac{L_{x2D}L_{y2D}}{L_{xD}L_{yD}}\right). \tag{6.15}$$

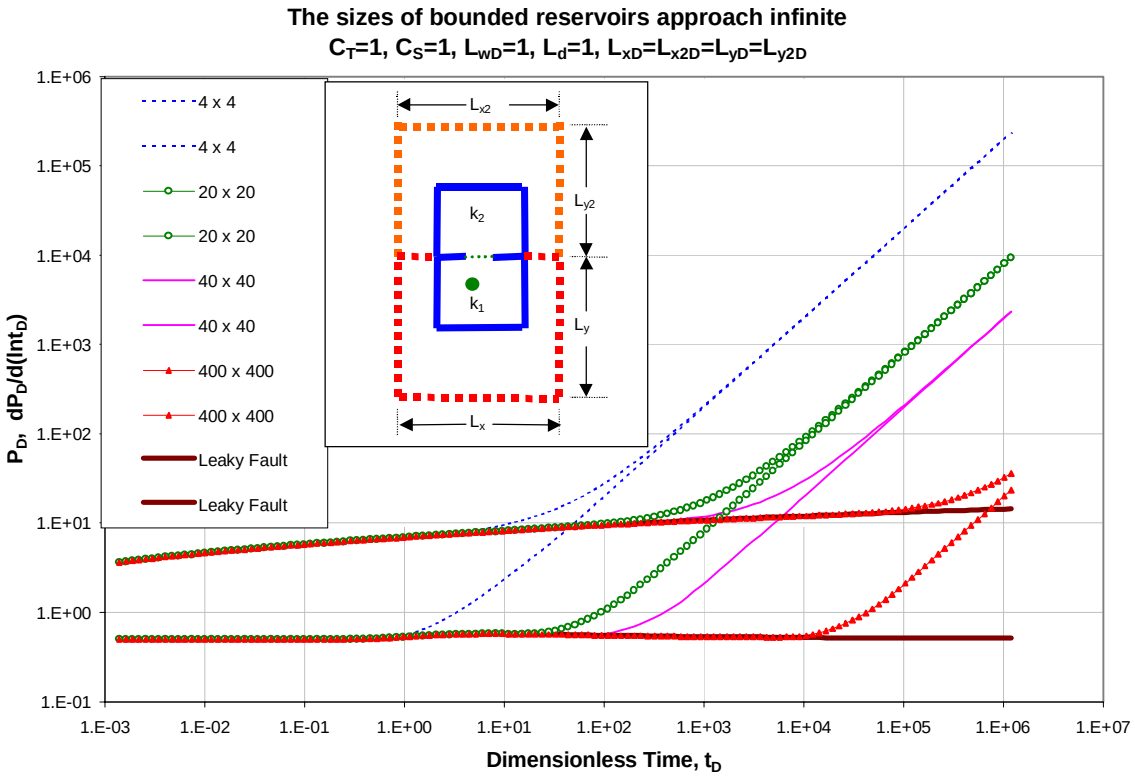

Figure 6.5: Increasing the sizes of Region 1 and Region 2 equivalently to approach the leaky fault infinite reservoir

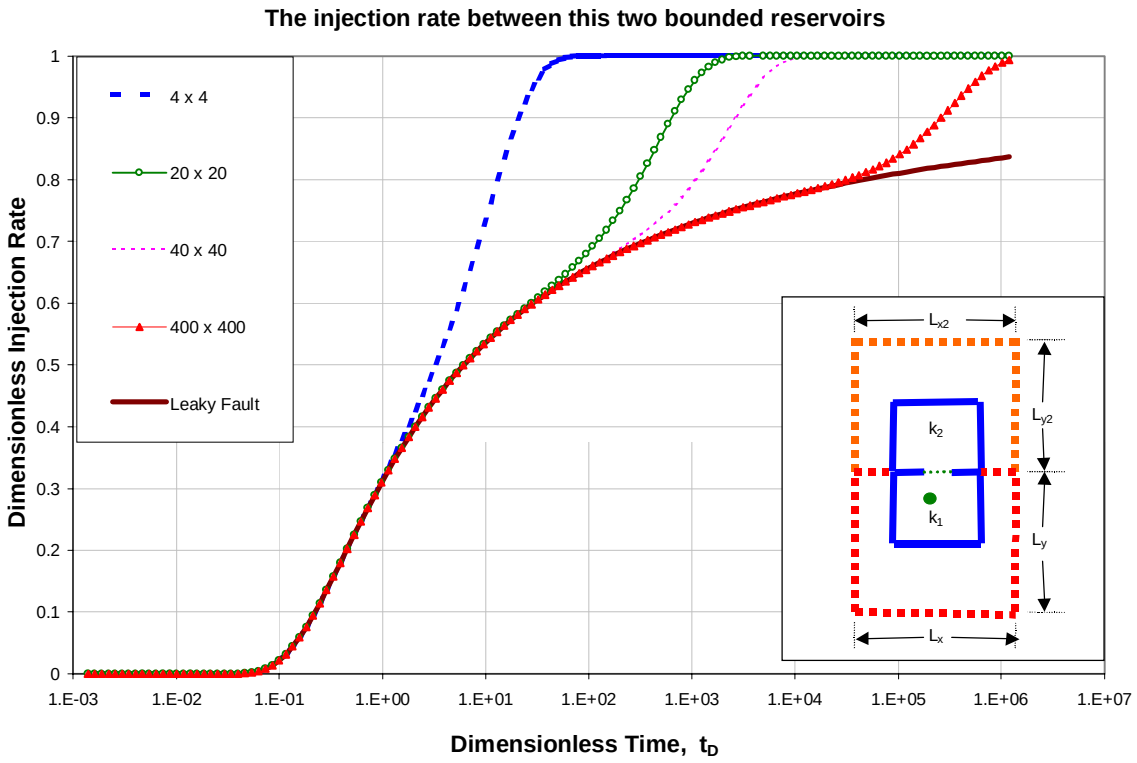

Figure 6.6: The total fluid injection rate compared with leaky fault infinite reservoir

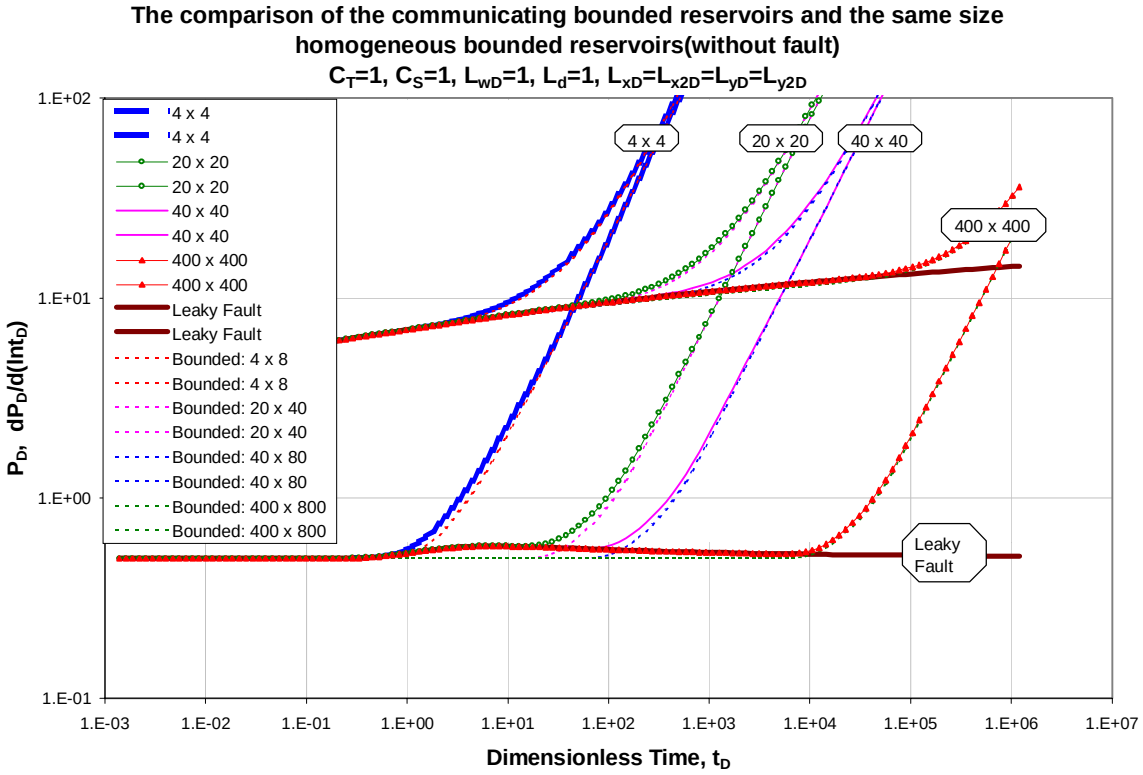

Figure 6.7: Comparison of communicating bounded reservoirs and "leaky-fault" reservoirs

For Fig. 6.8, the $t_{D,dev3}$ value estimate is 63.66 which is larger than the actual deviation time (around 20.0). Referring to Fig. 3.3, we know that $\frac{dp_D}{d(\ln t_D)}$ approaches the asymptotic limit of $\frac{1}{1+C_T}$ very slowly. Therefore the estimate $t_{D,dev3}$ will overestimate the actual value.

Line 4 is the derivative curve of a bounded unit volume reservoir, which displays a unit slope. Line 3 is the late time approximation of the bounded leaky fault reservoir. Choosing point A, (1.7, 10.0), and point B, (1300.0, 10.0), on line 4 and line 3 at the same $\frac{dp_D}{d(\ln t_D)}$ value, respectively and applying the related equations in Appendix D, we have

$$L_{xD}L_{yD} + C_S L_{x2D} L_{y2D} = \frac{t_{D,point,B}}{t_{D,point,A}} \tag{6.16}$$

$$= 764.7. \tag{6.17}$$

If we still use $C_S = 1$, then the estimated volume is 764.7 and the actual volume is $20 \times 20 + 20 \times 20 = 800$. The error is 4.4%.

6.2.4 Approximation of tee-shaped reservoirs

The tee-shaped reservoirs can also be approached by increasing L_{yD} and L_{x2D}. In order to compare with the results in Chapter 4, the distance from the well to the tee-channel, L_d, is chosen as the characteristic length. Let $C_T = C_S = C_R = 1$ in this case. Considering the $L_{yD} = 400, L_{x2D} = 400$ in Fig. 6.9 as an example, as $t_D < 0.1$, $\frac{dp_D}{d(\ln t_D)} = 0.5$. For $0.1 < t_D < 10^4$, the pressure derivative is the same as the behavior of a tee-shaped reservoir. When $t_D > 10^4$, the derivative curve is gradually increasing to a unit slope which indicates a bounded reservoir. The tee-shaped reservoir curve is the one shown in Fig. 4.5 and Fig. 4.7.

The total dimensionless injection rate from the vertically-fractured "injection" well is plotted in Fig. 6.10. At late time pseudosteady state flow is attained

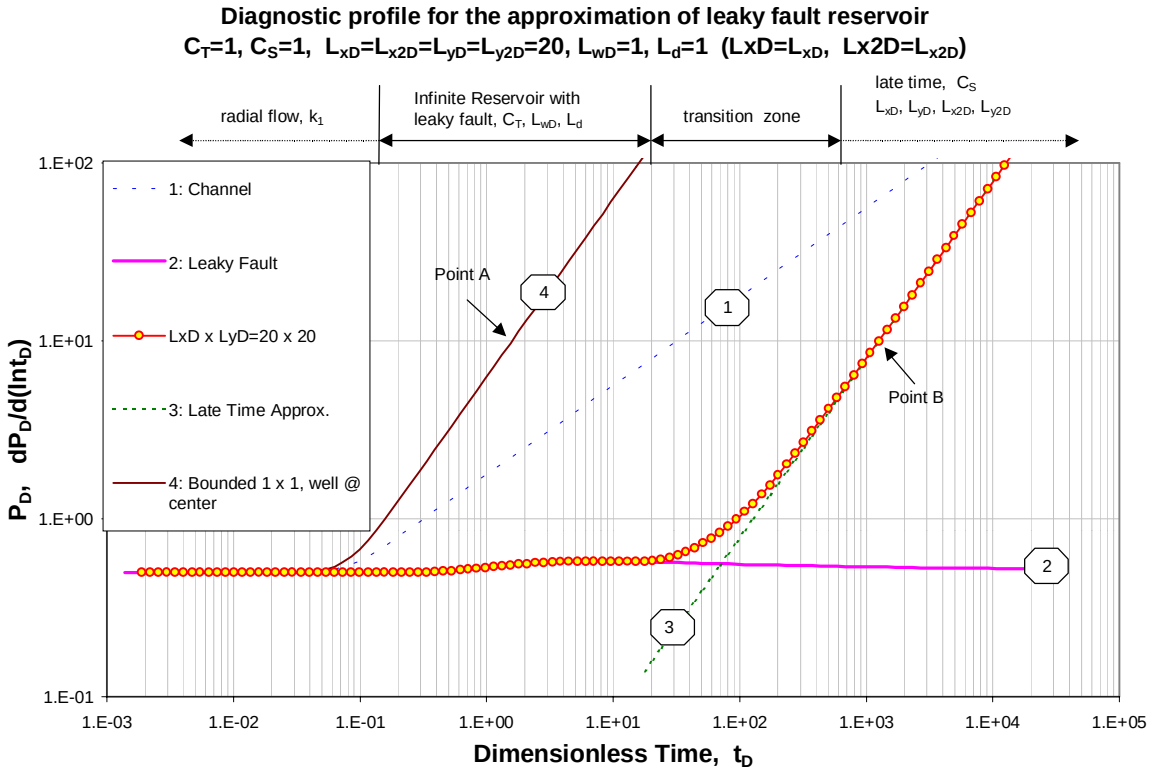

Figure 6.8: Diagnostic profile from the approximation of leaky fault reservoir

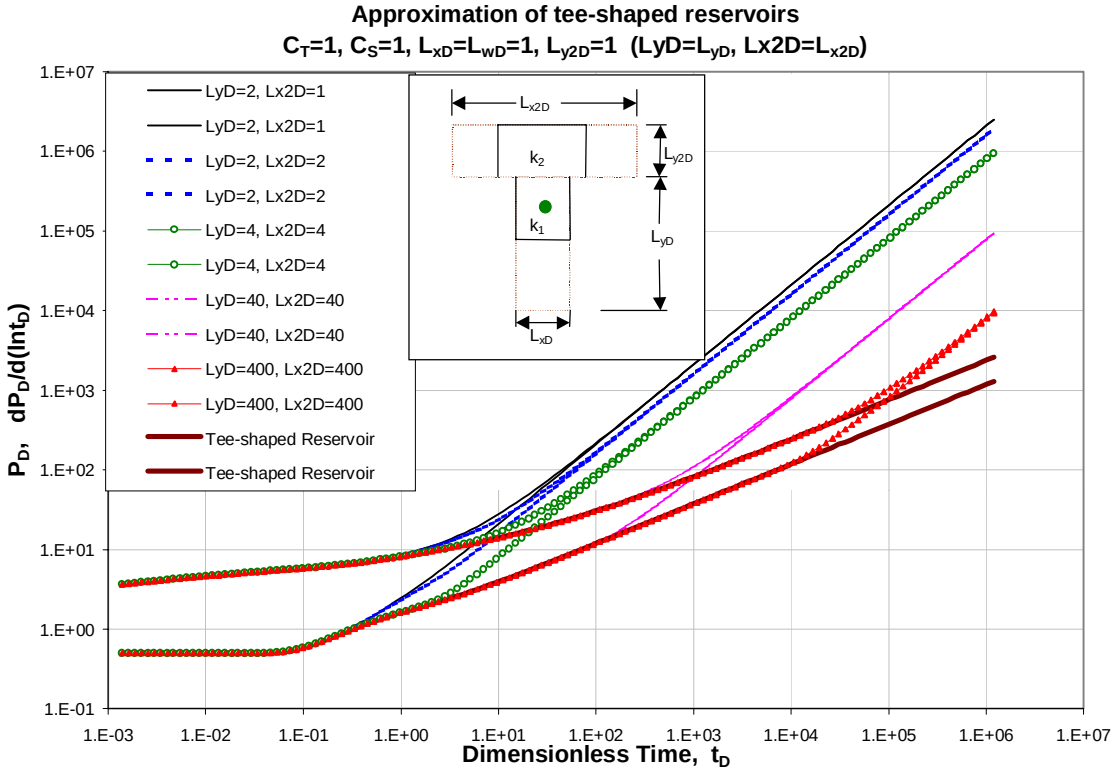

Figure 6.9: Approaching tee-shaped reservoirs by changing L_{yD} and L_{x2D} proportionally

since Q_{fD} is close to 1. Notice that the differences between Fig. 6.10 and Fig. 6.6 are because of the different boundary conditions.

In Fig. 6.11, line 1 is the late time behavior of the vertical channel, line 2 is the late-time derivative approximation of tee-shaped reservoir and line 3 is the late time approximation of the whole bounded system. Curve 4 is the derivative of a tee-shaped reservoir and line 5 is the $\frac{dp_D}{d(\ln t_D)}$ curve of a bounded unit volume reservoir which has a unit slope. The dimensionless time, $t_{D,dev4}$, when $\frac{dp_D}{d(\ln t_D)}$ deviates from the derivative curve of the tee-shaped reservoir can be derived by equating Eq. D.34 and Eq. 6.8; the expression for this time is

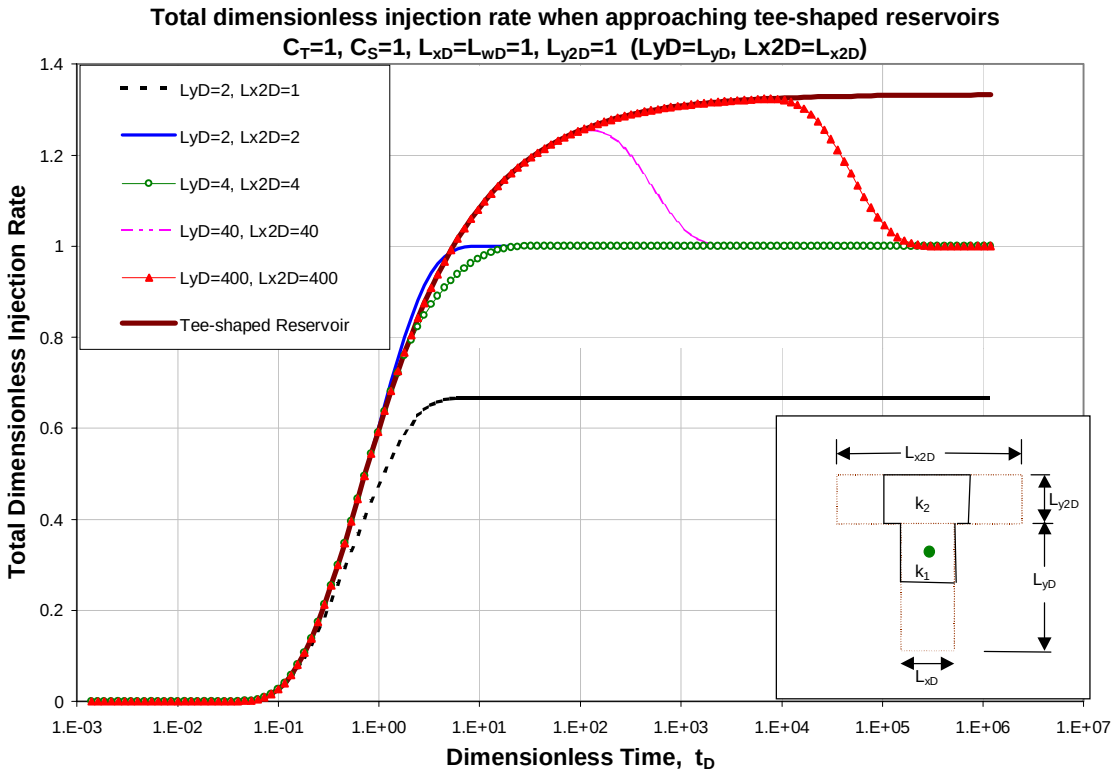

Figure 6.10: The total dimensionless injection rate with increasing L_{yD} and L_{x2D}

$$t_{D,dev4} = \frac{1}{\pi}\left(\frac{L_{xD}L_{yD} + C_S L_{x2D}L_{y2D}}{L_{xD} + 2\sqrt{C_T C_S}L_{y2D}}\right)^2 \tag{6.18}$$

where L_d is defined as the characteristic length. Using the conditions in Fig. 6.11, the $t_{D,dev4}$ value estimate is 22.64 which is a good estimate of the actual deviation time. We have noticed that, before $t_{D,dev4}$ the derivative curve can be reproduced successfully by tee-shaped reservoir model.

Referring to Lines 5 and 3, Eq. 6.16 is applicable. Applying the same method to point C on line 1 and point D on line 2, will give us

$$\sqrt{C_T C_S}L_{y2D} = \sqrt{\frac{t_{D,point,D}}{t_{D,point,C}}} - \frac{1}{2} \tag{6.19}$$

and

$$L_{xD}L_{yD} + C_S L_{x2D}L_{y2D} = \frac{t_{D,point,B}}{t_{D,point,A}}. \tag{6.20}$$

6.2.5 Approximation of two communicating parallel channels

By increasing L_{xD} and L_{x2D}, our model can approach the case of hydraulic communication between two parallel channels. To compare with the results in Chapter 5, L_{yD} is chosen as the characteristic length. Considering Fig. 6.12, parallel channel behavior is approached at very large L_{xD} and L_{x2D} values. The related total injection rate is shown in Fig. 6.13. Comparing this figure with Fig. 6.10 shows the effect of boundary conditions. Note that the lowest curve, which has a half slope, denoted as "parallel channels" in Fig.5.2, is one of the limiting cases in Fig. 5.2.

In Fig. 6.14, we focus on the analysis of the line with shaded circles. This line was computed for a bounded communicating parallel channel system with $C_T = 10$,

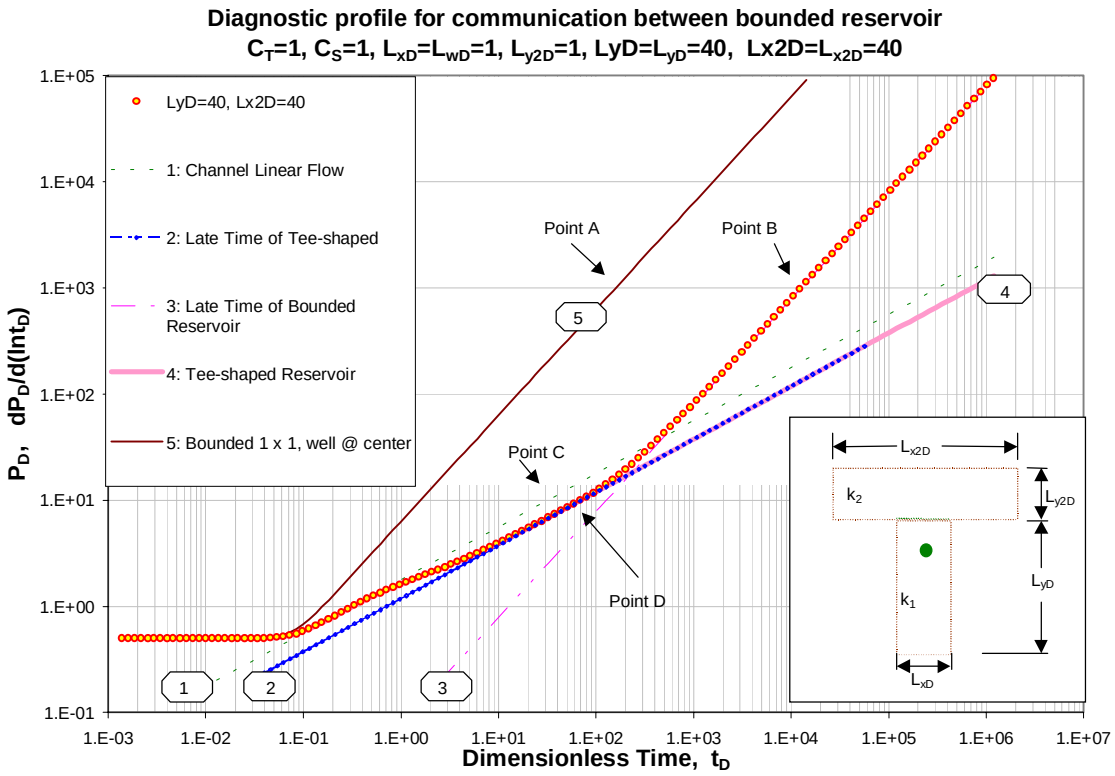

Figure 6.11: Diagnostic profile for communicating bounded reservoirs

$C_S = 1$, $L_{yD} = Ly_{2D} = 1$, $L_{wD} = 1$, $L_{xD} = L_{xD} = 400$ and $L_{x2D} = L_{x2D} = 400$, as stated in Fig. 6.14. The well is located at the center of the lower horizontal channel and is displaced from the center of the gap with a dimensionless distance 2, i.e., $X_{DV} = 2$. Line 5 is the late time derivative behavior of this case. Line 1 is the behavior of a well located at the center of a bounded unit volume, (dimensionless size is 1×1), reservoir. Line 2 is the behavior of a well, located at the channel center, in a channel which has a dimensionless width 1. Line 3 is the behavior of a well in an infinite parallel channel system, where the lower and upper bounded channels have a dimensionless width 1 and $C_T = 10$ is assumed. Line 4 is the late time derivative approximation of the two infinite parallel channels with the corresponding properties.

When $t_D < 10^2$, line 3 matches with the dotted circle line very well. The dimensionless time, $t_{D,dev5}$, when $\dfrac{dp_D}{d(\ln t_D)}$ deviates from the derivative curve of the parallel channel reservoir, is given by equating Eq. 6.8 and Eq. D.57

$$t_{D,dev5} = \frac{1}{4\pi}\left(\frac{L_{xD} + C_S L_{x2D} L_{y2D}}{1 + \sqrt{C_T C_S} L_{y2D}}\right)^2 \tag{6.21}$$

where L_y is defined as the characteristic length and $L_{yD} = 1$.

In Fig. 6.14, as before, from line 1 and 5 we have

$$L_{xD} L_{yD} + C_S L_{x2D} L_{y2D} = \frac{t_{D,point,B}}{t_{D,point,A}} \tag{6.22}$$

and from line 2 and 4, we get

$$\sqrt{C_T C_S} L_{y2D} = \sqrt{\frac{t_{D,point,D}}{t_{D,point,C}}} - 1. \tag{6.23}$$

In this case, Point A, Point B, Point C and Point D are read as $(16.0, 100.0)$, $(13000.0, 100.0)$, $(31.0, 10.0)$ and $(530.0, 10.0)$, respectively. Applying Eq. 6.22 we have

$$L_{xD}L_{yD} + C_S L_{x2D} L_{y2D} = \frac{13000}{16.0} - 1 = 811.5. \tag{6.24}$$

The real volume is $400 \times 1 + 400 \times 1 = 800$. Then the error of the above estimate is 1.4%. Applying Eq. 6.23 we have

$$\sqrt{C_T C_S} L_{y2D} = \sqrt{\frac{t_{D,point,D}}{t_{D,point,C}}} - 1 = \sqrt{\frac{530.0}{31.0}} - 1 = 3.135. \tag{6.25}$$

If we still assume $C_S = 1$ and $L_{y2D} = 1$ in Eq. 6.25, we have a estimate of C_T value as 9.83. Comparing to the real value, $C_T = 10$, the error is 1.7%.

6.2.6 Approximation of channel-splay reservoirs

The behaviors of the channel-splay reservoirs as we have studied in Chapter 5 can be approach by our communicating bounded reservoirs model. Fig. 6.15 shows the channel-splay reservoir approximation when L_{xD} is increased. The size of the splay in Fig. 6.15 is chosen as $L_{x2D} \times L_{y2D} = 1 \times 1$. Fig. 6.16 is the related dimensionless injection rate from the splay part. Take the dashed lines, with $L_{xD} = 40$, as an example; for $t_D < 0.1$, $\dfrac{dp_D}{d(\ln t_D)} = 0.5$. For $0.1 < t_D < 10$, the pressure derivative exhibits the same behavior as a channel-splay reservoir. For $10 < t_D < 10^2$, the pressure derivative indicates linear (channel) flow, i.e., half slope. When $t_D > 10^2$, the derivative curve gradually approaches a unit slope which indicates a bounded reservoir.

The dimensionless time, $t_{D,dev6}$, when the $\dfrac{dp_D}{d(\ln t_D)}$ curve deviates from that of channel and splay reservoir, is the cross point of line 1 and line 3 (or 2), and can be determined by equating Eq. 6.8 and Eq. D.40 as

$$t_{D,dev6} = \frac{L_{xD}^2}{4\pi} \tag{6.26}$$

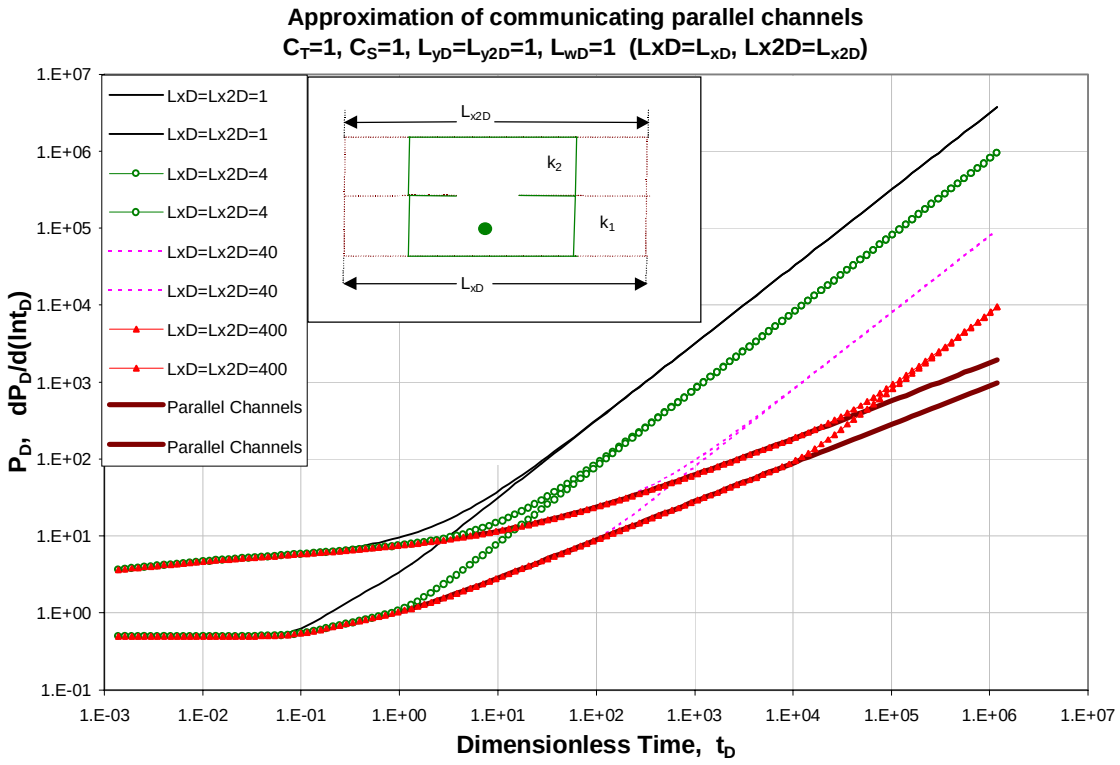

Figure 6.12: Approximation of two communicating parallel channels by increasing L_{xD} and L_{x2D}

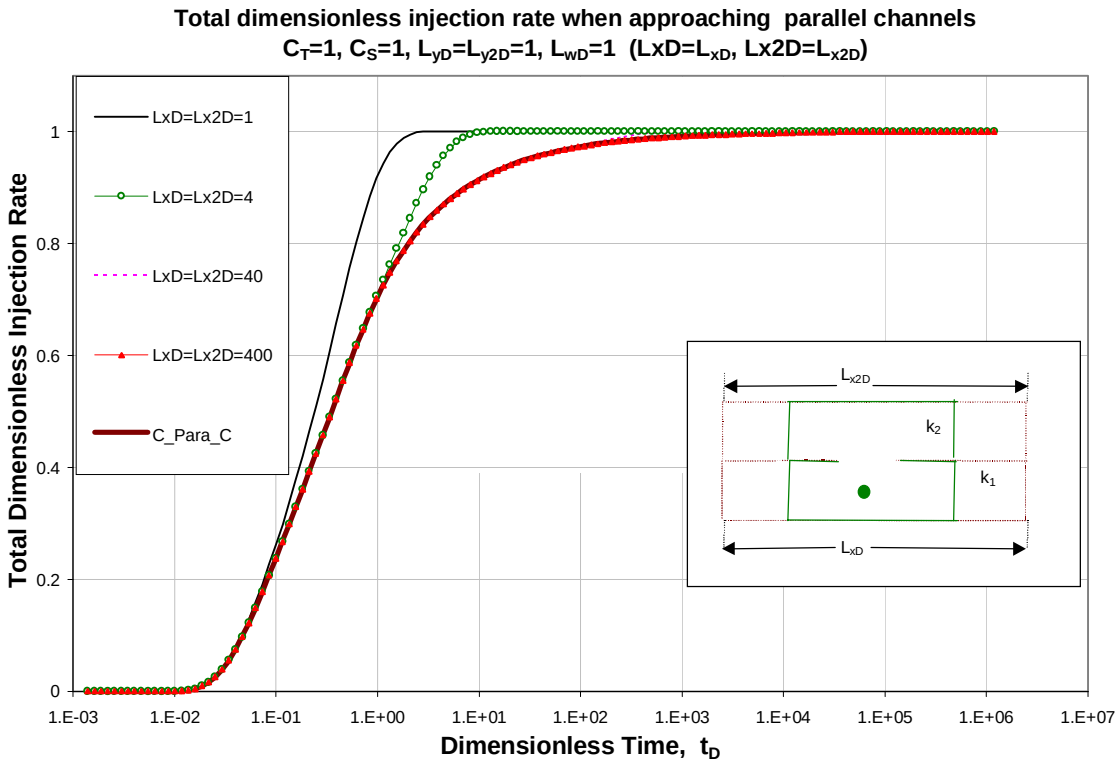

Figure 6.13: Total injection rate when increasing L_{xD} and L_{x2D} to approach communicating parallel channels

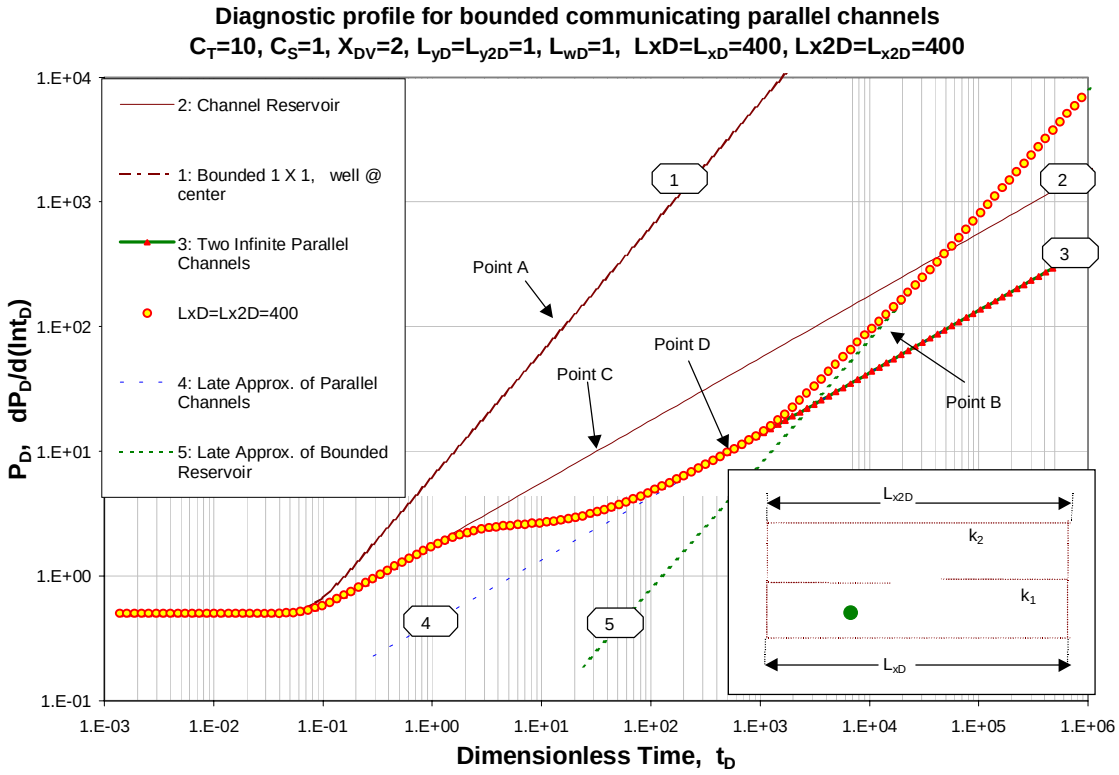

Figure 6.14: The diagnostic profile for the case of two bounded communicating parallel channels, $X_{DV} = 2$

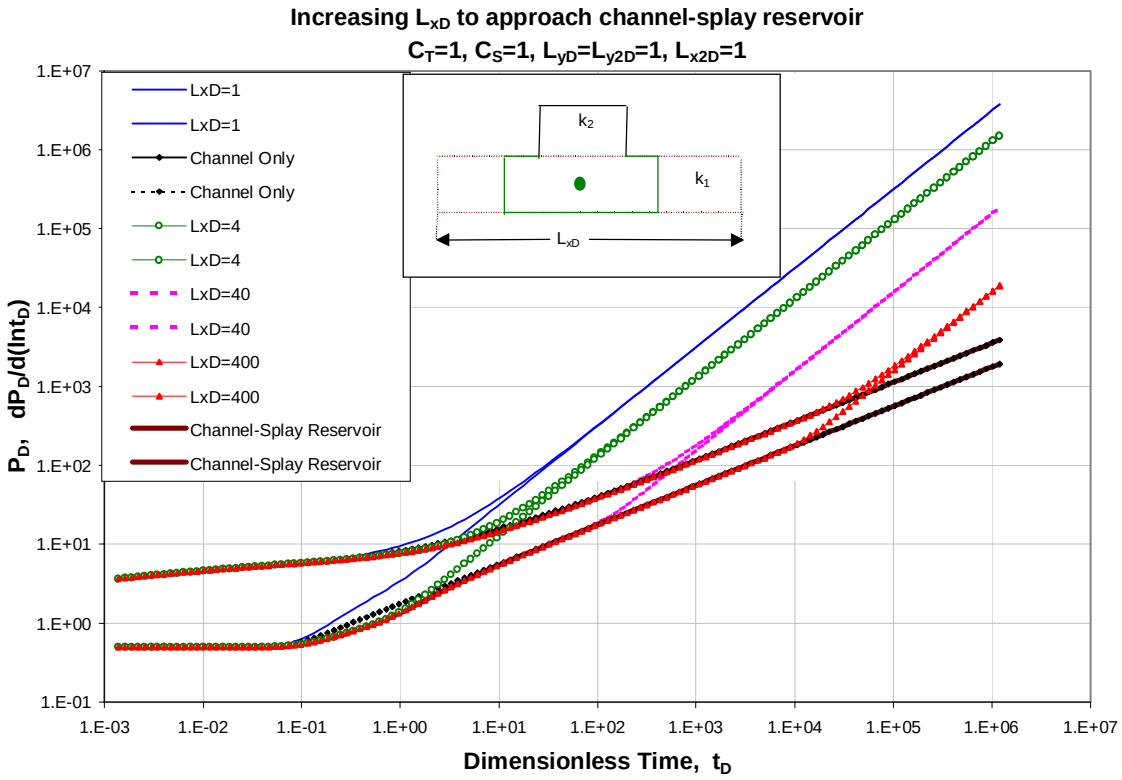

Figure 6.15: Approaching channel-splay reservoirs by increasing L_{xD}

where L_y is defined as the characteristic length and $L_{yD} = 1$. Eq. 6.16 is still applicable here.

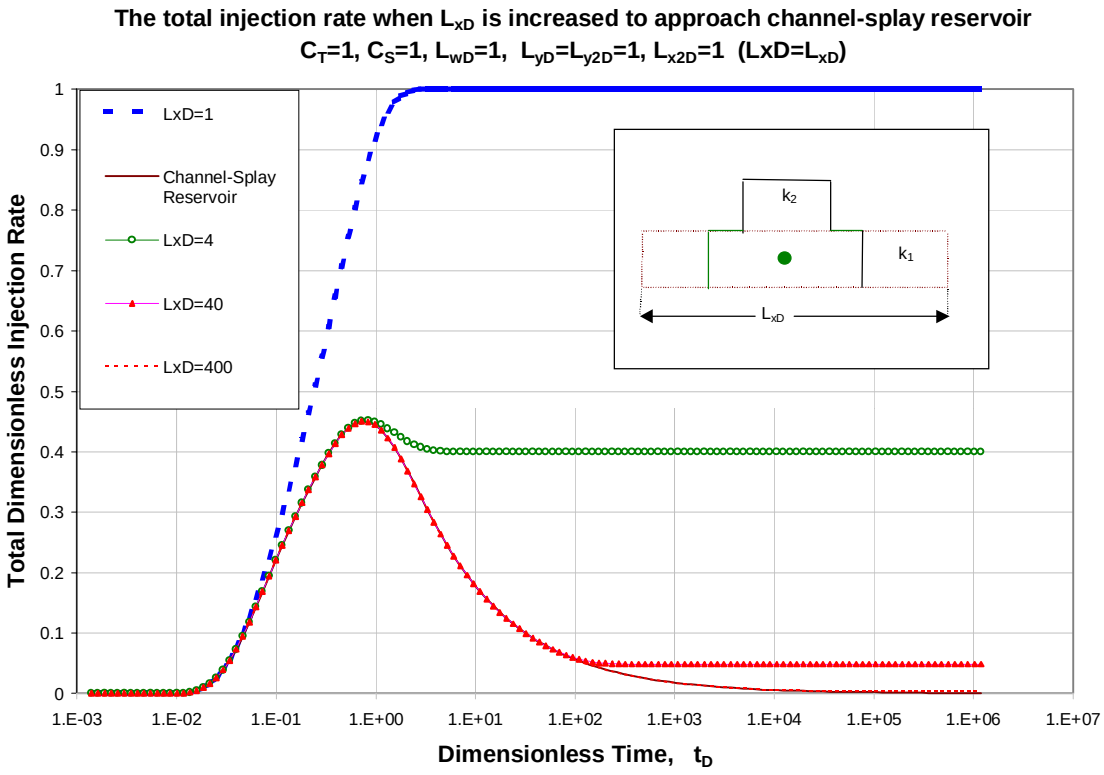

Figure 6.16: The total dimensionless injection rate as L_{xD} is increased

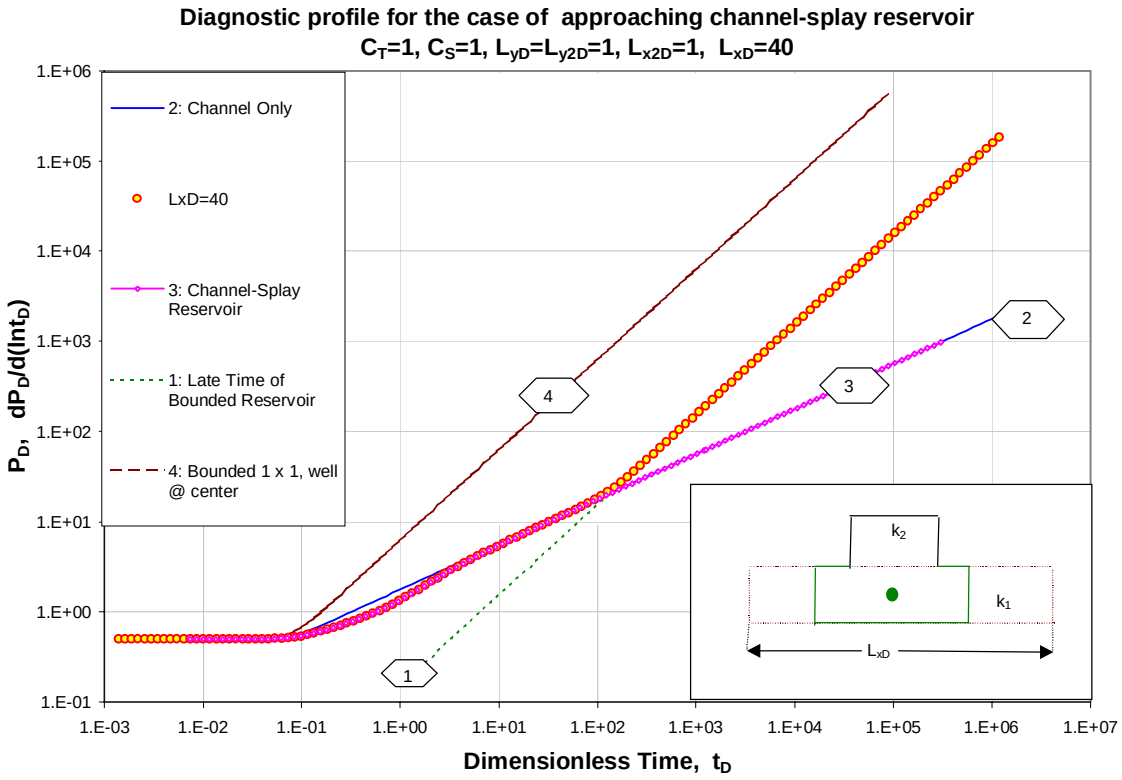

Figure 6.17: The diagnostic profile for the case of channel splay reservoir approximation, $L_{xD} = 40$

CHAPTER VII

CONCLUSIONS

In this dissertation, we have described a general method of modeling pressure drops in complex reservoirs typical of those found in fluvial-deltaic environments. The method consists of decomposing the complex reservoir into a series of simple-geometry homogeneous reservoirs for which analytical solutions are readily obtainable, then coupling the systems at the zones of hydraulic contact. The resulting system of equations are solved in Laplace space for the flow between the coupled reservoir systems. Since analytical Laplace transforms are not generally available for pressure drops written in terms of source/sink functions, we have had to resort to numerical Laplace transform techniques. In Appendix A, we provide a complete set of source functions for any system in terms of Elliptic Theta functions [12]. We also provide a new technique of finding Laplace transforms of the products of these functions (that arise in general pressure solutions), that provides the accuracy required for our computations at a reasonable speed.

We have presented results for a variety of different complex-geometry systems: a well in a semi-infinite system with a leaky fault that allows fluid transfer from another semi-infinite system, a well in one branch of a tee-shaped reservoir, a well in channel and splay reservoir, and a well in communicating bounded reservoir. For each of these systems, we have provided asymptotic expressions for long-time pressure derivative behavior. We have showed that our computed pressure responses agree favorably with the asymptotic expressions, and with well-known analytic results in limiting cases where the complex systems should physically approach the response of simple-geometry systems.

REFERENCES

[1] H. Stehfest, Numerical Inversion of Laplace Transforms, Communications of ACM **13, No. 1**, 47–49 (1970).

[2] L. Larsen, Pressure Transient Behavior of Reservoir Forming a Pattern of Coupled Linear Segments, in *paper SPE 26459 presented at the 68th Annual Technical Conference and Exhibition of the Society of Petroleum Engineers, Houston,TX, Oct. 3-6*, 1993.

[3] L. Larsen, Pressure Transient Behavior of Wells Producing from Complex Pattern of Interconnected Linear Segments, in *paper SPE 36549 presented at the Annual Technical Conference and Exhibition of the Society of Petroleum Engineers, Denver, CO. Oct. 6-9*, 1996.

[4] G. Stewart, A. Gupta, and P. Westaway, The Interpretation of Interference Tests in a Reservoir with Sealing and Partially Communicating Faults, in *paper SPE 12967 presented at the 1984 European Petroleum Conference, London, England, Oct.25-28*, 1984.

[5] L. M. Yaxley, Effect of Partially Communicating Fault on Transient Pressure Behavior, SPE Formation Evaluation , 590–595 (1987).

[6] A. K. Ambastha, P. G. McLeroy, and A. S. Grader, The Interpretation of Interference Tests in a Reservoir with Sealing and Partially Communicating Faults, SPE Formation Evaluation , 210–218 (1989).

[7] M. D. Abbaszadeh and H. Cinco-Ley, Pressure Transient Behavior in a Reservoir with a Finite-Conductivity Fault, in *SPE paper 24704 presented at the 1992 Annual Technical Conference and Exhibition of the Society of Petroleum Engineers, Washington DC, Oct. 4-7*, 1992.

[8] A. Sahni and D. G. Hatzignatiou, Pressure Transient Analysis in Multilayered Faulted Reservoirs, in *paper SPE 29674 presented at the 1995 Western Region Conference and Exhibition, Bakersfield, CA. March 8-10*, 1995.

[9] M. D. Abbaszadeh and H. Cinco-Ley, Interference Testing in Reservoirs With Conductive Faults or Fractures, in *paper SPE 38941 presented at the 1997 Annual Technical Conference and Exhibition of the Society of Petroleum Engineers, San Antonio, TX, Oct. 5-8*, 1997.

[10] L. Thompson and K. Temeng, Automatic Type-Curve Matching for Horizontal Wells, InSitu **18, Number 2**, 209–242 (1994).

[11] M. Onur and A. Reynolds, Well Testing Applications of Numerical Laplace Transformation of Sampled Data, in *paper SPE 36554 presented at the Annual Technical Conference and Exhibition of the Society of Petroleum Engineers, Denver, CO. Oct. 6-9*, 1996.

[12] F. Oberhettinger and L. Badii, *Table of Laplace Transforms*, Springer-Verlag, New York, 1973.

[13] W. T. V. William H. Press, Saul A. Teukolsky and B. P. Flannery, *Numerical Recipies in C - The Art of Scientific Computing*, Cambridge University Press, 1992.

[14] M. Abramowitz and I. A. Stegun, *Handbook of Mathematical Functions With*

Formulas, Graphs, and Mathematical Tables, United States Department of Commerce, National Bureau of Standards Applied Mathematics Series 55, 1972.

NOMENCLATURE

Ct = the total compressibility of the reservoir, 1/psi.

h = the thickness of the reservoir, ft.

k = the permeability of the reservoir, md.

l = the characteristic length, ft.

L_f = the half length of the fracture, ft.

$p(x, y, t)$ = pressure drop at (x, y), psi.

q_{0D} = production or injection rate of the well, rb/day.

q_{fD} = production or injection flux of the fracture well, rb/ft/day.

Q_{fD} = production or injection rate of the fracture well, rb/day.

t = the time variable, in days.

x = the horizontal coordinate, ft

y = the vertical coordinate, ft

η = the diffusivity of the reservoir.

ϕ = the porosity of the reservoir.

L_{xD} = the dimensionless width of the vertical channel.

L_{yD} = the dimensionless width of the horizontal channel.

q_{fD} = the dimensionless flux distribution of the fracture plane.

x'_D = the x direction coordinate of the well position.

y'_D is the y direction coordinate of the well position.

y''_D = the y direction coordinate of the image well position.

$x_{D,R}$ = the right hand side point of the fracture plane.

$x_{D,L}$ = the left hand side point of the fracture plane.

y_{fD} = the y direction coordinate of the fracture plane.

APPENDIX A

COMPUTATIONAL TECHNIQUES - SOURCE FUNCTIONS IN INFINITE AND BOUNDED SYSTEMS

A.1 One-Dimensional Source Functions

The following lists one-dimensional source functions in infinite and bounded systems with a variety of boundary conditions. Where possible, the source functions are expressed in terms of the elliptic theta functions[12] $\theta_2(z,t)$ and $\theta_3(z,t)$ where

$$\theta_2(z,t) = \frac{1}{\sqrt{\pi t}} \sum_{n=-\infty}^{\infty} (-1)^n \exp\left(-\frac{(z+n)^2}{t}\right) \tag{A.1a}$$

$$= \sum_{n=0}^{\infty} \cos\left((2n+1)\pi z\right) \exp\left(-\pi^2 \left(n+\frac{1}{2}\right)^2 t\right) \tag{A.1b}$$

and

$$\theta_3(z,t) = \frac{1}{\sqrt{\pi t}} \sum_{n=-\infty}^{\infty} \exp\left(-\frac{(z+n)^2}{t}\right) \tag{A.2a}$$

$$= \sum_{n=0}^{\infty} \varepsilon_n \cos\left(2n\pi z\right) \exp\left(-\pi^2 n^2 t\right) \tag{A.2b}$$

where

$$\varepsilon_n = \begin{cases} 1 & \text{for } n = 0 \\ 2 & \text{for } n = 1, 2, 3... \end{cases} \tag{A.3}$$

We also denote the leading term of Eq. A.1a and Eq. A.2a (i.e., when $n = 0$) as $\theta_L(z,t)$,

$$\theta_L(z,t) = \frac{1}{\sqrt{\pi t}} \exp\left(-\frac{z^2}{t}\right) \tag{A.4}$$

Infinite System: (L_x is arbitrary).

$$\Delta p_s\left(x,x',t,\tau\right)=\frac{dx'}{2L_x}\theta_L\left(\frac{x-x'}{2L_x},\frac{\eta\left(t-\tau\right)}{L_x^2}\right) \tag{A.5}$$

Semi-Infinite (with sealing fault at $x=0$) (L_x is arbitrary).

$$\Delta p_s\left(x,x',t,\tau\right)=\frac{dx'}{2L_x}\left(\theta_L\left(\frac{x-x'}{2L_x},\frac{\eta\left(t-\tau\right)}{L_x^2}\right)+\theta_L\left(\frac{x+x'}{2L_x},\frac{\eta\left(t-\tau\right)}{L_x^2}\right)\right) \tag{A.6}$$

Semi-Infinite (with constant pressure at $x=0$)

$$\Delta p_s\left(x,x',t,\tau\right)=\frac{dx'}{2L_x}\left(\theta_L\left(\frac{x-x'}{2L_x},\frac{\eta\left(t-\tau\right)}{L_x^2}\right)-\theta_L\left(\frac{x+x'}{2L_x},\frac{\eta\left(t-\tau\right)}{L_x^2}\right)\right) \tag{A.7}$$

Bounded by sealing faults at $x=0$ and $x=L_x$

$$\Delta p_s\left(x,x',t,\tau\right)=\frac{dx'}{2L_x}\left(\theta_3\left(\frac{x-x'}{2L_x},\frac{\eta\left(t-\tau\right)}{L_x^2}\right)+\theta_3\left(\frac{x+x'}{2L_x},\frac{\eta\left(t-\tau\right)}{L_x^2}\right)\right) \tag{A.8}$$

Bounded by a sealing fault at $x=0$ and constant pressure boundary at $x=L_x$

$$\Delta p_s\left(x,x',t,\tau\right)=\frac{dx'}{2L_x}\left(\theta_2\left(\frac{x-x'}{2L_x},\frac{\eta\left(t-\tau\right)}{L_x^2}\right)+\theta_2\left(\frac{x+x'}{2L_x},\frac{\eta\left(t-\tau\right)}{L_x^2}\right)\right) \tag{A.9}$$

Bounded by a constant pressure boundary at $x=0$ and a sealing fault at $x=L_x$

$$\Delta p_s\left(x,x',t,\tau\right)=\frac{dx'}{2L_x}\left(\theta_2\left(\frac{x-x'}{2L_x},\frac{\eta\left(t-\tau\right)}{L_x^2}\right)-\theta_2\left(\frac{x+x'}{2L_x},\frac{\eta\left(t-\tau\right)}{L_x^2}\right)\right) \tag{A.10}$$

Bounded by constant pressure boundaries at $x=0$ and $x=L_x$

$$\Delta p_s\left(x,x',t,\tau\right)=\frac{dx'}{2L_x}\left(\theta_3\left(\frac{x-x'}{2L_x},\frac{\eta\left(t-\tau\right)}{L_x^2}\right)-\theta_3\left(\frac{x+x'}{2L_x},\frac{\eta\left(t-\tau\right)}{L_x^2}\right)\right) \tag{A.11}$$

For a uniform flux line source between $x_1<x'<x_2$, the source functions are expressed in terms of integrals of elliptic theta functions. To our knowledge, there is no standard notation for these functions, so we introduce the following notation:

$$\Theta_2\left(z,t\right)=\frac{1}{2}\sum_{n=-\infty}^{\infty}\left(-1\right)^n\operatorname{erf}\left(\frac{z+n}{\sqrt{t}}\right) \tag{A.12a}$$

$$=\frac{1}{\pi}\sum_{n=0}^{\infty}\frac{\sin\left(\left(2n+1\right)\pi z\right)}{\left(2n+1\right)}\exp\left(-\pi^2\left(n+\frac{1}{2}\right)^2 t\right) \tag{A.12b}$$

$$\Theta_3(z,t) = \frac{1}{2}\sum_{n=-\infty}^{\infty} \operatorname{erf}\left(\frac{z+n}{\sqrt{t}}\right) \tag{A.13a}$$

$$= \frac{1}{2\pi}\sum_{n=0}^{\infty} \varepsilon_n \frac{\sin 2n\pi z}{n} \exp\left(-\pi^2 n^2 t\right) \tag{A.13b}$$

$$\Theta_L(z,t) = \frac{1}{2}\operatorname{erf}\left(\frac{z}{\sqrt{t}}\right) \tag{A.14}$$

In particular, since our functions will involve integrals of elliptic theta functions between two fixed points, we will employ the notation:

$$\widehat{\Theta}_2(z_1,z_2,t) = \Theta_2(z_2,t) - \Theta_2(z_1,t) \tag{A.15}$$

$$\widehat{\Theta}_3(z_1,z_2,t) = \Theta_3(z_2,t) - \Theta_3(z_1,t) \tag{A.16}$$

$$\widehat{\Theta}_L(z_1,z_2,t) = \Theta_L(z_2,t) - \Theta_L(z_1,t) \tag{A.17}$$

Infinite System: (L_x is arbitrary).

$$\Delta p_{sl}(x,t,\tau) = \widehat{\Theta}_L\left(\frac{x_1-x}{2L_x}, \frac{x_2-x}{2L_x}, \frac{\eta(t-\tau)}{L_x^2}\right) \tag{A.18}$$

Semi-Infinite (with sealing fault at $x=0$) (L_x is arbitrary).

$$\Delta p_{sl}(x,t,\tau) = \widehat{\Theta}_L\left(\frac{x_1-x}{2L_x}, \frac{x_2-x}{2L_x}, \frac{\eta(t-\tau)}{L_x^2}\right) + \widehat{\Theta}_L\left(\frac{x_1+x}{2L_x}, \frac{x_2-x}{2L_x}, \frac{\eta(t-\tau)}{L_x^2}\right) \tag{A.19}$$

: :

Semi-Infinite (with constant pressure at $x = 0$) (L_x is arbitrary).

$$\Delta p_{sl}(x,t,\tau) = \widehat{\Theta}_L\left(\frac{x_1 - x}{2L_x}, \frac{x_2 - x}{2L_x}, \frac{\eta(t-\tau)}{L_x^2}\right) - \widehat{\Theta}_L\left(\frac{x_1 + x}{2L_x}, \frac{x_2 - x}{2L_x}, \frac{\eta(t-\tau)}{L_x^2}\right) \tag{A.20}$$

Bounded by sealing faults at $x = 0$ and $x = L_x$

$$\Delta p_{sl}(x,t,\tau) = \widehat{\Theta}_3\left(\frac{x_1 - x}{2L_x}, \frac{x_2 - x}{2L_x}, \frac{\eta(t-\tau)}{L_x^2}\right) + \widehat{\Theta}_3\left(\frac{x_1 + x}{2L_x}, \frac{x_2 + x}{2L_x}, \frac{\eta(t-\tau)}{L_x^2}\right) \tag{A.21}$$

Bounded by a sealing fault at $x = 0$ and constant pressure boundary at $x = L_x$

$$\Delta p_{sl}(x,t,\tau) = \widehat{\Theta}_2\left(\frac{x_1 - x}{2L_x}, \frac{x_2 - x}{2L_x}, \frac{\eta(t-\tau)}{L_x^2}\right) + \widehat{\Theta}_2\left(\frac{x_1 + x}{2L_x}, \frac{x_2 + x}{2L_x}, \frac{\eta(t-\tau)}{L_x^2}\right) \tag{A.22}$$

Bounded by a constant pressure boundary at $x = 0$ and a sealing fault at $x = L_x$

$$\Delta p_{sl}(x,t,\tau) = \widehat{\Theta}_2\left(\frac{x_1 - x}{2L_x}, \frac{x_2 - x}{2L_x}, \frac{\eta(t-\tau)}{L_x^2}\right) - \widehat{\Theta}_2\left(\frac{x_1 + x}{2L_x}, \frac{x_2 + x}{2L_x}, \frac{\eta(t-\tau)}{L_x^2}\right) \tag{A.23}$$

Bounded by constant pressure boundaries at $x = 0$ and $x = L_x$

$$\Delta p_{sl}(x,t,\tau) = \widehat{\Theta}_3\left(\frac{x_1 - x}{2L_x}, \frac{x_2 - x}{2L_x}, \frac{\eta(t-\tau)}{L_x^2}\right) - \widehat{\Theta}_3\left(\frac{x_1 + x}{2L_x}, \frac{x_2 + x}{2L_x}, \frac{\eta(t-\tau)}{L_x^2}\right) \tag{A.24}$$

A.2 Laplace Transform of Products of Source Functions

In well-testing applications, we are most interested in finding the Laplace Transform (with respect to time) of the time integral of products of the previously

defined source functions. That is, a typical unit constant-rate pressure drop solution assumes the form

$$\Delta p_{cu}(x,y,z,t) = \frac{5.615}{\phi c_t}\int_0^t \frac{\Delta p_{sx}}{dx'}\frac{\Delta p_{sy}}{dy'}\frac{\Delta p_{sz}}{dz'}d\tau, \tag{A.25}$$

with Laplace transform

$$\overline{\Delta p}_{cu} = \frac{5.615}{\phi c_t}\int_0^\infty \frac{\Delta p_{sx}}{dx'}\frac{\Delta p_{sy}}{dy'}\frac{\Delta p_{sz}}{dz'}\frac{e^{-u\tau}}{u}d\tau. \tag{A.26}$$

(In the case where the point source is replaced by a uniform flux line source, for example in the x-direction, $\dfrac{\Delta p_{sx}}{dx'}$ in the above equations is replaced by Δp_{slx}.)

Each of the source functions in Eq. A.26 assumes a unique functional behavior at late time. In the following, ε is a small number on the order of machine round-off error. The late-time forms of each of these functions, as well as the times for which the late time approximations are valid, are listed in the following formulas. (The superscript "l" in the following formulas refers to late time approximation.)

Point Source, Infinite System:

$$\Delta p_s^l(x,x',t) = \frac{dx'}{2\sqrt{\pi\eta t}} \tag{A.27}$$

for $t > -\dfrac{(x-x')^2}{4\eta\ln(1-\varepsilon)}$.

Point Source, Semi-Infinite (with sealing fault at $x=0$)

$$\Delta p_s^l(x,x',t) = \frac{dx'}{\sqrt{\pi\eta t}} \tag{A.28}$$

for $t > \max\left(-\dfrac{(x-x')^2}{4\eta\ln(1-\varepsilon)}, -\dfrac{(x+x')^2}{4\eta\ln(1-\varepsilon)}\right)$.

Point Source, Semi-Infinite (with constant pressure at $x=0$)

$$\Delta p_s^l(x,x',t) = 0 \tag{A.29}$$

for $t > \max\left(-\dfrac{(x-x')^2}{4\eta\ln(1-\varepsilon)}, -\dfrac{(x+x')^2}{4\eta\ln(1-\varepsilon)}\right)$.

Point Source, Bounded by sealing faults at $x = 0$ and $x = L_x$

$$\Delta p_s^l\left(x, x', t\right) = \frac{dx'}{L_x} \tag{A.30}$$

for $t > -\dfrac{L_x^2 \ln \varepsilon}{\pi^2 \eta}$.

Point Source, Bounded by a sealing fault at $x = 0$ and constant pressure boundary at $x = L_x$

$$\Delta p_s^l\left(x, x', t\right) = 0 \tag{A.31}$$

for $t > -4\dfrac{L_x^2 \ln \varepsilon}{\pi^2 \eta}$.

Point Source, Bounded by a constant pressure boundary at $x = 0$ and a sealing fault at $x = L_x$

$$\Delta p_s^l\left(x, x', t\right) = 0 \tag{A.32}$$

for $t > -4\dfrac{L_x^2 \ln \varepsilon}{\pi^2 \eta}$.

Point Source, Bounded by constant pressure boundaries at $x = 0$ and $x = L_x$

$$\Delta p_s^l\left(x, x', t\right) = 0 \tag{A.33}$$

for $t > -4\dfrac{L_x^2 \ln \varepsilon}{\pi^2 \eta}$.

Line Source, Infinite System:

$$\Delta p_{sl}^l\left(x, t\right) = \frac{x_2 - x_1}{2\sqrt{\pi \eta t}} \tag{A.34}$$

for $t > \max\left[-\dfrac{(x_2 - x)^2}{4\eta \ln(1-\varepsilon)}, -\dfrac{(x_1 - x)^2}{4\eta \ln(1-\varepsilon)}\right]$.

Line Source, Semi-Infinite (with sealing fault at $x = 0$)

$$\Delta p_{sl}^l\left(x, t\right) = \frac{x_2 - x_1}{\sqrt{\pi \eta t}} \tag{A.35}$$

for $t > \max\left(-\dfrac{(x_2 - x)^2}{4\eta \ln(1-\varepsilon)}, -\dfrac{(x_1 - x)^2}{4\eta \ln(1-\varepsilon)}, -\dfrac{(x_2 + x)^2}{4\eta \ln(1-\varepsilon)}, -\dfrac{(x_1 + x)^2}{4\eta \ln(1-\varepsilon)}\right)$.

Line Source, Semi-Infinite (with constant pressure at $x = 0$)

$$\Delta p_{sl}^{l}(x,t) = 0 \tag{A.36}$$

for $t > \max\left(-\frac{(x_2-x)^2}{4\eta\ln(1-\varepsilon)}, -\frac{(x_1-x)^2}{4\eta\ln(1-\varepsilon)}, -\frac{(x_2+x)^2}{4\eta\ln(1-\varepsilon)}, -\frac{(x_1+x)^2}{4\eta\ln(1-\varepsilon)}\right)$.

Line Source, Bounded by sealing faults at $x = 0$ and $x = L_x$

$$\Delta p_{sl}^{l}(x,t) = \frac{x_2 - x_1}{L_x} \tag{A.37}$$

for $t > -\frac{L_x^2 \ln\varepsilon}{\pi^2\eta}$.

Line Source, Bounded by a sealing fault at $x = 0$ and constant pressure boundary at $x = L_x$

$$\Delta p_{sl}^{l}(x,t) = 0 \tag{A.38}$$

for $t > -4\frac{L_x^2 \ln\varepsilon}{\pi^2\eta}$.

Line Source, Bounded by a constant pressure boundary at $x = 0$ and a sealing fault at $x = L_x$

$$\Delta p_{s}^{l}(x,x',t) = 0 \tag{A.39}$$

for $t > -4\frac{L_x^2 \ln\varepsilon}{\pi^2\eta}$.

Line Source, Bounded by constant pressure boundaries at $x = 0$ and $x = L_x$

$$\Delta p_{s}^{l}(x,x',t) = 0 \tag{A.40}$$

for $t > -4\frac{L_x^2 \ln\varepsilon}{\pi^2\eta}$.

A.2.1 Numerical procedure for determination of Laplace transforms

Eq. A.26 is written as follows:

$$\overline{\Delta p_{cu}} = \frac{5.615}{\phi c_t}\int_0^{t^*} \frac{\Delta p_{sx}}{dx'}\frac{\Delta p_{sy}}{dy'}\frac{\Delta p_{sz}}{dz'}\frac{e^{-u\tau}}{u}d\tau + \overline{\Psi}, \tag{A.41}$$

where

$$\overline{\Psi} = \frac{5.615}{\phi c_t} \int_{t^*}^{\infty} \frac{\Delta p_{sx}}{dx'} \frac{\Delta p_{sy}}{dy'} \frac{\Delta p_{sz}}{dz'} \frac{e^{-u\tau}}{u} d\tau. \tag{A.42}$$

t^* is determined as follows. If the system contains at least one constant pressure boundary in any coordinate direction, then t^* is the *minimum* time at which any of the source functions approach zero. If there are no constant pressure boundaries, t^* is the minimum time at which *all* of the source functions attain their late-time functional forms. In Eq. A.41, the first integral is determined numerically using Chebyshev integration [13]. Here, we briefly describe the procedure used in its evaluation.

Determine the minimum time at which the first term in the exponential or error function forms of any of the functions in the product becomes non-negligible.

Consider an arbitrary elliptic theta function or integral of an elliptic theta function of the form $\theta_{\varrho}(z_i, \alpha_i t)$, where

$$\theta_{\varrho} \in \{\theta_2, \theta_3, \Theta_2, \Theta_3\} \tag{A.43}$$

At small values of time, the leading terms in each of these functions involves an exponential with argument $\frac{-z_i^2}{\alpha_i t}$. (Note that for small values of $\alpha_i t$,

$$\lim_{t \to 0} \left(\operatorname{erf} \left(\frac{z_i}{\sqrt{\alpha_i t}} \right) \right) = 1 - \frac{\sqrt{\alpha_i t} \exp\left(-\frac{z_i^2}{\alpha_i t} \right)}{\sqrt{\pi} z_i}. \tag{A.44}$$

Since the source functions always involve a difference in error function terms, the size of the source function in these cases is dominated by the size of the exponential term.) The exponential term in each of the source functions is negligible if

$$\frac{z_i^2}{\alpha_i t} > \epsilon, \tag{A.45}$$

where ϵ is a user-specified tolerance - we use $\epsilon \approx 87$. That is, the exponential functions are non-negligible for

$$\frac{z_i^2}{\alpha_i \epsilon} \leq t. \tag{A.46}$$

The minimum time that we are seeking is then the maximum value of t for which Eq. A.46 is satisfied for all source functions. Denote this time $t^*_{\min}$.

Determine the maximum time for the numerical integration.

The maximum time for numerical integration is the minimum time at which the approximations given by Eqs. A.27 - A.40 are satisfied by all the source function terms in the integral. Denote this time, $t^*_{\max}$.

Determine the integral.

We rewrite the first integral in Eq. A.41 as

$$\int_0^{t^*} \frac{\Delta p_{sx}}{dx'} \frac{\Delta p_{sy}}{dy'} \frac{\Delta p_{sz}}{dz'} \frac{e^{-u\tau}}{u} d\tau = \int_{t^*_{\min}}^{t^*_{\max}} \frac{\Delta p_{sx}}{dx'} \frac{\Delta p_{sy}}{dy'} \frac{\Delta p_{sz}}{dz'} \frac{e^{-u\tau}}{u} d\tau$$
$$= \sum_{i=0}^{n-1} \int_{t_i}^{t_{i+1}} \frac{\Delta p_{sx}}{dx'} \frac{\Delta p_{sy}}{dy'} \frac{\Delta p_{sz}}{dz'} \frac{e^{-u\tau}}{u} d\tau, \tag{A.47}$$

where n is the number of subintervals such that,

$$t_0 = t^*_{\min}, \tag{A.48}$$

$$t_{i+1} = t_i, \text{ for } i = 0, 1, ...n-2 \tag{A.49}$$

and

$$t_n = t^*_{\max}. \tag{A.50}$$

On each subinterval (t_i, t_{i+1}), the integrand $\left(\frac{\Delta p_{sx}}{dx'}\frac{\Delta p_{sy}}{dy'}\frac{\Delta p_{sz}}{dz'}\frac{e^{-u\tau}}{u}\right)$ is fit with a Chebyshev polynomial of degree 32, and the integral is evaluated using the procedure outlined in Chapters 5.8 and 5.9 of Ref. [13]. The total integral is obtained by summing the integrals over each subinterval as indicated in Eq. A.47.

A.2.2 Analytical late-time Laplace Transforms

In the following, we present appropriate expressions for the function $\overline{\Psi}$ (see Eq. A.42) for combinations of sealed and infinite boundary conditions. (The analytical Laplace transforms were determined using the symbolic mathematics program, Maple V release 5.1, (Waterloo-Maple Inc.).) We introduce the following simplifying notation:

$$\Lambda_\chi = \frac{\eta_\chi}{L_\chi^2} \tag{A.51}$$

where $\chi = x$, y, or z. For infinite or semi-infinite coordinate directions, the value of L_χ is arbitrary.

Point Source: Infinite x-direction, Infinite y-direction, Finite bounded z-direction

$$\overline{\Psi} = \frac{5.615}{\phi c_t L_x L_y L_z}\frac{E_1\left(ut^*\right)}{4\pi u\sqrt{\Lambda_x\Lambda_y}} \tag{A.52}$$

Point Source: A single fault in the x or y directions, Finite bounded z-direction

$$\overline{\Psi} = \frac{5.615}{\phi c_t L_x L_y L_z}\frac{E_1\left(ut^*\right)}{2\pi u\sqrt{\Lambda_x\Lambda_y}} \tag{A.53}$$

Point Source: Perpendicular single faults in the x and y directions, Finite bounded z-direction

$$\overline{\Psi} = \frac{5.615}{\phi c_t L_x L_y L_z} \frac{E_1\left(ut^*\right)}{\pi u \sqrt{\Lambda_x \Lambda_y}} \tag{A.54}$$

Point Source: Infinite in the x direction, Finite bounded in the y and z-directions

$$\overline{\Psi} = \frac{5.615}{\phi c_t L_x L_y L_z} \frac{\operatorname{erf} c\left(\sqrt{ut^*}\right)}{2\sqrt{\Lambda_x} u^{\frac{3}{2}}} \tag{A.55}$$

Point Source: Single fault in the x direction, Finite bounded in the y and z-directions

$$\overline{\Psi} = \frac{5.615}{\phi c_t L_x L_y L_z} \frac{\operatorname{erf} c\left(\sqrt{ut^*}\right)}{\sqrt{\Lambda_x} u^{\frac{3}{2}}} \tag{A.56}$$

Point Source: Finite bounded in the x, y and z-directions

$$\overline{\Psi} = \frac{5.615}{\phi c_t L_x L_y L_z} \frac{\exp\left(-ut^*\right)}{u^2} \tag{A.57}$$

A.3 Solutions Involving Line Sources

In the following, we consider a uniform flux line source in the x-direction with $x_1 < x < x_2$. Similar to point sources, the instantaneous line sources approach zero at late time in any system with a constant pressure boundary.

Line Source: Infinite x-direction, Infinite y-direction, Finite bounded z-direction

$$\overline{\Psi} = \frac{5.615\left(x_2 - x_1\right)}{\phi c_t L_x^2 L_y L_z} \frac{E_1\left(ut^*\right)}{4\pi u \sqrt{\Lambda_x \Lambda_y}} \tag{A.58}$$

Point Source: A single fault in the x or y directions, Finite bounded z-direction

$$\overline{\Psi} = \frac{5.615\,(x_2 - x_1)}{\phi c_t L_x^2 L_y L_z} \frac{E_1\,(ut^*)}{2\pi u\sqrt{\Lambda_x \Lambda_y}} \tag{A.59}$$

Line Source: Perpendicular single faults in the x and y directions, Finite bounded z-direction

$$\overline{\Psi} = -\frac{5.615\,(x_2 - x_1)}{\phi c_t L_x^2 L_y L_z} \frac{E_1\,(ut^*)}{\pi u\sqrt{\Lambda_x \Lambda_y}} \tag{A.60}$$

Line Source: Infinite in the x direction, Finite bounded in the y and z-directions

$$\overline{\Psi} = \frac{5.615\,(x_2 - x_1)}{\phi c_t L_x^2 L_y L_z} \frac{\operatorname{erf} c\left(\sqrt{ut^*}\right)}{2\sqrt{\Lambda_x} u^{\frac{3}{2}}} \tag{A.61}$$

Point Source: Single fault in the x direction, Finite bounded in the y and z-directions

$$\overline{\Psi} = \frac{5.615\,(x_2 - x_1)}{\phi c_t L_x^2 L_y L_z} \frac{\operatorname{erf} c\left(\sqrt{ut^*}\right)}{\sqrt{\Lambda_x} u^{\frac{3}{2}}} \tag{A.62}$$

Point Source: Finite bounded in the x, y and z-directions

$$\overline{\Psi} = \frac{5.615\,(x_2 - x_1)}{\phi c_t L_x^2 L_y L_z} \frac{\exp\left(-ut^*\right)}{u^2} \tag{A.63}$$

A.4 Derivatives of Source Functions

In this section, we present the derivatives of the one-dimensional source functions with respect to the dimensionless variables z and t. From these derivatives, we

can construct partial derivatives of the pressure function with respect to any reservoir parameter for nonlinear regression applications.

$$\frac{\partial \theta_2}{\partial z} = \frac{2}{\sqrt{\pi} t^{\frac{3}{2}}} \sum_{n=-\infty}^{\infty} (-1)^{n+1} (z+n) \exp\left(-\frac{(z+n)^2}{t}\right) \tag{A.64a}$$

$$= -2\pi \sum_{n=0}^{\infty} (2\,n+1) \sin((2\,n+1)\,\pi\,z) \exp\left(-\pi^2 \left(n+\frac{1}{2}\right)^2 t\right) \tag{A.64b}$$

$$\frac{\partial \theta_2}{\partial t} = -\frac{\theta_2\,(z,t)}{2t} + \frac{1}{\sqrt{\pi} t^{\frac{5}{2}}} \sum_{n=-\infty}^{\infty} (-1)^n (z+n)^2 \exp\left(-\frac{(z+n)^2}{t}\right) \tag{A.65a}$$

$$= -2\pi^2 \sum_{n=0}^{\infty} \left(n+\frac{1}{2}\right)^2 \cos((2\,n+1)\,\pi\,z) \exp\left(-\pi^2 \left(n+\frac{1}{2}\right)^2 t\right) \tag{A.65b}$$

$$\frac{\partial \theta_3}{\partial z} = -\frac{2}{\sqrt{\pi} t^{\frac{3}{2}}} \sum_{n=-\infty}^{\infty} (z+n) \exp\left(-\frac{(z+n)^2}{t}\right) \tag{A.66a}$$

$$= -4\pi \sum_{n=1}^{\infty} n \sin(2\,n\pi\,z) \exp\left(-\pi^2 n^2 t\right) \tag{A.66b}$$

$$\frac{\partial \theta_3}{\partial t} = -\frac{\theta_3\,(z,t)}{2t} + \frac{1}{\sqrt{\pi} t^{\frac{5}{2}}} \sum_{n=-\infty}^{\infty} (z+n)^2 \exp\left(-\frac{(z+n)^2}{t}\right) \tag{A.67a}$$

$$= -2\pi^2 \sum_{n=1}^{\infty} n^2 \cos(2\,n\pi\,z) \exp\left(-\pi^2 n^2 t\right) \tag{A.67b}$$

$$\frac{\partial \theta_L}{\partial z} = -\frac{2z}{\sqrt{\pi} t^{\frac{3}{2}}} \exp\left(-\frac{z^2}{t}\right) \tag{A.68}$$

$$\frac{\partial \theta_L}{\partial t} = \frac{(2z^2 - t)}{2\sqrt{\pi} t^{\frac{5}{2}}} \exp\left(-\frac{z^2}{t}\right) \tag{A.69}$$

$$\frac{\partial \Theta_2(z,t)}{\partial z} = \theta_2(z,t) \tag{A.70}$$

$$\frac{\partial \Theta_2(z,t)}{\partial t} = -\frac{1}{2\sqrt{\pi}\left(\sqrt{t}\right)^3} \sum_{n=-\infty}^{\infty} (-1)^n (z+n) \exp\left(-\frac{(z+n)^2}{t}\right) \tag{A.71a}$$

$$= -\frac{\pi}{2} \sum_{n=0}^{\infty} (2n+1) \sin\left((2n+1)\pi z\right) \exp\left(-\frac{1}{4}\pi^2 (2n+1)^2 t\right) \tag{A.71b}$$

$$\frac{\partial \widehat{\Theta}_2(z_1,z_2,t)}{\partial z_1} = -\frac{\partial \Theta_2(z_1,t)}{\partial z} \tag{A.72}$$

$$\frac{\partial \widehat{\Theta}_2(z_1,z_2,t)}{\partial z_2} = \frac{\partial \Theta_2(z_2,t)}{\partial z} \tag{A.73}$$

$$\frac{\partial \widehat{\Theta}_2(z_1,z_2,t)}{\partial t} = \frac{\partial \Theta_2(z_2,t)}{\partial t} - \frac{\partial \Theta_2(z_1,t)}{\partial t} \tag{A.74}$$

$$\frac{\partial \Theta_3(z,t)}{\partial z} = \theta_3(z,t) \tag{A.75}$$

$$\frac{\partial \Theta_3(z,t)}{\partial t} = -\frac{1}{2\sqrt{\pi}\left(\sqrt{t}\right)^3} \sum_{n=-\infty}^{\infty} (z+n) \exp\left(-\frac{(z+n)^2}{t}\right) \tag{A.76a}$$

$$= -\pi \sum_{n=1}^{\infty} n \sin(2n\pi z) \exp\left(-\pi^2 n^2 t\right) \tag{A.76b}$$

$$\frac{\partial \widehat{\Theta}_3(z_1,z_2,t)}{\partial z_1} = -\frac{\partial \Theta_3(z_1,t)}{\partial z} \tag{A.77}$$

$$\frac{\partial \widehat{\Theta}_3(z_1,z_2,t)}{\partial z_2} = \frac{\partial \Theta_3(z_2,t)}{\partial z} \tag{A.78}$$

$$\frac{\partial \widehat{\Theta}_3(z_1,z_2,t)}{\partial t} = \frac{\partial \Theta_3(z_2,t)}{\partial t} - \frac{\partial \Theta_3(z_1,t)}{\partial t} \tag{A.79}$$

A.4.1 Late Time Behavior

$$\frac{\partial \theta_2}{\partial z} = 0 \tag{A.80}$$

for $t > -\dfrac{4\ln\left(\frac{\varepsilon}{2\pi}\right)}{\pi^2}$.

$$\frac{\partial \theta_2}{\partial t} = 0 \tag{A.81}$$

for $t > -\dfrac{4\ln\left(\frac{2\varepsilon}{\pi^2}\right)}{\pi^2}$.

$$\frac{\partial \theta_3}{\partial z} = 0 \tag{A.82}$$

for $t > -\dfrac{\ln\left(\frac{\varepsilon}{4\pi}\right)}{\pi^2}$.

$$\frac{\partial \theta_3}{\partial t} = 0 \tag{A.83}$$

for $t > -\dfrac{\ln\left(\frac{\varepsilon}{2\pi^2}\right)}{\pi^2}$.

$$\frac{\partial \theta_L}{\partial z} = -\frac{2z}{\sqrt{\pi} t^{\frac{3}{2}}} \tag{A.84}$$

for $t > -\dfrac{z^2}{\ln(1-\varepsilon)}$.

$$\frac{\partial \theta_L}{\partial t} = \frac{(2z^2 - t)}{2\sqrt{\pi} t^{\frac{5}{2}}} \tag{A.85}$$

for $t > -\dfrac{z^2}{\ln(1-\varepsilon)}$.

$$\frac{\partial \Theta_2(z,t)}{\partial z} = 0 \tag{A.86}$$

for $t > -\dfrac{4\ln(\varepsilon)}{\pi^2}$.

$$\frac{\partial \Theta_2(z,t)}{\partial t} = 0 \tag{A.87}$$

for $t > -\dfrac{4\ln\left(\dfrac{4\varepsilon}{\pi}\right)}{\pi^2}$.

$$\frac{\partial \Theta_3(z,t)}{\partial z} = 1 \tag{A.88}$$

for $t > -\dfrac{\ln(\varepsilon)}{\pi^2}$.

$$\frac{\partial \Theta_3(z,t)}{\partial t} = 0 \tag{A.89}$$

for $t > -\dfrac{\ln\left(\dfrac{2\varepsilon}{\pi}\right)}{\pi^2}$.

APPENDIX B

WELL AND FRACTURE PLANE SOLUTIONS IN DIFFERENT RESERVOIR SYSTEMS

In this appendix, we record pertinent solutions to simple reservoir problems encountered in the modeling of complex-geometry reservoirs. The dimensionless variables used are the same as those defined in Chapter 2. The solutions are written in terms of the elliptic theta functions or integrals of elliptic theta functions defined in Appendix A. All solutions assume the presence of a single-phase slightly compressible fluid in a homogeneous anisotropic reservoir, and were obtained using the method of "sources and sinks".

B.1 One Well in an Infinite Reservoir

The dimensionless pressure drop at (x_D, y_D) caused by a well producing rate of $q_{0D}(t_D)$ at the point $\left(x_D^{'}, y_D^{'}\right)$ is given by

$$p_{D,wi}\left(x_D, x_D^{'}, y_D, y_{D,}^{'} t_D\right) = \frac{\pi}{2}\int_0^{t_D} q_{0D}(\tau)\,\theta_L\left(\frac{x_D - x_D^{'}}{2}, t_D - \tau\right)\theta_L\left(\frac{y_D - y_D^{'}}{2}, t_D - \tau\right)d\tau, \quad \text{(B.1)}$$

with Laplace transform,

$$\overline{p}_{D,wi}\left(x_D, x_D^{'}, y_D, y_{D,}^{'} u_D\right) = \overline{q}_{0D}(u_D)\,K_0\left(\sqrt{\left[\left(x_D - x_D^{'}\right)^2 + \left(y_D - y_D^{'}\right)^2\right]u_D}\right). \quad \text{(B.2)}$$

If unit production rate is assumed, then

$$\overline{q}_{0D}\left(u_D\right) = \frac{1}{u_D}. \tag{B.3}$$

The above formula can be expressed as

$$\overline{p}_{D,wi}\left(x_D, x_D^{'}, y_D, y_{D,}^{'} u_D\right) = \frac{1}{u_D} K_0 \left(\sqrt{\left[\left(x_D - x_D^{'}\right)^2 + \left(y_D - y_D^{'}\right)^2\right] u_D}\right). \tag{B.4}$$

Here, as before, K_0 is the modified Bessel function of the second kind.

B.2 Horizontal Uniform-flux Fracture Plane in an Infinite Reservoir

For a uniform-flux fracture plane, producing at an uniform flux of $q_{fD}\left(t_D\right)$, the dimensionless pressure drop at any point is given by

$$p_{D,hi}\left(x_D, y_D, x_{D,L}, x_{D,R}, y_{fD,} t_D\right) = \int_0^{t_D} q_{fD}\left(\tau\right) f_{hi}\left(x_D, y_D, x_{D,L}, x_{D,R}, y_{fD,} t_D - \tau\right) d\tau, \tag{B.5}$$

where, $x_{D,L}$ is the left hand side coordinate of the fracture, $x_{D,R}$ represents the right hand side coordinate of the fracture and y_{fD} is the y-direction position of the fracture plane, and,

$$f_{hi}\left(x_D, y_D, x_{D,L}, x_{D,R}, y_{fD,} t_D\right) = \pi \widehat{\Theta}_L \left(\frac{x_{D,L} - x_D}{2}, \frac{x_{D,R} - x_D}{2}, t_D\right) \theta_L \left(\frac{y_D - y_{fD}}{2}, t_D\right). \tag{B.6}$$

The Laplace transform of the pressure drop is given by

$$\overline{p}_{D,hi}\left(x_D, y_D, x_{D,L}, x_{D,R,} u_D\right) = \overline{q}_{fD}\left(u_D\right) \overline{f}_{hi}\left(x_D, y_D, x_{D,L}, x_{D,R,} u_D\right), \tag{B.7}$$

where, $\overline{f}_{hi}\left(x_D, y_D, x_{D,L}, x_{D,R,} u_D\right)$ is computed numerically as described in Appendix A.

B.3 Fully-Penetrating Well an Infinite Channel

For a well at the point (x'_D, y'_D) producing at a rate $q_{0D}(t_D)$ from a channel of width L_{xD} that is infinite in the y-direction, the dimensionless pressure drop at any point (x_D, y_D) is given by

$$p_{D,wv}(x_D, y_D, t_D) = \int_0^{t_D} q_{0D}(\tau) f_{wv}(x_D, y_D, L_{xD}, x'_D, y'_D, t_D - \tau)\, d\tau, \tag{B.8}$$

where

$$f_{wv}(x_D, y_D, L_{xD}, x'_D, y'_D, t_D) = \frac{\pi}{2L_{xD}} \left[\theta_3\left(\frac{x_D - x'_D}{2L_{xD}}, \frac{t_D}{L_{xD}^2}\right) + \theta_3\left(\frac{x_D + x'_D}{2L_{xD}}, \frac{t_D}{L_{xD}^2}\right)\right] \theta_L\left(\frac{y_D - y'_D}{2}, t_D\right). \tag{B.9}$$

The Laplace transform of the dimensionless pressure drop is given by

$$\overline{p}_{D,wv}(x_D, y_D, u_D) = \overline{q}_{0D}(u_D)\, \overline{f}_{wv}(x_D, y_D, L_{xD}, x'_D, y'_D, u_D), \tag{B.10}$$

where, as before, the Laplace transform of $f_{wv}(x_D, y_D, L_{xD}, x'_D, y'_D, t_D)$ is computed numerically using the methods in Appendix A.

B.4 A Horizontal Uniform-Flux Fracture Plane in an Infinite Vertical Channel

For a horizontal uniform-flux fracture for $(x_{D,L} < x < x_{D,R})$ in an infinite channel (in the y-direction) of width L_{xD}, the dimensionless pressure drop at any point (x_D, y_D) is given by

$$p_{D,hv}(x_D, y_D, t_D) = \int_0^{t_D} q_{fD}(\tau) f_{hv}(x_D, y_D, L_{xD}, x_{D,L}, x_{D,R}, y_{fD}, t_D - \tau)\, d\tau, \tag{B.11}$$

where

$$f_{hv}\left(x_D, y_D, L_{xD}, x_{D,L}, x_{D,R}, y_{fD}, t_D\right) =$$
$$\pi\left[\widehat{\Theta}_3\left(\frac{x_{D,L}-x_D}{2L_{xD}}, \frac{x_{D,R}-x_D}{2L_{xD}}, \frac{t_D}{L_{xD}^2}\right) + \widehat{\Theta}_3\left(\frac{x_{D,L}+x_D}{2L_{xD}}, \frac{x_{D,R}+x_D}{2L_{xD}}, \frac{t_D}{L_{xD}^2}\right)\right] \times$$
$$\theta_L\left(\frac{y_D - y_D^{'}}{2}, t_D\right). \quad \text{(B.12)}$$

The Laplace transform of the dimensionless pressure drop is given by

$$\overline{p}_{D,hv}\left(x_D, y_D, u_D\right) = \overline{q}_{fD}\left(u_D\right)\overline{f}_{hv}\left(x_D, y_D, L_{xD}, x_{D,L}, x_{D,R}, y_{fD}, u_D\right), \quad \text{(B.13)}$$

where, as before, the Laplace transform of $\overline{f}_{hv}\left(x_D, y_D, L_{xD}, x_{D,L}, x_{D,R}, y_{fD}, u_D\right)$ is computed numerically using the methods in Appendix A.

B.5 A Horizontal Uniform-Flux Fracture Plane in a Horizontal Channel

For a completely-penetrating horizontal fracture plane in a horizontal, x-direction, channel with thickness L_{yD}, the dimensionless pressure drop is given by

$$p_{D,hh}\left(x_D, y_D, t_D\right) = \int_0^{t_D} q_{fD}\left(\tau\right) f_{hh}\left(x_D, y_D, L_{xD}, x_{D,L}, x_{D,R}, y_{fD}, t_D - \tau\right) d\tau, \quad \text{(B.14)}$$

where

$$f_{hh}\left(x_D, y_D, L_{yD}, x_{D,L}, x_{D,R}, y_{fD}, t_D\right) =$$
$$\frac{\pi}{L_{yD}}\widehat{\Theta}_L\left(\frac{x_{D,L}-x_D}{2}, \frac{x_{D,R}-x_D}{2}, t_D\right) \times$$
$$\left[\theta_3\left(\frac{y_D - y_{fD}}{2L_{yD}}, \frac{t_D}{L_{yD}^2}\right) + \theta_3\left(\frac{y_D + y_{fD}}{2L_{yD}}, \frac{t_D}{L_{yD}^2}\right)\right] \quad \text{(B.15)}$$

and $x_{D,R}$ and $x_{D,L}$ refer to the x-coordinates of the right and left tips of the fracture. The corresponding Laplace transform of the dimensionless pressure drop is given by

$$\overline{p}_{D,hh}\left(x_D, y_D, u_D\right) = \overline{q}_{fD}\left(u_D\right)\overline{f}_{hh}\left(x_D, y_D, L_{yD}, x_{D,L}, x_{D,R}, y_{fD}, u_D\right). \tag{B.16}$$

The method of computation of the Laplace transform of the source function is detailed in Appendix A.

B.6 A Fully-Penetrating Well in a Bounded Rectangular Reservoir

For a completely-penetrating well at (x'_D, y'_D) in a rectangular sealed reservoir, with dimensions $L_{xD} \times L_{yD}$, the dimensionless pressure drop assumes the form

$$p_{D,wb}\left(x_D, y_D, t_D\right) = \int_0^{t_D} q_{0D}\left(\tau\right) f_{wb}\left(x_D, y_D, L_{xD}, L_{yD}, x'_D, y'_D, t_D - \tau\right) d\tau, \tag{B.17}$$

where

$$\begin{aligned} f_{wb}\left(x_D, y_D, L_{xD}, L_{yD}, x'_D, y'_D, t_D\right) = \\ \frac{\pi}{2}\left\{\frac{1}{L_{xD}}\left[\theta_3\left(\frac{x_D - x'_D}{2L_{xD}}, \frac{t_D}{L_{xD}^2}\right) + \theta_3\left(\frac{x_D + x'_D}{2L_{xD}}, \frac{t_D}{L_{xD}^2}\right)\right]\right\} \times \\ \left\{\frac{1}{L_{yD}}\left[\theta_3\left(\frac{y_D - y'_D}{2L_{yD}}, \frac{t_D}{L_{yD}^2}\right) + \theta_3\left(\frac{y_D + y'_D}{2L_{yD}}, \frac{t_D}{L_{yD}^2}\right)\right]\right\}. \end{aligned} \tag{B.18}$$

The corresponding Laplace transform function is given by

$$\overline{p}_{D,wb}\left(x_D, y_D, u_D\right) = \overline{q}_{0D}\left(u_D\right)\overline{f}_{wb}\left(x_D, y_D, L_{xD}, L_{yD}, x'_D, y'_D, u_D\right). \tag{B.19}$$

B.7 A Horizontal Uniform-Flux Fracture Plane in a Rectangular Bounded Reservoir

For a completely-penetrating horizontal fracture plane in a rectangular sealed reservoir, with dimensions $L_{xD} \times L_{yD}$, the dimensionless pressure drop assumes the

form

$$p_{D,hb}\left(x_D, y_D, t_D\right) = \int_0^{t_D} q_{fD}\left(\tau\right) f_{hb}\left(x_D, y_D, L_{xD}, L_{yD}, x_{D,L}, x_{D,R}, y_{fD}, t_D - \tau\right) d\tau, \tag{B.20}$$

where

$$f_{hb}\left(x_D, y_D, L_{xD}, L_{yD}, x_{D,L}, x_{D,R}, y_{fD}, t_D\right) = \frac{\pi}{L_{yD}} \left[\widehat{\Theta}_3\left(\frac{x_{D,L} - x_D}{2L_{xD}}, \frac{x_{D,R} - x_D}{2L_{xD}}, \frac{t_D}{L_{xD}^2}\right) + \widehat{\Theta}_3\left(\frac{x_{D,L} + x_D}{2L_{xD}}, \frac{x_{D,R} + x_D}{2L_{xD}}, \frac{t_D}{L_{xD}^2}\right)\right] \times \left[\theta_3\left(\frac{y_D - y_D^{'}}{2L_{yD}}, \frac{t_D}{L_{yD}^2}\right) + \theta_3\left(\frac{y_D + y_D^{'}}{2L_{yD}}, \frac{t_D}{L_{yD}^2}\right)\right]. \tag{B.21}$$

The corresponding Laplace transform is given by

$$\overline{p}_{D,hb}\left(x_D, y_D, u_D\right) = \overline{q}_{fD}\left(u_D\right) \overline{f}_{hb}\left(x_D, y_D, L_{xD}, L_{yD}, x_{D,L}, x_{D,R}, y_{fD}, u_D\right). \tag{B.22}$$

APPENDIX C

LAPLACE TRANSFORMATION OF SOME FUNCTIONS

The following Laplace transformation formulas are used in the verification of our proposed model and they are extremely practical when dealing with the communication between two infinite reservoirs.

$$L\left\{\frac{1}{\beta_1 t}\operatorname{erf}\left(\frac{\beta_2}{2\sqrt{\beta_1 t}}\right)\right\} = \frac{2\beta_2}{\beta_1\sqrt{\pi}}\sum_{m=0}^{\infty}\frac{\left(|\beta_2|\sqrt{\frac{u}{\beta_1}}\right)^m \cdot K_m\left(|\beta_2|\sqrt{\frac{u}{\beta_1}}\right)}{1\cdot 2\cdot 3\cdots(2m+1)} \tag{C.1}$$

let

$$Z_1 = |\beta_2|\sqrt{\frac{u}{\beta_1}}, \qquad Z_1 > 0. \tag{C.2}$$

Then,

$$L\left\{\frac{1}{\beta_1 t}\operatorname{erf}\left(\frac{\beta_2}{2\sqrt{\beta_1 t}}\right)\right\} = \frac{2\beta_2}{\beta_1\sqrt{\pi}}\sum_{m=0}^{\infty}\frac{Z_1^m \cdot K_m(Z_1)}{1\cdot 2\cdot 3\cdots(2m+1)} \tag{C.3a}$$

$$= \frac{2\beta_2}{\beta_1\sqrt{\pi}}\cdot f_1(Z_1) \tag{C.3b}$$

where,

$$f_1(Z_1) = \sum_{m=0}^{\infty}\frac{Z_1^m \cdot K_m(Z_1)}{1\cdot 2\cdot 3\cdots(2m+1)} \tag{C.4}$$

and β_1, β_2 are constants.

$$L\left\{\frac{1}{t}\exp\left(\frac{\beta_3}{4t}\right)\operatorname{erf}\left(\frac{\beta_2}{2\sqrt{t}}\right)\right\} = \frac{2\beta_2}{\sqrt{\pi}}\sum_{m=0}^{\infty}\frac{\left(\frac{\beta_2^2}{\beta_2^2+\beta_3}\right)^m}{1\cdot 2\cdot 3\cdots(2m+1)}\cdot \left(\sqrt{\left(\beta_2^2+\beta_3\right)u}\right)^m K_m\left(\sqrt{\left(\beta_2^2+\beta_3\right)u}\right) \quad \text{(C.5)}$$

let,

$$Z_2 = \sqrt{\left(\beta_2^2+\beta_3\right)u}, \quad Z_2 > 1 \quad \text{(C.6)}$$

$$r = \frac{\beta_2^2}{\beta_2^2+\beta_3} = \frac{1}{1+\frac{\beta_3}{\beta_2^2}}, \quad r \le 1 \quad \text{(C.7)}$$

Then,

$$L\left\{\frac{1}{t}\exp\left(\frac{\beta_3}{4t}\right)\operatorname{erf}\left(\frac{\beta_2}{2\sqrt{t}}\right)\right\} = \frac{2\beta_2}{\sqrt{\pi}}\sum_{m=0}^{\infty}\frac{r^m\cdot Z_2^m\cdot K_m\left(Z_2\right)}{1\cdot 2\cdot 3\cdots(2m+1)} \quad \text{(C.8a)}$$

$$= \frac{2\beta_2}{\sqrt{\pi}} f_2\left(r, Z_2\right) \quad \text{(C.8b)}$$

where,

$$f_2\left(r, Z_2\right) = \sum_{m=0}^{\infty}\frac{r^m\cdot Z_2^m\cdot K_m\left(Z_2\right)}{1\cdot 2\cdot 3\cdots(2m+1)} \quad \text{(C.9)}$$

and β_2, β_3 are constants. K_m is the modified Bessel function of the second kind and the computation of $f_2\left(r, Z_2\right)$ is stable when K_m is calculated in an ascendant order [14]. The expansion formulas of error function were listed in Chapter 7.1 of Ref. [14].

Note that Eq. C.3b and Eq. C.8b enable us to establish a tabulated function in our programming to compute the accurate Laplace transformation by using Chebyshev polynomial approximation.

APPENDIX D

LATE TIME DERIVATIVE APPROXIMATIONS

D.1 Basic Solutions

In this appendix, we derive solutions that describe the late time behavior of reservoir problems encountered in the modeling of complex-geometry reservoirs. The dimensionless variables used are the same as those defined in Chapter 2. The solutions are written in detail by substituting the relevant elliptic theta functions or integrals of elliptic theta functions into the corresponding solutions in Appendix B. All solutions assume the presence of a single-phase slightly compressible fluid in a homogeneous anisotropic reservoir, and were obtained using the method of "sources and sinks". Unit production rate is also assumed for all of the following solutions, so that

$$q_{0D}\left(t_D\right) = 1. \tag{D.1}$$

First, we write the late time derivative solutions for a producer located in an infinite reservoir, a well located in a vertical (or horizontal) channel reservoir, a well located in a bounded reservoir, a horizontal fracture plane in a vertical channel, a horizontal fracture plane in a horizontal channel reservoir and a horizontal fracture plane in a bounded reservoir. Then, the above solutions are applied for different complex-geometry reservoirs to get their late time approximations.

D.1.1 One Well in an Infinite Reservoir: Semilog Behavior

The dimensionless pressure drop at (x_D, y_D) caused by a well producing rate of $q_{0D}(t_D)$ at the point $\left(x_D^{'}, y_D^{'}\right)$ is given by Eq. B.1. The pressure derivative respect to $\ln(t_D)$ is

$$\frac{d}{d(\ln t_D)} p_{D,wi}\left(x_D, x_D^{'}, y_D, y_{D,}^{'} t_D\right) = \frac{\pi}{2}\theta_L\left(\frac{x_D - x_D^{'}}{2}, t_D\right)\theta_L\left(\frac{y_D - y_D^{'}}{2}, t_D\right) t_D. \tag{D.2}$$

At late time, $t_D > 25\max\left(\left(x_D - x_D^{'}\right)^2, \left(y_D - y_D^{'}\right)^2\right)$, the dimensionless pressure derivative is approximately given by

$$\frac{d}{d(\ln t_D)} p_{D,wi}\left(x_D, x_D^{'}, y_D, y_{D,}^{'} t_D\right) = \frac{1}{2}. \tag{D.3}$$

(In order to obtain the time bounds above, we used the formulas in Appendix A, Section A.2, with $\varepsilon = 10^{-10}$, the time bounds in all subsequent approximations were determined using the same value for ε.)

D.1.2 Horizontal Uniform-flux Fracture Plane in an Infinite Reservoir

For a uniform-flux fracture plane, producing at a rate of $Q_{fD}(t_D)$, the dimensionless pressure drop at any point is given by Eq. B.5. Then, its derivative is

$$\begin{aligned}
&\frac{d}{d(\ln t_D)} p_{D,hi}\left(x_D, y_D, x_{D,L}, x_{D,R}, y_{fD,} t_D\right) = \\
&\qquad \frac{Q_{fD}(t_D)}{2L_{fD}} f_{hi}\left(x_D, y_D, x_{D,L}, x_{D,R}, y_{fD,} t_D\right) t_D = \\
&\frac{\pi Q_{fD}(t_D)}{2L_{fD}}\widehat{\Theta}_L\left(\frac{x_{D,L} - x_D}{2}, \frac{x_{D,R} - x_D}{2}, t_D\right)\theta_L\left(\frac{y_D - y_{fD}}{2}, t_D\right) = \\
&\qquad \frac{Q_{fD}(t_D)}{2L_{fD}}\frac{\sqrt{\pi} t_D}{2\sqrt{t_D}}\exp\left[-\frac{(y - y_{fD})^2}{4t_D}\right] \times \\
&\qquad\qquad \left[\operatorname{erf}\left(\frac{x_{D,R} - x_D}{2\sqrt{t_D}}\right) - \operatorname{erf}\left(\frac{x_{D,L} - x_D}{2\sqrt{t_D}}\right)\right]
\end{aligned} \tag{D.4}$$

where, $x_{D,L}$ is the left hand side coordinate of the fracture, $x_{D,R}$ represents the right hand side coordinate of the fracture and y_{fD} is the y-direction position of the fracture plane. For small values of the argument, it is well known that

$$\mathrm{erf}(z) = \frac{2z}{\sqrt{\pi}} \exp\left(-z^2\right), \quad \text{as} \quad z \to 0. \tag{D.5}$$

The late time behavior of Eq. D.4 is approximately given by

$$\frac{d}{d(\ln t_D)} p_{D,hi}\left(x_D, y_D, x_{D,L}, x_{D,R}, y_{fD}, t_D\right) = \frac{Q_{fD}\left(t_D\right)}{2}, \tag{D.6}$$

for $t_D > 25 \max\left(\left(x_{D,R} - x_D\right)^2, \left(x_{D,L} - x_D\right)^2, \left(y_D - y_{fD}\right)^2\right)$.

D.1.3 Fully-Penetrating Well an Infinite Channel

For a well at the point (x'_D, y'_D) producing at a unit rate from a channel of width L_{xD} that is infinite in the y-direction, the dimensionless pressure drop at any point (x_D, y_D) is given by Eq. B.8. The derivative is

$$\frac{d}{d(\ln t_D)} p_{D,wv}\left(x_D, y_D, t_D\right) = f_{wv}\left(x_D, y_D, L_{xD}, x'_D, y'_D, t_D\right) t_D \tag{D.7}$$

where

$$f_{wv}\left(x_D, y_D, L_{xD}, x'_D, y'_D, t_D\right) = \frac{\pi}{2L_{xD}} \left[\theta_3\left(\frac{x_D - x'_D}{2L_{xD}}, \frac{t_D}{L_{xD}^2}\right) + \theta_3\left(\frac{x_D + x'_D}{2L_{xD}}, \frac{t_D}{L_{xD}^2}\right)\right] \theta_L\left(\frac{y_D - y'_D}{2}, t_D\right), \tag{D.8}$$

or, applying the late time formula we have

$$f_{wv}\left(x_D, y_D, L_{xD}, x_D^{'}, y_D^{'}, t_D\right)$$
$$= \frac{\sqrt{\pi}}{L_{xD}\sqrt{t_D}} \exp\left[-\frac{\left(y_D - y_D^{'}\right)^2}{4t_D}\right] \times$$
$$\left[1 + \sum_{n=1}^{\infty}\left(\cos\frac{n\pi\left(x_D - x_D^{'}\right)}{L_{xD}} + \cos\frac{n\pi\left(x_D + x_D^{'}\right)}{L_{xD}}\right)\exp\left(-\frac{n^2\pi^2 t_D}{L_{xD}^2}\right)\right]. \quad \text{(D.9)}$$

Then, for a fully-penetrating well an infinite channel the late time derivative approximation is

$$\frac{d}{d(\ln t_D)} p_{D,wv}\left(x_D, y_D, t_D\right) = \frac{\sqrt{\pi t_D}}{L_{xD}}, \quad \text{(D.10)}$$

for $t_D > \max\left(\frac{5L_{xD}^2}{\pi^2}, 25\left(y_D - y_D^{'}\right)^2\right)$.

D.1.4 A Horizontal Uniform-Flux Fracture Plane in an Infinite Vertical Channel

For a horizontal uniform-flux fracture for $(x_{D,L} < x < x_{D,R})$ in an infinite channel (in the y-direction) of width L_{xD}, the dimensionless pressure drop at any point (x_D, y_D) is given by Eq. B.11. Its derivative is

$$\frac{d}{d(\ln t_D)} p_{D,hv}\left(x_D, y_D, t_D\right) = \frac{Q_{fD}\left(t_D\right)}{2L_{fD}} f_{hv}\left(x_D, y_D, L_{xD}, x_{D,L}, x_{D,R}, y_{fD}, t_D\right) t_D \quad \text{(D.11)}$$

where

$$f_{hv}\left(x_D, y_D, L_{xD}, x_{D,L}, x_{D,R}, y_{fD}, t_D\right) =$$
$$\pi\left[\widehat{\Theta}_3\left(\frac{x_{D,L} - x_D}{2L_{xD}}, \frac{x_{D,R} - x_D}{2L_{xD}}, \frac{t_D}{L_{xD}^2}\right) + \widehat{\Theta}_3\left(\frac{x_{D,L} + x_D}{2L_{xD}}, \frac{x_{D,R} + x_D}{2L_{xD}}, \frac{t_D}{L_{xD}^2}\right)\right] \times$$
$$\theta_L\left(\frac{y_D - y_D^{'}}{2}, t_D\right), \quad \text{(D.12)}$$

or, applying late time formula we have

$$f_{hv}\left(x_D, y_D, L_{xD}, x_{D,L}, x_{D,R}, y_{fD}, t_D\right)$$
$$= \frac{\sqrt{\pi}}{L_{xD}\sqrt{t_D}} \exp\left[-\frac{\left(y_D - y_{fD}\right)^2}{4t_D}\right] \times$$
$$\left[2L_{fD} + \sum_{n=1}^{\infty} \frac{L_{xD}}{n\pi} \exp\left[-\frac{n^2\pi^2 t_D}{L_{xD}^2}\right] \times \right.$$
$$\left.\left(\sin\frac{n\pi\left(x_{D,R} - x_D\right)}{L_{xD}} - \sin\frac{n\pi\left(x_{D,L} - x_D\right)}{L_{xD}} + \sin\frac{n\pi\left(x_{D,R} + x_D\right)}{L_{xD}} - \sin\frac{n\pi\left(x_{D,L} + x_D\right)}{L_{xD}}\right)\right]. \tag{D.13}$$

Then, for a horizontal uniform-flux fracture plane in an infinite vertical channel the late time derivative approximation is

$$\frac{d}{d(\ln t_D)} p_{D,hv}\left(x_D, y_D, t_D\right) = Q_{fD}\left(t_D\right) \frac{\sqrt{\pi t_D}}{L_{xD}}, \tag{D.14}$$

for $t_D > \max\left(\frac{20 L_{xD}^2}{\pi^2}, 25\left(y_D - y_{fD}\right)^2\right)$

D.1.5 A Horizontal Uniform-Flux Fracture Plane in a Horizontal Channel

For a completely-penetrating horizontal fracture plane in a horizontal, x-direction, channel with thickness L_{yD}, the dimensionless pressure drop is given by Eq. B.14 and its derivative is

$$\frac{d}{d(\ln t_D)} p_{D,hh}\left(x_D, y_D, t_D\right) = \frac{Q_{fD}\left(t_D\right)}{2L_{fD}} f_{hh}\left(x_D, y_D, L_{xD}, x_{D,L}, x_{D,R}, y_{fD}, t_D - \tau\right) t_D \tag{D.15}$$

where

$$f_{hh}\left(x_D, y_D, L_{yD}, x_{D,L}, x_{D,R}, y_{fD}, t_D\right) =$$
$$\frac{\pi}{L_{yD}}\widehat{\Theta}_L\left(\frac{x_{D,L}-x_D}{2}, \frac{x_{D,R}-x_D}{2}, t_D\right) \times$$
$$\left[\theta_3\left(\frac{y_D-y_{fD}}{2L_{yD}}, \frac{t_D}{L_{yD}^2}\right)+\theta_3\left(\frac{y_D+y_{fD}}{2L_{yD}}, \frac{t_D}{L_{yD}^2}\right)\right], \quad \text{(D.16)}$$

or, applying the late time formula we have

$$f_{hh}\left(x_D, y_D, L_{yD}, x_{D,L}, x_{D,R}, y_{fD}, t_D\right)$$
$$= \frac{\pi}{L_{yD}}\left[\operatorname{erf}\left(\frac{x_{D,R}-x_D}{2\sqrt{t_D}}\right)-\operatorname{erf}\left(\frac{x_{D,L}-x_D}{2\sqrt{t_D}}\right)\right] \times$$
$$\left[1+\sum_{n=1}^{\infty}\left(\cos\frac{n\pi\left(y_D-y_{fD}\right)}{L_{yD}}+\cos\frac{n\pi\left(y_D+y_{fD}\right)}{L_{yD}}\right)\exp\left(-\frac{n^2\pi^2 t_D}{L_{yD}^2}\right)\right]. \quad \text{(D.17)}$$

Then, for a horizontal uniform-flux fracture plane in an horizontal channel the late time derivative approximation is

$$\frac{d}{d(\ln t_D)}p_{D,hh}\left(x_D, y_D, t_D\right) = Q_{fD}\left(t_D\right)\frac{\sqrt{\pi t_D}}{L_{yD}}, \quad \text{(D.18)}$$

$$\text{for } t_D > \max\left(25\left(x_{D,R}-x_D\right)^2, 25\left(x_{D,L}-x_D\right)^2, \frac{5L_{yD}^2}{\pi^2}\right).$$

D.1.6 A Fully-Penetrating Well in a Bounded Rectangular Reservoir

For a completely-penetrating well at (x'_D, y'_D) in a rectangular sealed reservoir, with dimensions $L_{xD} \times L_{yD}$, the dimensionless pressure drop assumes the form of Eq. B.17

$$\frac{d}{d(\ln t_D)}p_{D,wb}\left(x_D, y_D, t_D\right) = f_{wb}\left(x_D, y_D, L_{xD}, L_{yD}, x'_D, y'_D, t_D\right)t_D \quad \text{(D.19)}$$

where

$$f_{wb}\left(x_D, y_D, L_{xD}, L_{yD}, x'_D, y'_D, t_D\right) =$$
$$\frac{\pi}{2}\left\{\frac{1}{L_{xD}}\left[\theta_3\left(\frac{x_D - x'_D}{2L_{xD}}, \frac{t_D}{L^2_{xD}}\right) + \theta_3\left(\frac{x_D + x'_D}{2L_{xD}}, \frac{t_D}{L^2_{xD}}\right)\right]\right\} \times$$
$$\left\{\frac{1}{L_{yD}}\left[\theta_3\left(\frac{y_D - y'_D}{2L_{yD}}, \frac{t_D}{L^2_{yD}}\right) + \theta_3\left(\frac{y_D + y'_D}{2L_{yD}}, \frac{t_D}{L^2_{yD}}\right)\right]\right\}, \quad \text{(D.20)}$$

or, the late time expression is

$$f_{wb}\left(x_D, y_D, L_{xD}, L_{yD}, x'_D, y'_D, t_D\right)$$
$$= \frac{2\pi}{L_{xD}L_{yD}}\left[1 + \sum_{n=1}^{\infty}\left(\cos\frac{n\pi\left(x_D - x'_D\right)}{L_{xD}} + \cos\frac{n\pi\left(x_D + x'_D\right)}{L_{xD}}\right)\exp\left(-\frac{n^2\pi^2 t_D}{L^2_{xD}}\right)\right] \times$$
$$\left[1 + \sum_{n=1}^{\infty}\left(\cos\frac{n\pi\left(y_D - y'_D\right)}{L_{yD}} + \cos\frac{n\pi\left(y_D + y'_D\right)}{L_{yD}}\right)\exp\left(-\frac{n^2\pi^2 t_D}{L^2_{yD}}\right)\right]. \quad \text{(D.21)}$$

As the pseudosteady state flow regime is reached, the pressure derivative is

$$\frac{d}{d(\ln t_D)}p_{D,wb}\left(x_D, y_D, t_D\right) = \frac{2\pi t_D}{L_{xD}L_{yD}}, \quad \text{(D.22)}$$

for $t_D > \max\left(\frac{5L^2_{xD}}{\pi^2}, \frac{5L^2_{yD}}{\pi^2}\right)$.

D.1.7 A Horizontal Uniform-Flux Fracture Plane in a Bounded Rectangular Reservoir

For a completely-penetrating horizontal fracture plane in a rectangular sealed reservoir, with dimensions $L_{xD} \times L_{yD}$, the dimensionless pressure drop assumes the form of Eq. B.20 and its derivative is

$$\frac{d}{d(\ln t_D)}p_{D,hb}\left(x_D, y_D, t_D\right) = \frac{Q_{fD}\left(t_D\right)}{2L_{fD}}f_{hb}\left(x_D, y_D, L_{xD}, L_{yD}, x_{D,L}, x_{D,R}, y_{fD}, t_D\right)t_D \quad \text{(D.23)}$$

where

$$f_{hb}\left(x_D, y_D, L_{xD}, L_{yD}, x_{D,L}, x_{D,R}, y_{fD}, t_D\right) = \frac{\pi}{L_{yD}}\left[\widehat{\Theta}_3\left(\frac{x_{D,L}-x_D}{2L_{xD}}, \frac{x_{D,R}-x_D}{2L_{xD}}, \frac{t_D}{L_{xD}^2}\right) + \widehat{\Theta}_3\left(\frac{x_{D,L}+x_D}{2L_{xD}}, \frac{x_{D,R}+x_D}{2L_{xD}}, t_D\right)\right] \times \left[\theta_3\left(\frac{y_D - y_D^{'}}{2L_{yD}}, \frac{t_D}{L_{yD}^2}\right) + \theta_3\left(\frac{y_D + y_D^{'}}{2L_{yD}}, \frac{t_D}{L_{yD}^2}\right)\right], \quad \text{(D.24)}$$

or, the late time expression is

$$f_{hb}\left(x_D, y_D, L_{xD}, L_{yD}, x_{D,L}, x_{D,R}, y_{fD}, t_D\right) = \frac{2\pi}{L_{xD}L_{xD}} \times \left[1 + \sum_{n=1}^{\infty}\left(\cos\frac{n\pi\left(y_D - y_{fD}\right)}{L_{yD}} + \cos\frac{n\pi\left(y_D + y_{fD}\right)}{L_{yD}}\right)\exp\left(-\frac{n^2\pi^2 t_D}{L_{yD}^2}\right)\right] \times \left[2L_{fD} + \frac{L_{xD}}{\pi}\sum_{n=1}^{\infty}\frac{\exp\left(-\frac{n^2\pi^2 t_D}{L_{xD}^2}\right)}{n} \times \left(\sin\frac{n\pi\left(x_{D,R}-x_D\right)}{L_{xD}} - \sin\frac{n\pi\left(x_{D,L}-x_D\right)}{L_{xD}} + \sin\frac{n\pi\left(x_{D,R}+x_D\right)}{L_{xD}} - \sin\frac{n\pi\left(x_{D,L}+x_D\right)}{L_{xD}}\right)\right]. \quad \text{(D.25)}$$

When pseudosteady state flow is achieved, the pressure derivative is

$$\frac{d}{d(\ln t_D)}p_{D,hb}\left(x_D, y_D, t_D\right) = Q_{fD}\left(t_D\right)\frac{2\pi t_D}{L_{xD}L_{xD}}, \quad \text{(D.26)}$$

for $t_D > \max\left(\frac{5L_{xD}^2}{\pi^2}, \frac{5L_{yD}^2}{\pi^2}\right)$.

D.2 Late Time Derivative Approximations

D.2.1 System with a Leaky Fault

This system is defined as Fig. 1.1. Its late time asymptotic pressure derivative approximation is derived below. At very large times when all of the dimensionless pressure terms in Eq. 2.14 and Eq. 2.20 are given by late-time approximations (Eq. D.3 and Eq. D.5), and when the rate of fluid flow through the gap becomes approximately constant, the pressure derivative in Region 1 is approximately given by

$$\frac{dp_{D,1}}{d(\ln t_{D,1})} = 1 - \frac{Q_{fD}}{2}. \tag{D.27}$$

Similarly, the pressure derivative in Region 2 assumes the form,

$$\frac{dp_{D,2}}{d(\ln t_{D,2})} = \frac{Q_{fD}}{2C_S C_R} = \frac{Q_{fD}}{2C_T}. \tag{D.28}$$

Here Q_{fD} is the stabilized rate of flow through the gap in RB/D per RB/D of production from the actual well. Since the pressure derivatives along the gap must be the same for both regions, i.e., the right sides of Eq. D.27 and Eq. D.28 must be equal, it is easy to show that

$$Q_{fD} \rightarrow \frac{2C_T}{1 + C_T} \tag{D.29}$$

and

$$\frac{dp_{D,1}}{d(\ln t_{D,1})} \rightarrow \frac{1}{1 + C_T}. \tag{D.30}$$

Note that for a system with a vanishingly small gap width, the initial pressure derivative behavior will approximate that of a semi-infinite system, while at late time the derivative will approach the value given by Eq. 3.16.

D.2.2 Tee-shaped Channel Reservoir

The system is defined in Fig. 4.1. At very large times when flow in the vertical channel and horizontal channel become linear and parallel to the channel boundaries, and when the rate of fluid flow through the gap becomes approximately constant, the pressure derivative in the vertical and horizontal channels are approximately given by

$$\frac{dp_{D,1}}{d\left(\ln t_{D,1}\right)} = \frac{\sqrt{\pi}(2 - Q_{fD})}{L_{xD}}\sqrt{t_D} \tag{D.31}$$

and

$$\frac{dp_{D,2}}{d\left(\ln t_{D,2}\right)} = \frac{1}{\sqrt{C_T C_S}}\frac{\sqrt{\pi}Q_{fD}}{2L_{y2D}}\sqrt{t_D}, \tag{D.32}$$

respectively; see Eqs. D.10, D.14 and D.18. As before, Q_{fD} is the stabilized rate of flow through the gap in RB/D per RB/D of production from the actual well. Since the pressure derivatives along the gap must be the same for both regions, by equating the right sides of the above late time approximations, it is easy to show that

$$Q_{fD} \rightarrow \frac{2}{1 + \dfrac{L_{xD}}{2L_{y2D}\sqrt{C_T C_S}}} \tag{D.33}$$

and

$$\frac{dp_{D,1}}{d(\ln t_{D,1})} \rightarrow \frac{2\sqrt{\pi t_D}}{L_{xD} + 2L_{y2D}\sqrt{C_T C_S}} \tag{D.34}$$

$$= 2\alpha_T\sqrt{\pi t_D}, \tag{D.35}$$

where,

$$\alpha_T = \frac{1}{L_{xD} + 2L_{y2D}\sqrt{C_T C_S}}. \tag{D.36}$$

We find that if $\alpha_T = 1$ or $\alpha_T = \frac{1}{2}$, $\frac{dp_{D,1}}{d(\ln t_{D,1})}$ approaches the behavior of a semi-infinite channel and channel like reservoirs respectively. The smaller the α_T value, the better properties the communicating channel will have.

D.2.3 Channel and Splay Reservoir

Fig. 5.1 shows a channel and splay reservoir system. At very large times when flow in the horizontal channel becomes linear and parallel to the channel boundaries, and when the fluid flow through the junction reaches a steady value and the rate is approximately constant, the pressure derivative in the horizontal channel and splay are approximately given by

$$\frac{dp_{D,1}}{d(\ln t_{D,1})} = \frac{\sqrt{\pi t_D}}{L_{yD}}(1 - \frac{Q_{fD}}{2}), \tag{D.37}$$

and

$$\frac{dp_{D,2}}{d(\ln t_{D,2})} = \frac{1}{C_S}\frac{\pi Q_{fD}}{L_{x2D}L_{y2D}}t_D, \tag{D.38}$$

respectively.

As before, Q_{fD} is the stabilized injection rate at the vertically fractured injection well in RB/D per RB/D of production from the actual well. Equating the pressure derivatives along the gap for both regions, we can show that

$$Q_{fD} \rightarrow \frac{1}{\frac{1}{2} + \frac{1}{C_S}\frac{L_{yD}\sqrt{\pi t_D}}{L_{x2D}L_{y2D}}} \tag{D.39}$$

and

$$\frac{dp_{D,1}}{d(\ln t_{D,1})} \rightarrow \frac{\sqrt{\pi t_D}}{L_{yD} + C_S \frac{L_{x2D} L_{y2D}}{2\sqrt{\pi t_D}}} \tag{D.40}$$

$$= \alpha_{c\_s} \sqrt{\pi t_D}. \tag{D.41}$$

Recall that C_S is defined as

$$C_S = \frac{\phi_2 c_{t2} h_2}{\phi_1 c_{t1} h_1}. \tag{D.42}$$

Obviously, the term $C_S \frac{L_{x2D} L_{y2D}}{2 L_{yD} \sqrt{\pi t_D}}$ represents the relative fluid drainage ability in the splay.

D.2.4 Communicating Bounded Reservoir

The schematic of communicating bounded reservoir is plotted in Fig. 6.1. At very large times when flow in Region 1 and Region 2 become either linear flow or pseudosteady state depending on the boundary conditions, and when the rate of fluid flow through the leaky fault becomes approximately constant, the pressure derivative in the decomposed reservoir components are approximately given by

$$\frac{dp_{D,1}}{d(\ln t_{D,1})} = \frac{\pi t_D}{L_{xD} L_{yD}} (1 - \frac{Q_{fD}}{2}), \tag{D.43}$$

and

$$\frac{dp_{D,2}}{d(\ln t_{D,2})} = \frac{1}{C_S} \frac{\pi Q_{fD} t_D}{L_{x2D} L_{y2D}}, \tag{D.44}$$

respectively. Similarly, it is easy to show that

$$Q_{fD} \rightarrow \frac{2}{1+\frac{1}{C_S}\frac{L_{xD}L_{yD}}{L_{x2D}L_{y2D}}} \tag{D.45}$$

and

$$\frac{dp_{D,1}}{d(\ln t_{D,1})} \rightarrow \frac{2\pi t_D}{L_{xD}L_{yD}}\frac{1}{1+C_S\frac{L_{x2D}L_{y2D}}{L_{xD}L_{yD}}} \tag{D.46}$$

$$= \alpha_B \frac{2\pi t_D}{L_{xD}L_{yD}}, \tag{D.47}$$

where,

$$\alpha_B = \frac{1}{1+C_S\frac{L_{x2D}L_{y2D}}{L_{xD}L_{yD}}}. \tag{D.48}$$

Clearly, the term $C_S\frac{L_{x2D}L_{y2D}}{L_{xD}L_{yD}}$ is the ratio of the drainage volumes of the related bounded reservoirs. The smaller the α_B value, the better properties Region 2 will have.

D.2.5 Late Time Derivative Approximation for Other Limiting Cases

Other complex-geometry reservoirs which are essential for our analysis are plotted in the attached Fig. D.1. The same procedures are followed to derive the formulas. The dimensionless terms and assumptions are the same as before. Note that in all cases, the vertical channels have a width of L_{xD} and/or L_{x2D}; the horizontal channels have a width of L_{yD} and/or L_{y2D} and k_1 and k_2 represent Region 1 and Region 2 respectively. Late time behaviors are obtained by assuming late time linear flow inside the channel and semilog approximation for well and/or fracture plane in infinite reservoir.

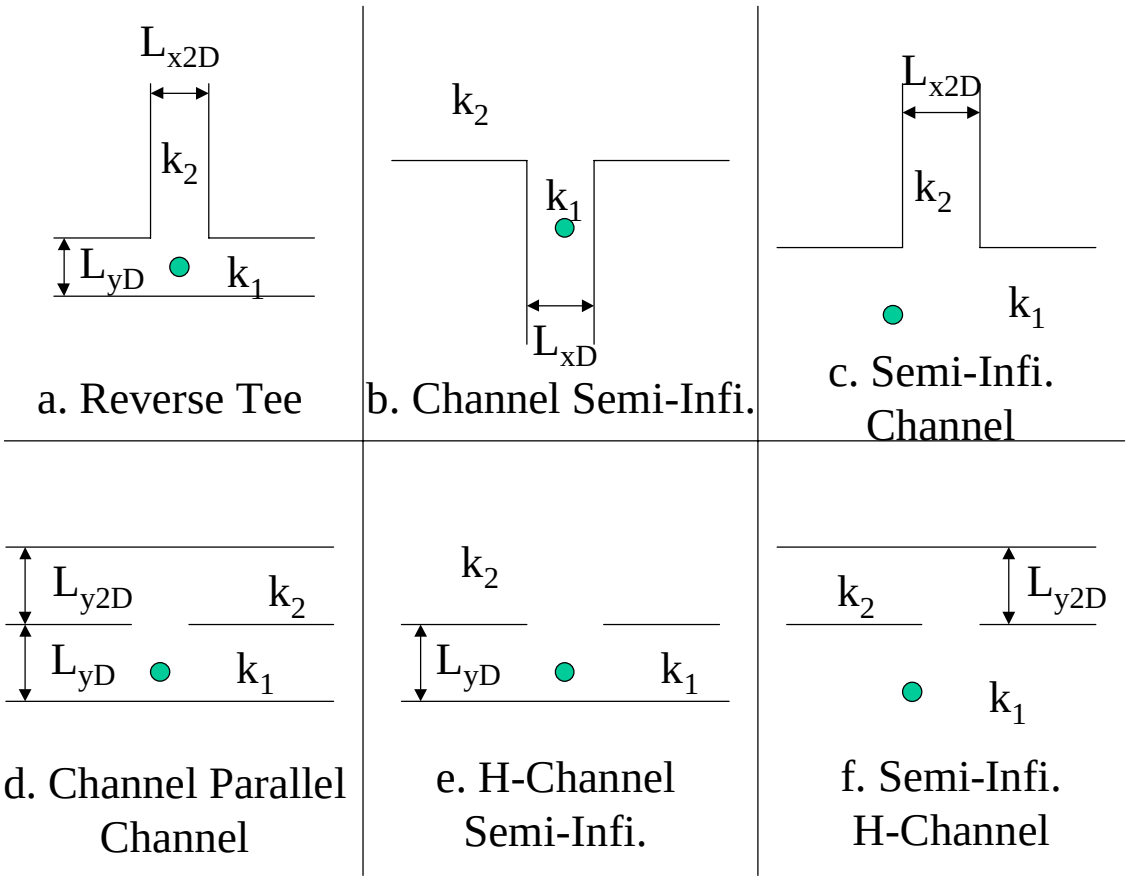

Figure D.1: Brief schematics of some important complex-geometry reservoirs

Reverse Tee

$$Q_{fD} \rightarrow \frac{2}{1+\frac{2}{L_{x2D}\sqrt{C_T C_S}}}. \tag{D.49}$$

$$\frac{dp_{D,1}}{d\left(\ln t_{D,1}\right)} \rightarrow \frac{\sqrt{\pi t_D}}{1+\frac{L_{x2D}\sqrt{C_T C_S}}{2}}. \tag{D.50}$$

Where L_y is defined as the characteristic length and $L_{yD} = 1$.

Channel and Semi-infinite System

$$Q_{fD} \rightarrow \frac{2}{1+\frac{1}{2C_T\sqrt{\pi t_D}}}. \tag{D.51}$$

$$\frac{dp_{D,1}}{d\left(\ln t_{D,1}\right)} \rightarrow \frac{2\sqrt{\pi t_D}}{1+2C_T\sqrt{\pi t_D}} \tag{D.52}$$

$$= \frac{1}{C_T+\frac{1}{2\sqrt{\pi t_D}}}. \tag{D.53}$$

Where L_x is defined as the characteristic length and $L_{xD} = 1$.

Semi-infinite and Channel System

$$Q_{fD} \rightarrow \frac{2}{1+\frac{2\sqrt{\pi t_D}}{L_{x2D}\sqrt{C_T C_S}}}. \tag{D.54}$$

$$\frac{dp_{D,1}}{d\left(\ln t_{D,1}\right)} \rightarrow \frac{1}{1+\frac{L_{x2D}\sqrt{C_T C_S}}{2\sqrt{\pi t_D}}}. \tag{D.55}$$

Where the distance from the well to the sealing fault, L_d, is defined as the characteristic length.

Two Communicating Parallel Channel System

$$Q_{fD} \rightarrow \frac{2}{1+\frac{1}{L_{y2D}\sqrt{C_T C_S}}}. \tag{D.56}$$

$$\frac{dp_{D,1}}{d\left(\ln t_{D,1}\right)} \rightarrow \frac{\sqrt{\pi t_D}}{1+L_{y2D}\sqrt{C_T C_S}}. \tag{D.57}$$

Where L_y is defined as the characteristic length and $L_{yD} = 1$.

Horizontal Channel and Semi-infinite System

$$Q_{fD} \rightarrow \frac{2}{1+\frac{1}{C_T\sqrt{\pi t_D}}}. \tag{D.58}$$

$$\frac{dp_{D,1}}{d\left(\ln t_{D,1}\right)} \rightarrow \frac{\sqrt{\pi t_D}}{1+C_T\sqrt{\pi t_D}}. \tag{D.59}$$

$$= \frac{1}{C_T+\frac{1}{\sqrt{\pi t_D}}}. \tag{D.60}$$

Where L_y is defined as the characteristic length and $L_{yD} = 1$.

Semi-infinite and Horizontal Channel System

$$Q_{fD} \rightarrow \frac{2}{1+\frac{2\sqrt{\pi t_D}}{L_{y2D}\sqrt{C_T C_S}}}. \tag{D.61}$$

$$\frac{dp_{D,1}}{d\left(\ln t_{D,1}\right)} \rightarrow \frac{1}{1+\frac{L_{y2D}\sqrt{C_T C_S}}{2\sqrt{\pi t_D}}}. \tag{D.62}$$

Where the distance from the well to the sealing fault, L_d, is defined as the characteristic length.